

Development of Innovative Gas- Assisted Foam Injection Molding Technology

By

Peter Ungyeong Jung

A thesis submitted in conformity with the requirements
for the degree of Doctor of Philosophy

Department of Mechanical and Industrial Engineering

University of Toronto

© Copyright by Peter Ungyeong Jung 2013

Development of Innovative Gas-Assisted Foam Injection Molding Technology

Peter Ungyeong Jung

Degree of Doctor of Philosophy, 2013

Department of Mechanical and Industrial Engineering
University of Toronto

ABSTRACT

Injection molding technology is utilized for a wide range of applications from mobile phone covers to bumper fascia of automotive vehicles. Foam injection molding (FIM) is a branched manufacturing process of conventional injection molding, but it was designed to take advantage of existing foaming technology, including material cost saving and weight reduction, and to provide additional benefits such as improvement in dimensional stability, faster cycle time, and so on. Gas-assisted injection molding (GAIM) is another supplemental technology of injection molding and offers several advantages as well. This thesis study takes the next step and develops innovative gas-assisted foam injection molding (GAFIM) technology, which is the result of a synergistic combination of two existing manufacturing technologies, FIM and GAIM, in order to produce a unique thermoplastic foam structure with proficient acoustic properties. The foam structure manufactured by GAFIM consists of a solid skin layer, a foam layer, and a hollow core; and its 6.4-mm thick sample outperformed the conventional 22-mm thick polyurethane foam in terms of the acoustic absorption coefficient. With respect to

foaming technology, GAFIM was able to achieve a highly uniform foam morphology by completely decoupling the filling and foaming phases. Moreover, the additional shear and extensional energies from GAFIM promoted a more cell nucleation-dominant foaming behavior, which resulted in higher cell density and smaller cell sizes with both CO₂ and N₂ as physical blowing agents. Lastly, it provided more direct control of the degree of foaming because the pressure drop and pressure drop rate was controlled by a single parameter, that being the gas injection pressure. In summary, innovative, gas-assisted foam injection molding technology offers not only a new strategy to produce acoustically functioning thermoplastic foam products, but also technological advantages over the conventional foam injection molding process. Gas-assisted foam injection molding can become the bedrock for more innovative future applications.

ACKNOWLEDGEMENT

First of all, I would like to thank God the Father for presenting this opportunity to me six years ago and giving me courage to accept this challenging task. I truly believe that He walked this long journey with me and I could not have finished it without His love, guidance, and blessings.

I cannot say enough how grateful I am for my supervisor, Prof. Chul B. Park, for his excellent guidance and the valuable life lessons that I learned from him. He has been very supportive and patient throughout my program and presented numerous opportunities for me to mature as a researcher and a person. I also would like to thank Prof. Hani E. Naguib for being my Ph.D. thesis committee member and always encouraging me as one of his own students. I am also very appreciative to Prof. Chandra for his time and effort as my Ph.D. thesis committee member and his very valuable technical advice. I am grateful for Prof. Ashgriz and Prof. Turng for becoming my exam committee members in such a short notice and for their valuable feedback.

I am indebted to my colleagues at the Microcellular Plastics Manufacturing Lab for sharing my ups and downs on daily basis, which is not an easy task. I sincerely thank my previous and current colleagues, Dr. Anson Wong, Reza Nofar, Kamlesh Majithiya, Nemat Hossieny, Hassan Mahmood, Dr. Amir Ameli, Davoud Jahani, Dr. Saleh Amani, Konstantin Kovalski, Medhi Saniei, Dr. Jing Wang, Dr. Sunny Leung, Dr. Mohamed Hassan, Dr. Yanting Guo, Lun Howe Mark, Mo Xu, Ali Rizvi, Alireza Naeini, Vahid Shaayegan, Weidan Ding, Anna Zhao, Sai Wang, Dr. Reza Bazegari, Dr. Adhikary Kamal. I am also grateful to the many undergraduate students who have assisted me in

my research throughout the years, especially, Hyunwoo Lee, Taewon Park, and Chenkun Li.

There are two of my colleagues with whom I have shared a lot of struggles and frustrations; together, we were able to overcome obstacles, and they have supported me incredibly throughout the years. Thus, my special thanks go to Raymond Chu and Dr. Changwei Zhu.

I was very fortunate to get to know so many hyungs and establish valuable friendships with them throughout the years. They helped me to get through difficult times of my life, and shared their personal experiences and wisdoms with me. I would like to thank Dr. Kevin Y.H. Lee, Dr. Richard Eungkee Lee, Dr. Ryan S.G. Kim, Dr. Yongark Moon, Dr. Myungjae Lee, Dr. Kyungmin Lee, Dr. John W.S. Lee, Dr. Taekyun Lee, and Dr. Patrick Lee. I was also privileged to share special friendships with Esther Lee, Prof. Dongwoo Cho, Prof. Bosung Shin, Dr. Youngseok Kim, and Prof. Simon Park.

Last, but definitely not the least, I would like to thank very special people in my life. I owe a big thank to Donna Lee for being a huge part of my life and inspiring me with her caring support, positive energy, and love. I cannot thank enough my beloved family, my dad, mom, and sister, Maria, for their unconditional love, endless support, having faith in me when I was doubting myself, encouraging me when I was struggling, and motivating me every day to try my best at everything I do to become a better person. I really am indebted to my mom, especially, for packing my lunch (and dinner sometimes) every weekday for the last six years, which have been fuel to my engine. I thank everyone else who helped me to get through this tall, challenging task.

TABLE OF CONTENTS

ABSTRACT.....	II
ACKNOWLEDGEMENT.....	IV
TABLE OF CONTENTS	VI
LIST OF TABLES.....	XII
LIST OF FIGURES.....	XIII
LIST OF SYMBOLS.	XIX
NOMENCLATURE.....	XXI
CHAPTER 1 INTRODUCTION.....	1
1.1 Thermoplastic Foams	1
1.2 Open-Cell and Closed-Cell Foams	1
1.3 Thermoplastic Foam Processing	1
1.4 Injection Molding.....	2
1.5 Foam Injection Molding.....	4
1.6 Acoustic Thermoplastic Foams.....	5

1.7	Research Motivation	6
1.8	Thesis Objectives and Scope of Research.....	7
1.9	Organization of Thesis	8
CHAPTER 2	LITERATURE REVIEW AND THEORETICAL BACKGROUND	11
2.1	Thermoplastic Foam Processing.....	11
2.1.1	Fundamentals of Blowing Agents.....	11
2.1.2	Formation of Polymer/Gas Solution	14
2.1.3	Theoretical Principles of Cell Nucleation and Growth Mechanisms...	17
2.2	Manufacturing of Open-Celled Foam Structures	21
2.2.1	Open-Celled Structures with Foam Extrusion Technology	21
2.2.2	Porous Structures by using Sacrificial Fillers	22
2.3	Foam Injection Molding Technologies.....	23
2.3.1	Conventional Foam Injection Molding and Microcellular Injection Molding Technologies	23
2.3.2	Low Pressure and High Pressure Foam Injection Molding Technologies	25
2.3.3	Investigation of Foaming Behaviors in Foam Injection Molding Using Mold Pressure Profile.....	27
2.3.4	Effect of Gas Counter Pressure on Foam Injection Molding Behavior	29

2.4	Gas-Assisted Injection Molding.....	30
2.4.1	Conventional Gas-Assisted Injection Molding Technology	30
2.4.2	Effect of Gas Channel	32
2.4.3	Computer Simulation Analysis	33
2.4.4	Effect of GAIM on Polymer Crystalline Morphology.....	35
2.5	Acoustic Absorption and Insulation.....	37
2.5.1	Principles of Acoustic Absorption	37
2.5.2	Principles of Acoustic Insulation	38
2.5.3	Thermoplastic Foams for Acoustic Applications.....	40
CHAPTER 3	PROPOSED DESIGN OF GAS-ASSISTED FOAM INJECTION MOLDING TECHNOLOGY.....	57
3.1	Motivation.....	57
3.1.1	Advantages of Gas-Assisted Injection Molding	57
3.1.2	Advantages of Foam injection molding.....	58
3.1.3	Synergistic Effects of the Proposed Gas-Assisted Foam Injection Molding Technology	58
3.2	Fundamental Foaming Principles of the Proposed Technology	62
3.2.1	Coupled Nature of Conventional Foam Injection Molding Technology	62
3.2.2	Decoupling of the Filling and Foaming Mechanism.....	64
3.3	System Implementation of the Proposed Technology.....	68

3.3.1	Schematic of the Proposed Technology	68
3.3.2	Required Equipment for the Proposed Technology	69
CHAPTER 4	EXPERIMENTAL STUDIES OF GAS-ASSISTED FOAM INJECTION MOLDING TECHNOLOGY	76
4.1	Introduction	76
4.2	Experimental Materials	76
4.3	Experimental Set-up	77
4.3.1	Advanced Structural Foam Molding System	77
4.3.2	Arburg Injection Molding Machine with MuCell® System	77
4.3.3	Gas-Assisted Injection Molding System	78
4.3.4	Moldflow® Simulation Study	81
4.4	Experimental Procedure.....	81
4.4.1	Manufacturing of Foams	81
4.4.2	Foam Structure Characterization.....	81
4.4.3	Acoustic Characterization	82
4.5	Effects of Processing Parameters of Gas-Assisted Injection Molding Technology.....	83
4.5.1	Effect of Delay Time.....	83
4.5.2	Effect of Gas Injection Pressure Profile.....	85
4.5.3	Simulation Study Using MoldFlow®	87

4.6	Low Cavity Pressure Case of the Proposed Technology	89
4.6.1	Experiment with CO ₂	90
4.6.2	Experiment with N ₂	92
4.6.3	Foaming Mechanism Analysis	93
4.7	Highly Pressurized Case of the Proposed Technology.....	95
4.7.1	Experiment with Low Gas Injection Pressure.....	96
4.7.2	Experiment with High Gas Injection Pressure	99
4.7.3	Foaming Mechanism Analysis.....	102
4.8	Summary	108
CHAPTER 5	ACOUSTIC PROPERTY CHARACTERIZATION OF THE MANUFACTURED FOAMS.....	147
5.1	Introduction	147
5.2	Strategies to Improve Acoustic Properties of Injection Foam Molded Samples	148
5.2.1	Perforation.....	148
5.2.2	Implementation of Mold Opening Technology	153
5.2.3	Utilization of Gas-Assisted Foam Injection Molding Technology	157
5.3	Relationships between Cellular Morphologies and Acoustic Properties	159
5.4	Summary	161

CHAPTER 6	CONCLUSIONS AND RECOMMENDATIONS FOR FUTURE RESEARCH	178
6.1	Summary of Major Contributions.....	178
6.2	Recommendations for Future Research	182
	REFERENCES.....	185

LIST OF TABLES

Table 2.1 DSC parameters of different zones of G6.7 and G11.6 samples [165]	45
Table 4.1 Physical properties of Pellethane [®] 2355-75A.....	110
Table 4.2 Common fixed processing conditions of injection molding process for GAIM experiments.....	110
Table 4.3 GAIM processing conditions for the delay time study.....	111
Table 4.4 GAIM processing conditions for the gas injection pressure study	111
Table 4.5 GAIM processing conditions for the gas injection pressure profile	112
Table 4.6 Fixed processing parameters for Moldflow [®]	112
Table 4.7 GAIM processing parameters for CO ₂ experiment.....	113
Table 4.8 Common processing parameters for the pressurized case	113
Table 4.9 GAIM processing conditions for the pressurized case	114
Table 5.1 Fixed processing conditions for the mold-opening experimental study	164
Table 5.2 Processing conditions of FIM process for the perforation study	164
Table 5.3 Variable processing parameters for the perforation roller study	164

LIST OF FIGURES

Figure 1.1 Schematics of closed-cell and open-cell foam structures.....	10
Figure 2.1 Gas bubble shape changes with different contact angles on a planar surface [135].....	46
Figure 2.2 Conical cavity for bubble nucleation [135].....	46
Figure 2.3 Schematic for creating porous structure with using sacrificial fillers	47
Figure 2.4 SEM picture of foamed porous structure by leaching of NaCl particulates [36]	47
Figure 2.5 Measurement of cavity pressure profile [127].....	48
Figure 2.6 Pressure profiles in foam extrusion and FIM [127].....	49
Figure 2.7 Comparison of estimated cell density from foam extrusion and actual cell density from FIM of (a) HDPE, (b) PP, and (c) TPO [127]	50
Figure 2.8 Schematic of conventional gas-assisted injection molding technology	51
Figure 2.9 Fingering effect of GAIM TPU	52
Figure 2.10 R_{eq} values of semi-circular and rectangular gas channels on thin plates [154]	52
Figure 2.11 SEM pictures of etched GAIM PP at (a) skin layer and (b) near inner core [164].....	53
Figure 2.12 Acoustic functional mechanisms of a porous medium [167]	53
Figure 2.13 Transmission loss values of ABS and ABS/carbon-black composites with various carbon-black contents [173].....	54
Figure 2.14 Acoustic absorption behavior of PP/PE blend foams with various thicknesses	

[91].....	54
Figure 2.15 Acoustic absorption coefficients of PP/PE blend foams with different perforation density [91].....	55
Figure 2.16 Acoustic absorption behaviors of various types of 3 mm-thick PLLA composites [176].....	55
Figure 2.17 Acoustic absorption of 6.5-mm PP samples with different sizes of voids [31]	56
Figure 3.1 Technological innovations for the proposed GAFIM	71
Figure 3.2 Foaming mechanisms of conventional foam injection molding.....	72
Figure 3.3 Effect of injection flow rate on the final cell structure [127].....	72
Figure 3.4 Effect of void fraction setting on the final cell structure [127]	73
Figure 3.5 Schematic of the proposed gas-assisted foam injection molding technology .	74
Figure 3.6 Effect of additional shear on cell density [178].....	74
Figure 3.7 Effect of extensional strains on cell density [179]	75
Figure 4.1 Schematic of advanced structural foam molding machine [75]	115
Figure 4.2 Arburg ALLROUNDER 270C [187]	115
Figure 4.3 Schematic of MuCell [®] system setup	116
Figure 4.4 Original cavity drawing.....	116
Figure 4.5 Modified cavity with gas channels and measurement locations	117
Figure 4.6 Engineering drawing of cavity with gas channels.....	118
Figure 4.7 Picture of actual cavity insert with gas channels.....	119
Figure 4.8 Drawing of sample part with gas channels.....	120
Figure 4.9 Spring-loaded check valve	121

Figure 4.10 Schematic of ‘through nozzle’ gas injection system	121
Figure 4.11 Effect of gas injection delay time	121
Figure 4.12 Cavity pressure profile when GAIM was applied	122
Figure 4.13 Effect of gas injection pressure	122
Figure 4.14 Cavity pressure profile of Exp. 4.6.....	123
Figure 4.15 Cavity pressure profile of Exp. 4.7.....	124
Figure 4.16 Filled polymer volumes by gas injection pressure changes based on Moldflow [®]	124
Figure 4.17 Voids created by GAIM based on Moldflow [®]	125
Figure 4.18 Gas voids from different GAIM pressure profiles	125
Figure 4.19 The effects of shot sizes on the degree of filling of GAIM samples.....	126
Figure 4.20 The effects of melt temperature on the degree of filling of GAIM samples	126
Figure 4.21 SEM pictures of FIM and GAFIM samples with 35 vol% of void fraction setting.....	127
Figure 4.22 Cell density values of both FIM and GAFIM samples.....	128
Figure 4.23 Cellular morphologies of FIM and GAFIM samples with N ₂ as PBA.....	129
Figure 4.24 Cell density values of FIM and GAFIM at three different locations	130
Figure 4.25 Cavity pressure profiles of (a) FIM and (b) GAFIM for 35 vol% void fraction setting and N ₂ as PBA.....	130
Figure 4.26 Measurement locations of non-gas injection and gas injection regions in a foamed sample	131
Figure 4.27 Cavity pressure profiles of medium GAIM pressure experiment	132
Figure 4.28 SEM images of gas injection (GI) and non-gas injection (NGI) regions of	

GAFIM sample	133
Figure 4.29 SEM pictures of FIM and GAFIM samples at gas injection (GI) regions ..	134
Figure 4.30 SEM pictures of both FIM and GAFIM (6.89 MPa of gas injection pressure) samples at gas injection regions.....	134
Figure 4.31 Magnified SEM images of both FIM and GAFIM samples at non-gas injection regions.....	135
Figure 4.32 Cell density changes at both gas injection (GI) and non-gas injection (NGI) regions due to the implementation of GAFIM.....	136
Figure 4.33 Average cell diameters at both gas injection (GI) and non-gas injection (NGI) regions of FIM and GAFIM samples.....	137
Figure 4.34 Average foam density values at gas injection (GI) and non-gas injection (NGI) regions of FIM and GAFIM samples.....	138
Figure 4.35 Cavity pressure profile of highly pressurized cavity case with 13.79 MPa of gas injection pressure.....	139
Figure 4.36 SEM pictures of gas injection (GI) regions for FIM and two GAFIM cases	140
Figure 4.37 Magnified SEM pictures of gas injection (GI) regions for FIM and two GAFIM cases	141
Figure 4.38 SEM images of non-gas injection regions (NIG) for FIM and two GAFIM cases	142
Figure 4.39 Magnified SEM images of non-gas injection (NGI) regions for FIM and both GAFIM cases	143
Figure 4.40 Cell density changes of gas injection (GI) and non-gas injection (NGI) areas	

due to the increase of gas injection pressure of GAFIM 144

Figure 4.41 Average cell diameter values of gas injection (GI) and non-gas injection (NGI) regions for FIM and two GAFIM cases 145

Figure 4.42 Average foam density values at gas injection (GI) and non-gas injection (NGI) regions of FIM and two GAFIM cases 146

Figure 4.43 Images from the visualization batch foaming system with respect to time. 146

Figure 5.1 Impedance tube testing setups for acoustic absorption of (a) high frequency range with 30 mm diameter tube and (b) low frequency range with 100 mm diameter tube 165

Figure 5.2 Impedance tube testing set-ups for acoustic transmission loss of (a) 30 mm diameter tube and (b) 100 mm diameter tube 165

Figure 5.3 Acoustic absorption coefficients with different open area ratios of rigid cover plate (a) 0.4, (b) 0.1, (c) 0.025, and (d) 0.005 166

Figure 5.4 Manually perforated samples with different hole sizes 166

Figure 5.5 Acoustic absorption coefficients of polyurethane foam with the manually perforated samples 167

Figure 5.6 Acoustic absorption behaviors of perforated samples 167

Figure 5.7 Acoustic absorption coefficients of perforated samples followed by regular foamed samples 168

Figure 5.8 Effects of perforation on the acoustic absorption coefficients for (a) Exp. 1, (b) Exp. 2, and (c) Exp. 3 169

Figure 5.9 Acoustic absorption coefficients of mold opening samples 170

Figure 5.10 Foam samples with various degrees of mold opening 170

Figure 5.11 Transmission losses of different mold opening samples.....	171
Figure 5.12 Acoustic absorption behaviors of two different injection flow rate settings.....	171
Figure 5.13 Cellular morphologies of (a) high injection flow rate samples and (b) low injection flow rate samples	172
Figure 5.14 Transmission loss values for two different injection flow rate settings	173
Figure 5.15 Acoustic absorption coefficients of two injection flow rate settings at higher frequency range.....	173
Figure 5.16 Acoustic insulation behaviors of two injection flow rate settings.....	174
Figure 5.17 Acoustic absorption coefficients of FIM and GAFIM samples	174
Figure 5.18 Transmission loss behaviors of FIM and GAFIM samples.....	175
Figure 5.19 Acoustic absorption coefficients of GAFIM samples with two gas injection pressures, 13.79 and 6.89 MPa	176
Figure 5.20 Transmission loss values of GAFIM samples with two different gas injection pressures, 13.79 and 6.89 MPa	177

LIST OF SYMBOLS

A	=	area of the micrograph, m^2
A_b	=	surface area of bubble, m^2
C_o	=	concentration of gas molecules, mol/m^3
D_o	=	diffusivity coefficient constant, m^2/s
D	=	diffusivity, m^2/s
E	=	elastic modulus of polymer, Pa
f_o	=	frequency factor of gas molecules joining the nucleus, dimensionless
$F(\theta_c)$	=	shape factor
k	=	Boltzmann constant, m^2kg/s^2-K
M	=	magnification factors of the micrograph, dimensionless
\dot{N}_{hom}	=	nucleation rate of homogenous nucleation ($= J_{hom}$), $\#/m^3-s$
n	=	number of bubbles in the micrograph, dimensionless
r	=	cell radius, m
R_g	=	universal gas constant, J/K-mol
T_{sys}	=	system temperature, K
V_b	=	volume of bubble, m^3

W = required amount of work for a cell nucleation, J

Greek Letters

σ = local tensile stress, Pa

β = angle of conical heterogeneous nucleation site, rad

ΔE_D = activation energy for diffusion, J

ΔG^*_{het} = free energy barrier for heterogeneous nucleation, J

ΔG^*_{hom} = free energy barrier for homogeneous nucleation, J

ΔP = system pressure change, Pa

ε = extensional strain, dimensionless

Φ = expansion ratio, dimensionless

ρ_o = polymer bulk density, kg/m³

ρ_f = polymer foam sample density, kg/m³

γ_{pb} = surface tension at polymer-bubble boundary, N/m

θ_c = contact angle, rad

NOMENCLATURE

ASFM	=	Advanced Structural Foam Molding
CBA	=	Chemical Blowing Agent
FIM	=	Foam Injection Molding
GAIM	=	Gas-Assisted Injection Molding
GAFIM	=	Gas-Assisted Foam Injection Molding
GCP	=	Gas-Counter Pressure
HDPE	=	High Density Polyethylene
NCU	=	Nitrogen Control Unit
PBA	=	Physical Blowing Agent
PP	=	Polypropylene
PU	=	Polyurethane
PVOH	=	Polyvinylalcohol
SCF	=	Super Critical Fluid
TPO	=	Thermoplastic Polyolefin
TPU	=	Thermoplastic Polyurethane

Chapter 1 Introduction

1.1 Thermoplastic Foams

Plastic foams or polymer foam structures can easily be seen in numerous and various applications in our daily lives, such as sponges, seat cushions, food trays, packaging materials, insulating materials for construction applications, automotive door modules, inner layer of automobile bumpers, and so on. In order to create these foam structures in polymer, at least two phases are required – solid polymer phase and gaseous phase [1]. Foamed plastic products can provide a number of advantages over their solid counterparts. The advantages are as follows: lighter part weight, savings in material cost, more accurate dimensional stability, increased fatigue life, enhanced toughness, better thermal insulation, and improvements in acoustic properties [2-5].

1.2 Open-Cell and Closed-Cell Foams

Depending on the cell structure within the foam structure, thermoplastic foams can be characterized as open-cell and closed-cell foams. A closed-cell is a cell which is totally enclosed by its cell walls, and hence, no interconnection is available with other adjacent cells [1]. On the other hand, an open-cell is a cell which is not entirely closed by its cell walls, and hence, interconnecting with other adjacent cells via pores or openings [1]. Schematics of these different cellular structures are exhibited in Figure 1.1.

1.3 Thermoplastic Foam Processing

Thermoplastic foams can be manufactured via various processes such as batch

foaming [6-15], bead foaming [16-30], compression molding [31-34], rotational molding [35-46], extrusion foaming [47-56], and foam injection molding [57-74]. In general, a significant amount of research has focused on extrusion and injection molding processes because they are highly utilized in the plastic industry due to high productivity. However, bead foaming technology has been broadening its applications from packaging to automotive products for the last few years. Despite significant differences in terms of their processing equipment, the thermoplastic foam processes generally consist of three stages: (i) gas dissolution within the polymer matrix, (ii) nucleation of bubbles, and (iii) bubble growth. The fundamental theories and related literature on thermoplastic foam processing are discussed in Chapter 2.

1.4 Injection Molding

In today's plastics industry, injection molding is the most widely employed thermoplastic shaping process. The injection molding process involves injecting molten plastic into a mold cavity to shape three dimensional plastic parts. Due to its unique ability to produce detailed and complicated three-dimensional (3-D) products, injection molding has become the most successful and established manufacturing technology among all the thermoplastic processing technologies [75]. For the last few years, the injection molding manufacturing sector has been growing at a fast rate because of its applications in consumer products such as electronics and in automotive products. It has a total product value of almost \$200 billion dollars per year and currently is the fourth largest manufacturing industry in the United States [76].

An injection molding machine has three fundamental components: an injection

unit, a clamping unit, and a mold cavity [76]. The objectives of the injection unit are as follows:

- Melting of the polymer,
- Accumulating the molten polymer in a screw chamber or a separate shot pot,
- Injection of molten polymer through the nozzle into a cavity, and
- Maintaining the packing or holding pressure during the cooling phase.

The clamping unit is used to open and close the mold cavity, as well as to apply high pressure to prevent the flash during injection and cooling stages. The mold cavity is used to finalize the shape of the product and is usually custom designed because every product has its own unique design.

The injection molding process has a number of advantages over other thermoplastic processes. Firstly, it is capable of manufacturing complex 3-D design products, whereas the extrusion process can only produce 2-D shapes. Secondly, it is able to produce parts with a wide variety of materials, including non-traditional materials such as metals and ceramics [77-80]. Thirdly, injection molding is well suited for mass production because it is capable of providing a relatively short cycle time and is able to manufacture a number of products in one shot. Lastly, there are several special injection molding processes, including co-injection molding [81-83], fusible core injection molding, gas-assisted injection molding [84], injection-compression molding, in-mold decoration/lamination, low-pressure injection molding, micro-injection molding [85], and foam injection molding [86-88].

Unfortunately, injection molding has several negative traits, in terms of

dimensional characteristics such as shrinkage, warpage, and residual stress. Shrinkage usually affects 8 to 10 vol%, but it is unavoidable because the specific volume of polymer changes as it solidifies during the filling and cooling phases. As an effort to compensate for the shrinkage, a high packing pressure is usually applied during the cooling phase. The packing process forces more molten polymer to be further injected to compensate for the volume lost by shrinkage. However, it is impossible to prevent the shrinkage completely with the conventional injection molding process. Warpage is a distortion where the surfaces of the molded part do not follow the original design. It occurs because of molded-in residual stress, which is caused by non-uniform shrinkage within the cavity [89, 90]. This residual stress is a process-induced stress, frozen in a molded product. It can be either flow-induced or thermal-induced. The residual stresses are the main reasons for shrinkage and warpage. If the processing conditions and design elements can reduce the shear stress during the filling, then the flow-induced residual stress will be reduced. On the other hand, uniform cooling and efficient packing will provide the less amount of thermal-induced residual stress [90]. Furthermore, the residual stress variations can be also caused by polymer molecular orientations as well as the fiber orientations.

1.5 Foam Injection Molding

Foam injection molding (FIM) is an advanced manufacturing technology, which has been developed from conventional injection molding process. In foam injection molding, gas is added to the molten polymer by using either a physical blowing agent (PBA) or chemical blowing agent (CBA), depending on the gas producing method. Gas and molten polymer get mixed thoroughly for uniform distribution of a blowing agent. Then, a mixture of polymer and gas is injected into a cavity, and its shaping is finalized

after its cooling is completed. Foam injection molding technology can provide advantages such as weight reduction, material cost saving, faster cycle time, improved dimensional stabilities, absence of sink mark on surfaces, and so on [86-88]. In other words, FIM technology can overcome the aforementioned negative traits of the conventional injection molding process. However, the implementation of FIM technology deteriorates the mechanical properties of foam products when compared to their solid counterparts. Furthermore, FIM can leave flow swirl marks on the surface due to the fountain flow pattern resulting from premature cell nucleation and aggressive cell growth at the flow front.

There are various supplemental manufacturing technologies derived from FIM technology. This thesis study discusses the effects of gas counter pressure and breathing mold (or mold opening) technologies with FIM in later chapters. Furthermore, the fundamental foaming mechanisms and the effects of various processing parameters will be discussed in Chapter 2. In this thesis, lastly, the term of foam injection molding includes the microcellular injection molding technology as well.

1.6 Acoustic Thermoplastic Foams

Noise can be defined as the irregular and chaotic sound which people find disturbing and consider harmful to their health as well. In recent years, the public's exposure to noise has increased significantly because of mechanic and electronic devices that surround them in everyday life, from mobile phones to automotive vehicles. As the public's dependency on technological equipment increases, the noise from these equipment becomes unavoidable. Therefore, noise has been recognized as a form of

environmental pollution. A number of acoustic and material science researchers have developed new noise reduction materials, and these materials are actively utilized in different applications as mandatory features of different products.

Traditionally, thermosetting polymer foam structures, such as polyurethane (PU) foams, have been and still are actively employed for the noise reduction applications. However, these thermoset polymer materials are not recyclable, and their acoustic functionalities deteriorate significantly when they are exposed to a high moisture environment. In addition, a relatively large thickness for these structures is required to accomplish effective acoustic absorption [91]. It is also very difficult to manufacture these foams in complex shapes because of their foaming mechanism. Furthermore, due to their very high flexibilities, the number of possible applications is limited.

In order to overcome the aforementioned disadvantages, there have been some efforts made to develop new thermoplastic materials that have a similar level of acoustic properties as the traditional thermoset foams. Because of inherited material properties and the different foaming mechanisms of thermoplastic materials, however, this research has elucidated several challenges and various strategies to overcome them.

1.7 Research Motivation

The manufacturing of acoustically effective thermoplastic foam structure has been a challenging research topic in the last few years. Although researchers have developed various foam structures, these structures have had several disadvantages, such as the need for additional processing techniques, relatively large thickness, very long process time, and geometrical constraints. Consequently, this thesis proposes a new manufacturing

technology that can produce an innovative thermoplastic foam structure with adequate acoustic performance. The proposed technology is based on conventional foam injection molding and gas-assisted injection molding technologies, so it can enhance the manufacturability of acoustic thermoplastic foams significantly. Furthermore, by taking advantage of the unique foam structure produced by the proposed technology, the foam structure can be produced in complex designs with relatively thin sample thickness without a significant sacrifice in acoustic performance while maintaining the advantages of conventional FIM technology.

1.8 Thesis Objectives and Scope of Research

The main objective of this research was to develop an innovative manufacturing technology that can produce new type of thermoplastic foam injection molded structure with improved acoustic properties. This new technology is the synergistic marriage of two commercially available manufacturing technologies, which being gas-assisted injection molding (GAIM) and FIM processes.

In order to successfully accomplish the main objective of this thesis, a few short-term objectives have to be achieved in this thesis, and they are as follows:

- To optimize gas-assisted injection molding technology,
- To determine different foaming mechanisms of GAFIM technology, and
- To elucidate the relationships between morphology and the final acoustic properties.

This study was conducted in three main parts to achieve the objectives above. Firstly, extensive experimental and computer simulation studies were carried out to

maximize the impact of the GAIM technology. Secondly, research was focused on the development of innovative gas-assisted foam injection molding (GAFIM) technology to manufacture a new type of foam structure. In addition, its foaming mechanisms were investigated to provide a better understanding of the proposed technology. Lastly, different strategies were studied to improve the acoustic performances of various thermoplastic foam samples, and the acoustic characteristics of the newly developed foam structure by GAFIM were evaluated as well. Furthermore, the studies to describe the relationships between cellular morphologies and acoustic properties were carried out.

1.9 Organization of Thesis

This thesis is organized into six chapters. Chapter 1 contains an introduction that describes in brief the following topics relevant to the thesis topic: thermoplastic foams, their classifications, processing technologies, injection molding, foam injection molding, and acoustic thermoplastic foams.

Chapter 2 reviews various literature related to the research subjects, such as the fundamentals of foam processing, basic principles of foam injection molding technology, existing GAIM technology and its effect on polymer crystalline morphology, and fundamental mechanisms for acoustic absorption and insulation.

Chapter 3 explains the motivation behind the proposed gas-assisted foam injection molding (GAFIM) technology and the possible benefits that the successful development of GAFIM could provide. Furthermore, the foaming mechanisms of GAFIM are hypothesized and their fundamental reasons are explained. The actual implementation of GAFIM and its related strategies are then described in detail.

Chapter 4 illustrates the actual experimental and simulation studies that were conducted for this thesis study. Firstly, it describes the experimental material, equipment, and procedures of the experiments. Secondly, both experimental and simulation studies for the existing GAIM technology are discussed to compare their differences and to optimize the technology for the purpose of this thesis study. Thirdly, the actual foaming mechanisms of GAFIM are elucidated by extensive analysis of the morphological results of the comprehensive experimental studies and their cavity pressure profiles.

Chapter 5 focuses on the acoustic aspects of this thesis study. First, it lists the evaluation criteria and describes their testing methods. Second, it introduces effective strategies to enhance the acoustic functionalities and the supporting experimental results. Third, it examines the impacts of GAFIM on the acoustic properties of TPU foam structures. Finally, the interrelationships between cellular morphologies and acoustic performance are discussed.

Chapter 6 summarizes the significant findings and describes the impacts of this thesis study. Furthermore, it provides recommendations and possible guidelines for potential future research related to the newly developed GAFIM technology.


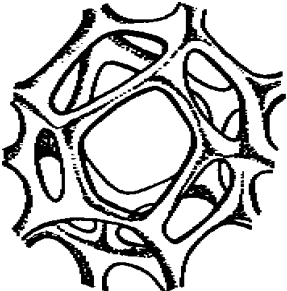
Category	Cell Structure
Closed-cell Foam	 A schematic diagram of a closed-cell foam structure. It shows a cluster of interconnected, roughly spherical cells. Each cell is completely enclosed by a thick, dark border representing the cell walls. The cells are packed together, with some overlapping, creating a dense, three-dimensional network of closed cells.
Open-cell Foam	 A schematic diagram of an open-cell foam structure. It shows a cluster of interconnected, roughly spherical cells. The cell walls are thin and form a continuous, porous network. The cells are not fully enclosed, and there are many openings between them, creating a highly porous, interconnected structure.

Figure 1.1 Schematics of closed-cell and open-cell foam structures

Chapter 2 Literature Review and Theoretical Background

2.1 Thermoplastic Foam Processing

2.1.1 Fundamentals of Blowing Agents

A plastic foam, in general, consists of a gaseous phase, generated from a blowing agent within a polymer matrix. A cellular structure can be initiated by dissolving a blowing agent into a polymer followed by nucleation and the growth of numerous bubbles. There are many varieties of blowing agents that can be selected depending on the desired foam structures, manufacturing processes, or applications of foam products. Blowing agents can be classified into chemical blowing agents (CBAs) and physical blowing agents (PBAs) by how gas is introduced into the polymer melt.

2.1.1.1 Chemical Blowing Agents

CBAs are individual compounds or mixtures of compounds that generate gases by thermal decomposition. There are two major types of CBAs, exothermic and endothermic, depending on the types of reactions that release gases [1, 92]. As the type of chemical reaction indicates, endothermic CBAs absorb energy, often in the form of heat from the neighboring environment, and then liberate gases back to the environment. In most cases, the primary gas released by endothermic CBAs is carbon dioxide (CO₂). On the other hand, exothermic CBAs, such as azodicarbonmide, generate energy to the neighboring

environment during its thermal decomposition in the form of heat, and liberate nitrogen (N₂) gas. In addition, there is another type of CBA that utilizes both types of reactions and releases different types of gases simultaneously.

The primary advantage of CBAs is that they do not require any major modification of the existing processing equipment; however, they are often more expensive than PBAs. In addition, the following requirements must be considered when selecting CBAs for their successful implementations [1]:

- The temperature of decomposition of CBA must be close to the melting point or lower than the processing temperature to ensure full decomposition of CBA.
- The decomposition of CBA should not generate an excessive amount of heat, which can cause the thermal degradation of the polymer.
- The rate of gas liberation of CBA must not decrease significantly during the thermal decomposition process due to the increase in system pressure.
- The CBA and the liberated gas must be readily dispersed or dissolved in the polymer matrix.

Although these requirements are satisfied, there is still no guarantee of how much gas is actually generated because it is almost impossible to measure the amount of generated gas *in situ* inside of barrel.

2.1.1.2 Physical Blowing Agents

In contrast to CBAs, PBAs are materials that generate gases as a result of physical transformations, and they are injected directly into the processing equipment in either the liquid or gas phase [1, 92]. The traditional PBAs are aliphatic and halogenated

hydrocarbons, such as chlorofluorocarbons (CFCs) and hydrochlorofluorocarbons (HCFCs). CFCs have been utilized with a variety of polymers, such as polyurethanes, polystyrenes, and polyethylene, to create foam structures because of their non-combustibility, low toxicity, low diffusion coefficient, and lower thermal conductivity [93]. The primary drawback of CFCs, however, is that they deplete the ozone layer and cause irreversible environmental damages. HCFCs are second generation PBAs that have been developed after CFCs by inheriting their advantages while reducing their environmental impact. These PBAs can result in high volume expansion at a low processing pressure due to low diffusivities associated with a larger molecular size [94]; thus, CFCs and HCFCs are very effective PBAs for creating low density foam products. Due to their ozone-depleting potentials, nevertheless, the Montreal Protocol [95] and the related regulations have banned these PBAs.

As alternatives to CFCs and HCFCs, volatile organic compounds (VOCs) can be used, but they are flammable, harmful to health, and still have negative impacts on the ozone layer [96]. Therefore, the foam industry shifted its interest to another potential replacement, hydrofluorocarbons (HFCs), and studies have been conducted to investigate their effectiveness as alternate PBAs [97, 98]. A number of studies have also investigated the plastic foaming behaviors using CO₂, as well as inert gases such as N₂, argon (Ar), and helium (He) [99-107]. Furthermore, HFCs, CO₂, N₂, Ar, and He have lower solubility and higher diffusivity in polymer melts than their less environmental-friendly counterparts [108-111]. These characteristics have added technological challenges for accomplishing desired foam morphologies. In addition, the implementation of PBAs requires a considerable amount of major modifications on the existing equipment, such as

the gas injection port, a new extrusion screw, and a new type of nozzle, as well as additional equipment that can pressurize the gas and inject it to the processing equipment with a set flow rate.

Despite the challenges mentioned above, however, the utilization of PBAs can provide active and very accurate control of the actual gas amount in a polymer melt, as well as material cost savings.

2.1.2 Formation of Polymer/Gas Solution

The formation of a uniform polymer/gas mixture is very critical for achieving a high quality plastic foam structure [75, 96]. This uniform formation requires adequate system pressure and temperature during the melt extrusion phase of both foam extrusion and foam injection molding technologies. A non-uniform polymer/gas matrix will lead to a non-uniform cell structure with low cell density in the produced foam products. The most critical requirement to ensure the uniform polymer/gas matrix is providing the suitable system pressure prior to foaming, which should be considerably higher than the solubility pressure of gas in a specific polymer melt at a certain processing temperature. The satisfaction of this requirement will ensure the complete mixing and dissolution of gas into a polymer matrix. Otherwise, un-dissolved gas will result in the formation of excessively large voids in the foam structures. Therefore, it is crucial to accurately measure the solubility of the blowing agent that can be dissolved into the polymer at different processing pressures and temperatures [110, 112].

Solubility is defined as the content of blowing agent that can be dissolved into the polymer matrix at a particular temperature and pressure with respect to the unit weight of

the polymer matrix. The researchers have employed various methods to measure the solubilities of different gases in polymers in the past. In particular, the pressure decay method, which measures pressure changes inside a chamber as gas sorption by a polymer occurs, was commonly utilized because of the simplicity of the system setup and low construction cost [113]. Despite these advantages, it was challenging to implement this method to molten polymers since it requires a high resolution pressure sensor that can tolerate a high temperature. Furthermore, a large polymer sample is required for this method, which leads to a very long measurement time. Another common method is using an electrobalance to measure the mass uptake during sorption processes [114, 115]. This method provides more accurate solubility measurements with a shorter measurement time. However, the shortcoming of this method is the low operating temperature due to the operation limits of electrobalance. Thus, the researchers have decoupled the system to independently control the temperature of the pressure chamber and the electrobalance [116, 117]. This measuring technique still had a drawback, which deteriorated the accuracy of the solubility measurement due to the effect of the convection-induced gas density variation. This issue was resolved by another gravimetric method that employs a magnetic suspension balance (MSB) [118]. In this method, the microbalance avoids the convection effect via measuring the sample weight in a compartment isolated from the chamber. Hence, the gas solubility and diffusivity in the polymer matrix at elevated temperatures and pressures were measured accurately. Although various researchers have utilized this method to measure the solubility of PBA in a polymer, the mass reading of the dissolved PBA is observed as apparent solubility, which is smaller than the actual solubility because of the buoyancy effect of polymer swelling upon gas dissolution. In

order to estimate the effect of polymer swelling and to compensate the buoyancy effect, different equations of state (EOS) were employed [109, 110, 112, 119-123]. Among those equations, the Sanchez-Lacombe EOS (SL EOS) and Simha-Somcynski EOS (SS EOS) are two common choices [124, 125]. Recently, a visualization system was developed to directly obtain the pressure-volume-temperature (PVT) characteristics of polymer/gas mixtures and this adaptation of direct PVT measurement led to more accurate solubility data [126].

As the solubility of PBA dictates the system pressure at a certain processing temperature, the diffusivity of PBA determines the processing time requirement in a continuous process. The diffusivity can be estimated as follows [55, 87]:

$$D = D_o \exp\left(-\frac{\Delta E_D}{R_g T_{sys}}\right) \quad \text{Equation 2.1}$$

where D_o is the diffusivity coefficient constant; ΔE_D is the activation energy for diffusion; R_g is the universal gas constant; and T_{sys} is the system temperature in absolute temperature. Although the rate of gas diffusion increases as the system temperature increases, based on the above equation, the typical gas diffusion process with polymer is still not fast enough for the general continuous thermoplastic manufacturing processes. Thus, it is required to provide additional means to accelerate the diffusion process [55]. The utilization of a screw with high mixing and energy transfer capability can be an effective strategy to overcome this challenge. Furthermore, a designated mixing equipment such as a static mixer can be attached to enhance the overall mixing quality between polymer and gas. In addition, a secondary cooling screw can be incorporated to provide a more uniform temperature field [87]. Consequently, these strategies improve

the gas dissolution behavior and help to form a more homogeneous polymer/gas mixture during the thermoplastic foaming processes.

2.1.3 Theoretical Principles of Cell Nucleation and Growth

Mechanisms

2.1.3.1 Cell Nucleation

Cell nucleation is the first stage of the thermoplastic foaming process. Cell nucleation can be defined as the transformation of small clusters of gas molecules to energetically stable pockets or groups [127]. A minimum amount of energy must be provided to the polymer/gas mixture in order to create cells, and the amount of energy has to be large enough to break the free energy barrier. The energy can be provided via thermodynamic changes, such as elevation of temperature or pressure drop, as aforementioned. In general, there are two types of nucleation, homogeneous and heterogeneous, depending upon the circumstances that nucleation occurs. Homogeneous nucleation is when cells are nucleated randomly throughout the molten polymer matrix. On the other hand, heterogeneous nucleation is what occurs at certain preferable sites, such as phase boundaries or additive particles.

The classical nucleation theory has been used to describe the nucleation behavior of homogeneous nucleation [128, 129]. According to this theory, the required amount of work to generate a cell, W , with a certain radius, r , in a liquid can be defined as follows:

$$W = \gamma_{pb}A_b - \Delta PV_b \quad \text{Equation 2.2}$$

where γ_{pb} is surface tension; A_b is the surface area of bubble; ΔP is the system pressure

change; and V_b is the volume of a bubble. Once the geometric variable of a bubble is substituted, the actual required work is defined as follows:

$$W = 4\pi r^2 \gamma_{pb} - \frac{4}{3} \pi r^3 \Delta P \quad \text{Equation 2.3}$$

The induced energy has to be larger than the maximum energy barrier to maintain the already nucleated cells. Otherwise, the radius of the nucleated bubble is smaller than the critical bubble radius and eventually collapses. The free energy barrier is defined by differentiating W in terms of r from the equation above.

$$\Delta G_{hom}^* = \frac{16\pi \gamma_{pb}^3}{3\Delta P^2} \quad \text{Equation 2.4}$$

The corresponding nucleation rate is defined as follows:

$$\dot{N} = C_o f_o \exp\left(-\frac{\Delta G^*}{kT}\right) \quad \text{Equation 2.5}$$

where C_o is the concentration of gas molecules; f_o is the frequency factor of gas molecules joining the nucleus; and k is the Boltzman constant. An increase of ΔP yields a reduction of ΔG_{hom}^* , and this leads to a higher cell nucleation rate at the saturation pressure. Furthermore, the nucleation rate increases as the amount of gas within the polymer matrix increases.

Although classical nucleation theory explains the effect of pressure drop on cell nucleation rate, it lacks the explanation for the effect of pressure drop rate on nucleation behavior. This theory assumes instantaneous pressure drop followed by instantaneous nucleation. In the actual circumstances, however, the pressure drop is not instantaneous and occurs over a certain period of time. Therefore, nucleation rate is also affected by the

pressure drop rate. Park et al. studied the effects of pressure drop rate on cell nucleation rate and the competition mechanism between nucleation and growth during the extrusion foaming process [130]. When thermodynamic instability is being introduced by pressure drop, some cells are nucleated. As gas diffuses to already nucleated cells, low gas concentration regions are produced around these cells. In the low gas concentration regions, additional cell nucleation cannot take place. The size and distribution of depleted gas regions around the already nucleated cells should be carefully investigated in order to check for the possibility of additional cell nucleation. In the case where the size of the depleted gas regions is smaller than the distance between the nucleated cells, the additional cells will be nucleated. As the pressure drop rate increases, cell density increases as well because a higher pressure drop rate requires a shorter period of time for the pressure drop to take place so the nucleated cells do not have enough time to grow excessively.

Heterogeneous nucleation occurs when cells are nucleated at some preferred sites. Because of its complexity and numerous possible scenarios, the mechanism of heterogeneous nucleation has not been thoroughly studied. In general, however, it is well known that higher cell density can be achieved when additives are utilized as nucleating agents within the polymer matrix [131-134]. Heterogeneous nucleation can occur at different types of surfaces of preferred sites, and the planar surface type of heterogeneous nucleation is shown in Figure 2.1 [135]. As the contact angle, θ_c , decreases, the surface area of liquid and gas boundary increases and this can eventually lead to become very close to homogeneous nucleation. Therefore, heterogeneous nucleation occurs by replacing high energy, solid-liquid interface to low energy, solid-gas interface, and by

reducing the surface area of the liquid-gas interface. Due to these characteristics, the required free energy barrier is significantly smaller than that for homogeneous nucleation. Thus, the energy barrier for heterogeneous nucleation and the shape factor, $F(\theta_c)$, are defined as follows [127, 135]:

$$\Delta G_{het}^* = \frac{16\pi\gamma pb^3}{3\Delta P^2} F(\theta_c) = \Delta G_{hom}^* F(\theta_c) \quad \text{Equation 2.6}$$

$$F(\theta_c) = \frac{2+3 \cos \theta_c - \cos^3 \theta_c}{4} \quad \text{Equation 2.7}$$

These equations show that the shape factor, $F(\theta_c)$, decreases as the contact angle, θ_c , increases, and this trend leads to the further reduction of the free energy barrier of heterogeneous nucleation. Although this planar surface is an appropriate estimation when nucleating agents have a plate-like shape, it would not be suitable for particle-like nucleating agents such as talc. If nano-clays are fully and individually dispersed in the polymer melt, they can be treated as plate-like nucleating agent. However, it can also be particle-like nucleating agent because it is very challenging to fully disperse them within the polymer matrix. Since these particle-like nucleating agents are more commonly employed in various foaming processes, a new model assuming the conical cavity as the preferred site, instead of the planar surface, has been developed. The conical cavity is displayed in Figure 2.2 and its shape factor is defined as follows [135]:

$$F(\theta_c, \beta) = \frac{1}{4} \left[2 - 2 \sin(\theta_c - \beta) + \frac{\cos \theta_c \cos^2(\theta_c - \beta)}{\sin \beta} \right] \quad \text{Equation 2.8}$$

Despite the aforementioned advantages of heterogeneous nucleation, it still presents a few critical challenges to achieving a fine cell structure. The first challenge is that the overall foam structure is highly dependent on the characteristics of the additives.

Secondly, since a higher content of additives generally leads to a higher cell density, an adequate amount of nucleating agents has to be used but they also have to be uniformly dispersed within the polymer matrix to yield a uniform foam structure.

2.2 Manufacturing of Open-Celled Foam Structures

2.2.1 Open-Celled Structures with Foam Extrusion Technology

Over the last few years, researchers have developed various extrusion processing technologies to manufacture open-cell foam structures [136-143]. These studies have indicated that the key to achieving a high open-cell content is the utilization of non-uniformity within the melt structure, which is accomplished by inducing hard and soft regions via partial cross-linking and by blending in a small amount of a second phase material [142]. Second, in order to obtain a high open-cell content over a wide range of processing temperatures, the mixture must be plasticized using an additional amount of blowing agent [137, 138]. Third, two semi-crystalline polymers with significantly different crystallization temperatures must be employed to create a melt structure with both hard and soft regions [141]. Finally, a significant temperature differential between the core and the surface of extruded foam must be induced in order to increase the chance of cell opening. The latter is achieved by softening the cell walls and increasing the gas pressure within the cell walls [143]. Although these strategies were proven to be effective to induce open-cell structures, their limitation is the necessity of a relatively high volume expansion ratio. In other words, these strategies are effective only for batch and extrusion foaming applications since regular FIM process cannot produce foam structures due to the confined volume of a mold cavity.

2.2.2 Porous Structures by using Sacrificial Fillers

Recently, researchers have made the effort to fabricate plastic porous structures using either a solid sacrificial domain, such as sodium chloride (NaCl), polymeric sacrificial domain, or a combination of both. These sacrificial domains should be leachable in water so that they leave voids after the completion of the leaching process. In general, NaCl particulates are utilized to create cube-shaped voids, and water-dissolving polymers are employed to create channel-like voids. The introduction of foaming increases void fraction and enhances the leaching efficiency as well. The schematic of these overall procedures to create porous structures with sacrificial fillers is exhibited in Figure 2.3, and the actual sample is shown in Figure 2.4. The final characteristics such as porosity and acoustic properties are then measured.

For the most of these studies, NaCl was selected as a solid sacrificial domain because it is inexpensive and environmentally friendly. Thermoplastic porous structures are relatively new research topics, and studies have been carried out for different applications. Kramschuster and Turng incorporated polyvinyl alcohol (PVOH) as a polymeric sacrificial domain, as well as NaCl, as parts of injection foam molded polylactide (PLA) [144]. They have developed a unique porous structure for tissue scaffold applications. They also utilized CO₂ as a plasticizer to improve the moldability of blends with a high NaCl content and to further reduce the processing temperature, which is especially desirable for biodegradable polymer such as PLA. As a result, the maximum 75 % of the porosity was accomplished once the NaCl particulates and the PVOH were leached out.

The other studies investigated the acoustic functionalities of thermoplastic porous

structures. Chu et al. employed NaCl as a solid sacrificial domain and used a rotation molding process to manufacture a porous foam structure. In order to induce foaming, CBA was utilized and the acoustic absorption coefficients were evaluated [36, 145]. The authors claimed that smaller voids created by leached NaCl particulates that led to higher acoustic absorption coefficients. As the overall sample thickness was increased, the acoustic absorption enhanced because of a dissipation mechanism. A similar study was conducted by Mosanenzadeh et al. that utilized NaCl as a solid sacrificial domain and polyethylene glycol (PEG) as a polymeric sacrificial domain in the PLA matrix [146]. The porous structures were obtained by leaching out both NaCl and water-soluble PEG from the PLA matrix. The acoustic absorption behaviors of these porous structures were then evaluated.

2.3 Foam Injection Molding Technologies

2.3.1 Conventional Foam Injection Molding and Microcellular

Injection Molding Technologies

Foam injection molding (FIM) technology is a variant of the conventional injection molding process. Similar to other thermoplastic foam manufacturing technologies, it melts the polymer first and mixes a blowing agent with the polymer melt. Then, the mixture of polymer and gas is injected into a cavity through a shut off nozzle. During this injection phase, the polymer/gas matrix goes through a large magnitude of pressure drop since the cavity is usually in the atmospheric pressure. Due to the pressure drop, foam is induced and the injected material volume with its volume expansion fills the cavity completely. The advantages of FIM are as follows [127];

- Absence of sink mark on the surface,
- Reduction of part weight,
- Savings in material cost,
- Faster cycle time,
- Lower residual stress,
- Improved dimensional stability,
- Lower clamp force required,
- Possible lower processing temperature due to lower viscosity,
- Minimum damages on fiber-type fillers, and
- High stiffness-to-weight ratio.

A microcellular plastic was developed by Dr. Suh and his students at the Massachusetts Institute of Technology in the early 1980s to achieve two goals: reduction of material and increase in material stiffness by very small bubbles that act as crack arrestors [86]. In order to successfully serve these purposes, cell diameters should typically be between 5 to 50 μm [147] and cell density should be higher than 10^6 [86]. In contrast, other researchers have claimed that the microcellular structure should have a cell density higher than 10^9 with a cell size smaller than 10 μm [127]. An additional requirement is that the majority of cells must be closed cells with less amount of weight reduction. At first, research focused on developing microcellular structures with batch foaming processes. Then, the research efforts shifted to the implementation of a microcellular structure to continuous polymer manufacturing processes such as extrusion and injection molding. Microcellular injection molding technology and the necessary processing equipment have been further developed by a number of researchers and

companies. Trexel Inc. was the pioneer company that cooperated with the research team at MIT to develop the MuCell[®] system that effectively injects PBAs such as N₂ and CO₂. Nowadays, the term “microcellular injection molding” is often used to broadly describe general FIM technologies.

The main difference between microcellular injection molding process and commercial FIM is that the mold filling is completed without foaming [86]. In other words, the microcellular injection molding injects a full shot of polymer material into a cavity because its main purpose is to compensate the volume shrinkage during the cooling process. On the other hand, the low pressure FIM often utilizes higher set void fraction. Although conventional FIM employs either PBA or CBA, the microcellular process only utilizes PBAs to manufacture the foam structure. Because of the reduced viscosity from the plasticization effect due to the presence of gas within the polymer matrix, this method can also be adopted to manufacture very thin-walled products. Similar to conventional FIM, the microcellular injection molding process still can provide excellent dimensional stability because the volume expansion compensates for shrinkage and warpage by eliminating residual stress. A faster cycle time is achieved since there is no need for the packing and holding phases. However, microcellular foam applications share the same disadvantages as conventional FIM, which are poor surface quality, limited applications to nontransparent products, requirement of a strictly balanced runner system, complicated processing technology, and considerable amount of capital investment for modifications of the existing equipment [86].

2.3.2 Low Pressure and High Pressure Foam Injection Molding Technologies

2.3.2.1 Low Pressure FIM

Low pressure FIM can be defined by its two characteristics such as relative cavity pressure, ranging from 0.5 to 10 MPa, and smaller injection shot size, which is usually from 65 to 80 vol% of the full shot volume. This smaller shot size also results in a lower injection pressure, which can lead to a lower tonnage in the injection molding machine. Furthermore, the adaptation of low pressure FIM might save a considerable amount of tooling cost. Since it allows a significant portion of cavity volume to be filled by expansion, it is often utilized for applications with large and thick-walled products. Other advantages include the reduction of residual stress, better dimension stability, and material cost saving. Consequently, the typical applications are products that serve simple functions, which are packaging materials, pallets, and so on.

The relatively large expansion within a cavity presents some technological challenges such as severe flow swirl marks on the product surface and non-uniform cellular morphology. The flow swirl marks are generated because the cells are nucleated at the flow front and smeared on the cavity surface. Since a relatively large amount of cavity volume needs to be filled by foaming, the nucleated cells have to travel a further distance for a longer time before they reach their final destinations. Thus, the cells are exposed to excessive cell growth, which leads to a severe degree of cell coalescence. Furthermore, the low injection pressure limits the part thickness of products because a greater portion of solid skin layer is formed when the overall part thickness is small, due to faster cooling from the cavity surface. In other words, the polymer flow has to overcome a greater amount of resistance to fill the cavity, which is very challenging at a low injection pressure. In this context, applications with a thickness less than 0.25" are

avoided in general.

2.3.2.2 High Pressure FIM

High pressure FIM is defined by the following characteristics: fast and complete filling of cavity; separation of core foaming and solid skin layer formation; and core foaming because of polymer shrinkage during the cooling phase. For high pressure FIM, the volume expansion is equal to the amount of shrinkage because the cavity is completely filled first with the full shot size injection, and a small degree of volume becomes available during the cooling phase due to polymer shrinkage. The main advantage of high pressure FIM is the uniformity of the foam structure. Since a complete filling is achieved before excessive foaming, the foaming is carried out without any significant cell migration. In addition, high pressure FIM can improve the surface quality by minimizing the effects of flow swirls. However, the degree of volume expansion is very small, which makes it difficult to save in the cost of materials.

2.3.3 Investigation of Foaming Behaviors in Foam Injection Molding Using Mold Pressure Profile

Various researchers attempted to investigate the foaming mechanisms of FIM technology with different strategies, but it was often challenging because there are different factors coupled together that determine final cellular morphology. As one of the strategies, Lee investigated the foaming behaviors in the FIM process using mold pressure profiles [127, 148]. A simple plaque-shaped mold with various fan gates was utilized and cavity pressures were measured at three different locations, which were named Location A, Location B, and Location C, as shown in Figure 2.5. The foaming of

FIM was compared with the foaming of foam extrusion, based on the pressure profile that each foaming process provides, under the assumption that cell nucleation occurs when the system pressure becomes considerably lower than the solubility pressure. In the case of foam extrusion, the polymer/gas matrix experiences a steady state as it comes out from the die to the atmosphere, and cell growth occurs in the steady state. In the case of FIM, on the other hand, the cavity environment changes as the degree of filling increases because the polymer/gas flow front experiences different cavity pressures. As the cavity pressure keeps changing, cell nucleation locations vary with respect to the degree of polymer/gas injection in the cavity. Furthermore, the magnitudes of pressure drop vary as the cavity gets filled with more material and the pressure of flow front increases. The pressure profiles of both foam extrusion and FIM are displayed in Figure 2.6.

In order to effectively compare the foaming behaviors from two different processing technologies, most of the processing parameters were kept identical except for the pressure drops and the pressure drop rates which were varied. In terms of polymer materials, polypropylene (PP), thermoplastic poly-olefin (TPO), and high density polyethylene (HDPE) were utilized in both foam extrusion and FIM processes. N₂ was utilized as the PBA for both independent experimental studies. First, the cell density values were measured from the foam extrusion process while varying the processing parameters in order to estimate the required pressure drops and pressure drop rates for the desired cell density values with respect to all three materials. The foam samples were manufactured using FIM, and the cell density values at the three aforementioned locations were measured. When the pressure drop values from extrusion foaming and FIM were compared, it was assumed that a larger pressure drop, whether it occurs at

nozzle or at gate, would determine the final cell density. The comparison results are exhibited in Figure 2.7, and the actual cell density values of FIM were very close to the estimated cell density values from the foam extrusion for all three materials. In most of the cases, the variation was less than one order of magnitude. Consequently, the cell density values of the foam structure by FIM could be estimated based on foam extrusion data and the cavity pressure profile. In other words, the processing parameters can be varied to obtain the desired pressure drop as an effort to accomplish the desired cell density values in the injection foam molded samples.

2.3.4 Effect of Gas Counter Pressure on Foam Injection Molding Behavior

Gas counter pressure (GCP) technology has been developed as a strategy to improve the surface quality of conventional FIM products because the surface quality often determines the cosmetic quality of products, and it also affects the mechanical properties of products [64-66, 88, 149, 150]. GCP is a supplemental process that pressurizes a cavity prior to the injection of the polymer/gas matrix. Since it suppresses aggressive cell growth at the leading edge of the flow front, the surface swirl by fountain flow is prevented [151].

In order to effectively implement GCP technology, a pressure-tight cavity design is required to minimize pressure loss during the GCP process and it usually employs N₂ gas to pressurize the cavity. Once the cavity is pressurized to a desired pressure, the predetermined volume (i.e., shot size) of compressed polymer/gas matrix is injected into the cavity. During this injection phase, controlled venting is required to maintain a

consistent counter pressure as the unfilled cavity volume is being reduced. When an appropriate thickness of solid, smooth skin layer is formed after the injection has completed, the counter pressure is fully released to induce foaming from the melt core [149]. Since GCP technology enables the polymer/gas matrix to experience a uniform pressure drop cycle throughout the cavity and prevents the inherited time dependence nature of the FIM foaming behavior, it significantly improves the uniformity of cellular morphology in the foam molded samples [127]. However, it is critically important to maintain GCP considerably higher than the solubility pressure of the polymer and gas that are utilized in the actual processing conditions. If GCP is lower than the solubility pressure, the effectiveness of the technology will be significantly deteriorated because it might not be able to provide uniform cell nucleation and aggressive cell growth will not be prevented. Furthermore, since the flow front is paused during the filling phase, a flow mark may form [149]. Releasing GCP prior to the completion of the filling phase can minimize the possibility of the formation of these flow marks. In summary, GCP and the timing of GCP release are the two most critical processing parameters in determining final morphology for GCP technology.

2.4 Gas-Assisted Injection Molding

2.4.1 Conventional Gas-Assisted Injection Molding Technology

Gas-assisted injection molding (GAIM) is a technology to pressurize an injection molded part during its cooling stage [84]. Pressurizing an injected polymer within a cavity is a very difficult task for the conventional injection molding process because pressure can only be applied to the polymer melt through different parts of cavity such as

the gate, runner, and/or sprue bushings. This pressurizing process is called the packing or holding stage, and it is usually utilized to compensate for shrinkage, which the molten polymer experiences during its cooling cycle. However, if the already injected polymer in any of the cavity features is solidified and becomes rigid enough, the melt pressure applied by the injection molding machine does not get transmitted to the already injected polymer in the cavity, regardless of the amount of pressure or duration of the packing cycle. In order to overcome the aforementioned limitations of conventional injection molding, GAIM technology employs an independent gas injection approach into the cavity to pressurize the injected polymer during the cooling phase. The conventional GAIM technology employs N₂ gas to apply pressure to the injected polymer to replace the traditional melt pressure method of the conventional injection molding process.

When GAIM is implemented, 80 to 100 vol% of the polymer is injected in general [84]. N₂ gas injection begins either towards the end of polymer injection or after the completion of polymer injection. Once the injected polymer is pressurized and maintained for a desirable amount of time during the cooling phase, N₂ gas is then vented out by either sprue-break or other vent feature in the cavity. Figure 2.8 shows the schematic of how this conventional GAIM takes places with respect to the regular injection molding process. GAIM can provide a number of advantages [84, 152]:

- Lower clamping force,
- Faster cycle time,
- Less material,
- Better dimensional stability, and
- Elimination of sink marks.

2.4.2 Effect of Gas Channel

For relatively thick applications, the implementation of GAIM is not difficult and does not involve a significant amount of modification. When GAIM is applied to thin-wall products, however, the adaptation of gas channel(s) is necessary [84]. The gas channel is a type of runner cut into a mold to direct the gas flow, so it forms a hollow core with the pressurized gas during the GAIM process [84, 153]. The fundamental principle of the gas channel is to create an intended path for gas flow because gas always tends to travel along the path that provides the least amount of flow resistance [84, 154, 155]. When GAIM is utilized without gas channels for relatively wide products, the injected gas can cause a ‘fingering’ phenomenon [84, 156]. It is a term to describe the uncontrolled spread of injected gas within the polymer matrix, which often takes the shape of spread fingers as shown in Figure 2.9. Consequently, the location, dimension, and shape of the gas channel should be carefully determined to yield an optimal result. Implementation of good gas channel designs can provide the following benefits [84]:

- Increase in resin flow length,
- Lower polymer injection pressure,
- Lower clamping force, and
- Uniformly distributed packing by gas.

In addition, it would be very difficult to correct the gas channels once they are machined into a cavity. Therefore, it is very critical to design the gas channels properly prior to the actual cavity modification. Inappropriate gas channel design can provide negative traits in the final product properties. Oversized gas channels often results in

insufficient gas penetration, which can lead to incomplete filling, and undesired race-track effect on the polymer melt. Meanwhile, undersized gas channels cause the gas to spread out laterally rather than penetrate further in the flow direction.

A number of studies have been carried out to investigate the effects of various shapes and design parameters of gas channels [153, 154, 156, 157]. Geng et al. studied six different shapes of gas channels using Moldflow[®], and a rib design with inner chamfers provided an approximately 15% increase in terms of flow length when compared to a simple semicircular channel [153]. Chien et al. conducted a comparison study between semicircular and rectangular-shaped gas channels with various part thicknesses [154]. When the cross-sectional areas of different gas channel designs were equal, the semicircular gas channel was able to outperform the rectangular channels for all the evaluated part thicknesses. In addition, the authors recommended designing the equivalent radius (R_{eq} , shown in Figure 2.10) of gas channels to be greater than 2 in order to provide an adequate molding window. As an effective strategy to prevent gas fingering, Lu et al. recommended that the overall height of gas channel to nominal part thickness ratio should be from 2.5 to 3.0 for acrylonitrile butadiene styrene (ABS) and high impact polystyrene (HIPS) materials; whereas the ratio should be between 3.5 and 4.0 for polycarbonate (PC) [156]. Furthermore, semicircular and rectangular shapes of gas channels were preferred over trapezoidal shape because the chances of gas fingering for those two shapes were significantly lower.

2.4.3 Computer Simulation Analysis

Computer simulation analysis is especially critical for GAIM technology because it is very difficult and costly to repair a cavity back to its original state once the necessary

modifications are completed. Effective utilization of computer simulation can save a significant amount of time, effort, and cost during the design stage. In addition, it can help to optimize the processing conditions by reducing the necessary trial and error type experimental studies. Therefore, a number of research studies have been conducted using either modified computer-aided engineering (CAE) software, or a commercial software, Moldflow[®] from Autodesk Inc. For the studies that implemented different CAE software, their research primary focuses were on developing new or modified analytical program logics for the GAIM process [158-161]. Gao developed a three-dimensional finite element model combined with a volume tracking technique to simulate the mold filling phase during the GAIM process [161]. This volume-tracking method was utilized to track two different flow interfaces, the polymer melt flow front, and the polymer-gas interface. However, this study did not provide any experimental data to support the reported simulation logics and their results. Zhou et al. utilized the matching asymptotic expansion method and compared the analytical results with Moldflow[®] and actual experimental results [158]. Chen et al. adopted M-Flow, which was a modified CAE based software, to investigate the effects of processing parameters of both conventional injection molding and GAIM technologies [159]. Based on experimental results, higher melt temperature, higher gas pressure, longer gas packing time, and slower injection speed were the preferred conditions for yielding a lesser degree of warpage. In addition, the study conducted by Li et al. compared the difference between their newly developed surface model and the mid-plane model of Moldflow[®] [160]. The authors showed that their surface model was able to reduce the required software runtime and also provided more accurate gas penetration results than the results from Moldflow[®].

The commercial software, Moldflow[®], has been commonly utilized as a tool to simulate numerous GAIM applications. The principal advantages of Moldflow are its availability and easy-to-use user interface. Therefore, one can easily start to utilize the software without expertise on related topics such as viscous fluid dynamics, multiphase flow dynamics, and so on. These research efforts were focused on the verification of Moldflow[®] simulation results by comparing them to the actual experimental findings [162, 163]. Parvez et al. utilized Moldflow for their GAIM study and they found that Moldflow provided over-predicted results in gas penetration length in most of the cases [163]. In addition, the authors claimed that the shot size of polymer and the delay time of gas injection were the two most dominant parameters of gas penetration length.

2.4.4 Effect of GAIM on Polymer Crystalline Morphology

GAIM technology provides several advantages over the conventional injection molding process as previously described. However, it is also capable of changing the crystalline morphology of the injected polymer and little research has been conducted to understand this change [164-166]. Zheng et al. studied the effect of GAIM on the crystalline morphology of polypropylene (PP) at the surface layer and inner core layer, and they observed two different crystalline structures, microfibrillar and spherulite, respectively, at each location [164]. At the skin layer, the polymer molecular chains were highly oriented along the flow direction and formed microfibrillar bundles due to the large amount of shear energy provided by GAIM. GAIM can provide significantly larger shear energy than conventional injection molding because N₂ gas transmits pressure very effectively directly inside the polymer melt. The polymer at the skin layer experienced direct contact with the cold mold surface, which increased the shear energy furthermore.

On the other hand, spherulite crystalline structures were obtained in the inner core layer because the shear energy was considerably smaller than that of the skin layer due to a higher melt temperature and slower cooling rate. Figure 2.11 shows these two crystalline structures from two different locations within the GAIM PP sample. The different crystalline structures yielded approximately a 10 °C difference in terms of melting peaks based on differential scanning calorimetry (DSC) results. When higher gas injection pressure was implemented, the microfibrillar crystallites became more oriented with the flow direction.

In the case of PP/glass fiber (GF) composite with the GAIM process, the aforementioned trend was witnessed as well. A significantly larger amount of crystallites was formed within the GAIM PP/GF sample than the conventional injection molding PP/GF sample because of a higher shear energy from GAIM [165]. However, an unexpected and uncontrolled cellular structure near the inner core layer was also obtained as a result of GAIM on the PP/GF composite.

Wang et al. conducted a similar research study with high density polyethylene (HDPE), and the effect of GAIM on the crystalline structure of HDPE was investigated [166]. In order to evaluate the crystalline structures of the samples, melting peaks and degrees of crystallinity were measured at three different regions of GAIM HDPE samples, skin zone, sub-skin zone, and gas channel zone, using DSC. Based on the experimental results shown in Table 2.1, the melting peaks and the crystallinity values were increased as the measurement locations moved from the skin layer to the gas channel core. Furthermore, the melting peaks and the degree of crystallinity increased when the gas injection pressure increased from 6.7 to 11.6 MPa. In this study, the effect of these

different crystalline structures on the mechanical properties, specifically tensile modulus, storage modulus, and loss modulus, was also investigated. The results suggested that with a higher gas injection pressure, the more uniform the orientation of HDPE samples and the more enhanced the mechanical properties become.

According to the above research studies and their findings, GAIM provided significant amounts of additional extensional and shear energies to the polymer melt, which affected the orientations of polymer molecular chains and promoted a higher amount of polymer crystallization. This higher degree of crystallization and formation of crystallites in various shapes are expected to influence foaming behaviors immensely.

2.5 Acoustic Absorption and Insulation

2.5.1 Principles of Acoustic Absorption

The acoustic absorption mechanism by a porous structure is displayed in Figure 2.12 [167]. When the incident acoustic wave hits the structure, some portion of the wave gets reflected, whereas the rest is transmitted into the structure. Acoustic absorption is a representation of how effectively the transmitted wave is dissipated or lost within the structure. Common acoustic porous materials are curtains, carpets, fibrous materials, mineral wool, cotton, and open-celled thermoset foam structures.

There are three types of losses occurring when acoustic waves travel through the porous structure, and the acoustic absorption coefficients become higher as the amount of losses increases [168]. The first type of loss is viscous loss that occurs due to the relative motion of air in the structure. The second is thermal loss, which results from heat conduction between regions of wave compression and regions of wave refraction. The

third type of loss is from the conversion of compression energy into internal energy of molecular vibration.

There are various models that explain and estimate the acoustic absorption behaviors of foam products. However, these models are based on several assumptions of the material properties of foam products – that the foams are very highly porous, have open-celled cellular morphology, and are very flexible (i.e., low elastic modulus). Recently, the Johnson-Allard model has been developed to fundamentally explain the acoustic absorption mechanism of conventional flexible and porous PU foam structure [169]. The model estimates the acoustic absorption coefficients of porous structure based on five characteristics: porosity, airflow resistivity, tortuosity, viscous characteristic length, and thermal characteristic length. The model has been implemented on PP porous structures in other studies, and these studies have shown fairly good agreements between the estimated value and the actual measurements [31, 167]. However, since this model is only applicable to open-celled and highly porous structures, it was not employed in this thesis study.

It is a well-known fact that the acoustic absorption of higher frequency acoustic waves is relatively easier than that of lower frequency acoustic waves. Traditionally, the absorption of lower frequency waves can be achieved by either increasing the overall thickness or leaving an air-gap behind the structure [170]. The recent study using the aforementioned Johnson-Allard model confirmed the positive impact of an air-gap within the multilayer acoustic structure on acoustic absorption at lower frequencies [169].

2.5.2 Principles of Acoustic Insulation

Acoustic insulation is commonly understood as another form of acoustic absorption although they are two very different strategies to reduce noise. In general, acoustic insulation can be achieved with the utilization of an acoustic barrier, which serves the main purposes of maximum reflection and minimum transmittance. Unlike effective acoustic absorption structures, therefore, the acoustic insulation structures can be rigid, heavy, and solid parts. 30 dB of transmission loss can make the difference between being exposed to an automotive vehicle passing by and being in a quiet room [171]. Therefore, achieving a 20 to 30 dB of transmission loss can be recognized as a considerable amount of noise reduction.

According to the study by Kang et al., the air-gap was utilized as a middle layer of a sandwich panel structure in order to improve acoustic insulation [172]. Lee et al. investigated the acoustic insulation behaviors of ABS/carbon black composites, and the most predominant factor for their transmission loss values was the carbon-black content [173]. The increase of carbon-black content within the ABS matrix improved the transmission loss by higher elastic modulus, which provided a higher degree of acoustic wave reflection. When the carbon-black content was increased from 0 to 5 wt%, the average transmission loss increased from 7 to 10 dB over the entire range of measured frequency as exhibited in Figure 2.13. Ni et al. investigated the effects of filler sizes on the acoustic insulation performance of insulation sheet materials, which consisted of a fiber sheet core and PU outer layers [174]. When the nano-silica particle size was increased from 73 to 254 μm , there was a slight improvement in transmission loss values because larger particles were able to reflect more acoustic waves. This was due to the acoustic waves propagating over the small particles in the polymer matrix although the

overall impact of filler size change was not significant. In addition, the increase of filler content provided a considerable enhancement of transmission loss values because a decrease in the viscoelasticity of material increased the reflection coefficient. This trend agreed with the aforementioned research as well.

The effective acoustic insulation materials developed in the research above were mostly very rigid materials with a high elastic modulus because their reflection coefficients had to be maximized. In the process of maximizing the reflection coefficients by increasing the modulus, however, a significant sacrifice of acoustic absorption performance was inevitable.

2.5.3 Thermoplastic Foams for Acoustic Applications

Various researchers have studied the acoustic properties of different thermoplastic foam structures [31, 91, 175, 176]. These thermoplastic foams were prepared using various manufacturing technologies from the conventional extrusion foaming to simple compression molding. As a result, they had a wide range of morphologies and the corresponding acoustic behaviors.

Soto et al. investigated the acoustic absorption behaviors of various commercial thermoplastic foam products and polyurethane (PU) foam products [175]. In the case of closed cell PE foams, the foam structures with larger cells (i.e., approximately 0.75 mm of average cell diameter) were able to achieve higher acoustic absorption coefficients. As the base polymer matrix was changed from PE to a PP/PE blend, the maximum absorption coefficient decreased by about 50%. When the cells were highly interconnected, the maximum absorption coefficient was only about 0.2 for PP foam

samples. Therefore, the material flexibility was the more critical property than the cellular morphology when determining acoustic absorption functionality. Furthermore, this result indicated that the majority of absorption was due to viscous loss.

Suh et al. manufactured PE-based foam extrusion products, and these were closed-cell structures unlike the traditional acoustic foams [177]. As an effort to improve the acoustic absorption functionalities of closed-cell structures, the perforation technique was utilized. Based on the study, acoustic absorption was enhanced as cell size increased, and the authors claimed that the cells should be larger than 5 mm in order to accomplish effective acoustic absorption. The foam structure also needs to have very thin cell walls and large cells because the outer cells need to transmit the acoustic wave into the inner cells. This transmittance allows the acoustic wave to propagate in the foam structure thoroughly until the wave gets dissipated through vibration damping.

Subramonian et al. conducted an extensive study on the acoustic absorption behaviors of PE and PP/PE blend foam samples [91]. The samples were manufactured with conventional extrusion foaming technology, and hydrocarbon was utilized as a blowing agent. As foam thickness was increased from 10 to 25 mm, the efficiency for absorbing low frequency improved significantly according to Figure 2.14. When the foam thickness was increased further to 50 mm, the maximum absorption peak shifted towards a lower frequency. With respect to perforation, the acoustic absorption coefficients were increased approximately by 20% once the surface was perforated. As perforation density increased from 1 hole/cm² to 4 holes/cm² (Figure 2.15), the absorption coefficients improved by about 5% because increasing the number of surface pores provided more friction loss of air flow, which led to more acoustic wave dissipation

within the foam structure. The effect of base polymer material property on the acoustic absorption behavior was investigated as well. In order to increase the flexibility of the PP/PE blend foam, the amount of PE was increased since PE has a lower modulus than PP. As a result, the maximum acoustic absorption coefficient increased from 0.4 to 0.8 when the PE content increased from 0 (i.e., neat PP) to 40 wt%. This study also confirmed that the foam structure, which consists of closed cells smaller than 2 mm, was not acoustically active. The aforementioned strategies were proven to be effective for improving the acoustic absorption behavior of PE or PP/PE blend extruded foams, but with the following drawback: the overall foam thickness was relatively thick (i.e., 50 mm), which can limit its applications.

Chen et al. investigated the changes in acoustic absorption properties of ramie reinforced poly(L-lactic acid) (PLLA) composites [176]. The acoustic absorption coefficients of various combinations of PLLA composites were measured in this study, and the most effective additive was flame retardant, although the maximum coefficient was still less than 0.4. The authors claimed that poor compatibility between the polymer matrix and the fire retardant created micro pores, which improved acoustic absorption. In addition, the authors claimed that the randomly oriented ramie fibers in the PLLA matrix also helped to enhance the acoustic absorption property. However, this needs to be studied further because even the increased acoustic absorption coefficient was still around 0.1.

McRae et al. studied the acoustic absorption behaviors of porous PP structures [31]. In order to manufacture porous PP samples, powder-type PP was blended with salt particles and compression molded at an elevated temperature. The samples were then

cooled and put into water for a very long time to leach out the salt particles from the PP samples. After the leaching process, the samples were dried and tested for their acoustic absorption coefficients. When the sample thickness was 6.5 mm, a small void size (106~250 μm) sample outperformed the samples with the other two void sizes (250~500 μm and 500~850 μm) as shown in Figure 2.17. In the case of 13-mm thick samples, the medium void size sample achieved the highest absorption coefficient although the small void size sample still performed better at a lower frequency range, which was less than 2700 Hz. Both large and medium void size samples achieved similar results at a lower frequency range, around 1700 Hz. The effects of sample density were also varied depending upon the sample thickness. For the 6.5-mm sample, the sample with the highest density, 0.24 g/cm^3 , dominated the rest of samples. In the case of 13-mm thick samples, on the other hand, all the samples achieved quite similar maximum coefficients over frequencies ranging from 2800 to 5500 Hz. When the sample thickness was 26 mm, the acoustic behavior was improved and the maximum coefficients were achieved at lower frequencies as the sample density was decreased.

The aforementioned research studies investigated the acoustic absorption behaviors of various types of thermoplastic foams, which were produced via different manufacturing technologies. In general, relatively thin samples were not able to achieve very effective acoustic absorption performances because the acoustic waves were not dissipated within the sample structures. Large cells were preferred for achieving high absorption coefficients at a lower frequency range in very thick thermoplastic open-celled foam samples. The perforation technique was able to improve the acoustic absorption behaviors by certain degrees. The elastic modulus or flexibility of foam structures was

also a very critical characteristic in determining acoustic absorption coefficients.

Table 2.1 DSC parameters of different zones of G6.7 and G11.6 samples [166]

Sample	Position	T_{peak} [°C]	ΔH_f [J/g]	X_c [%]
G6.7	Skin zone	129.5	145.3	49.6
	Sub-skin zone	130.9	160.1	54.6
	Gas channel zone	131.0	161.2	55.0
G11.6	Skin zone	129.7	154.7	52.8
	Sub-skin zone	131.5	161.5	55.1
	Gas channel zone	131.9	167.1	57.0

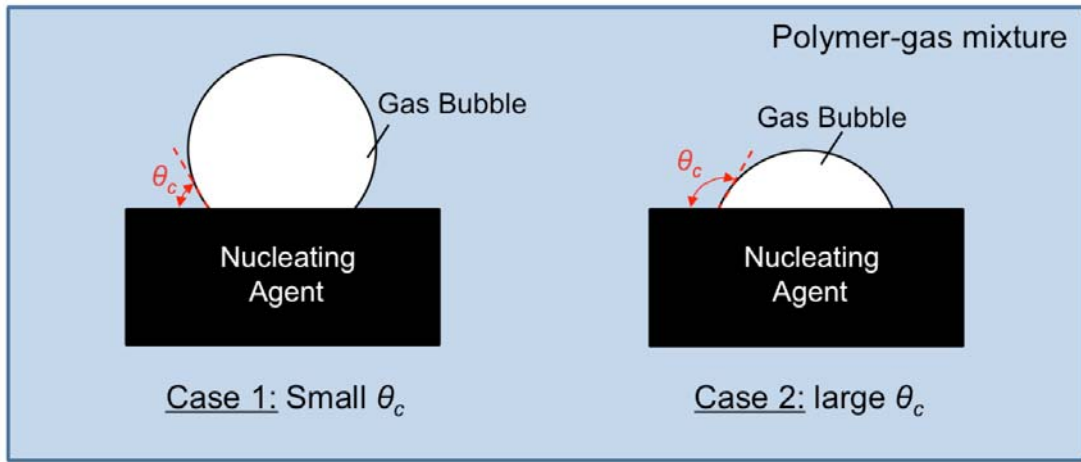


Figure 2.1 Gas bubble shape changes with different contact angles on a planar surface

[135]

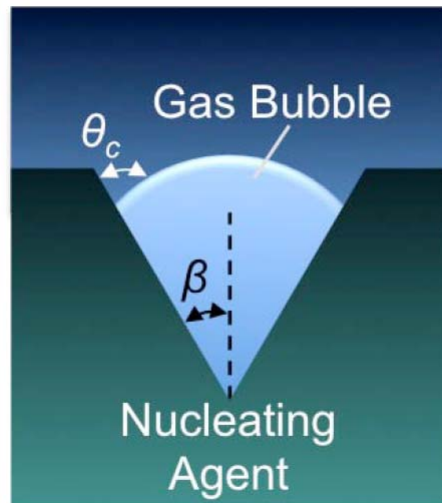


Figure 2.2 Conical cavity for bubble nucleation [135]

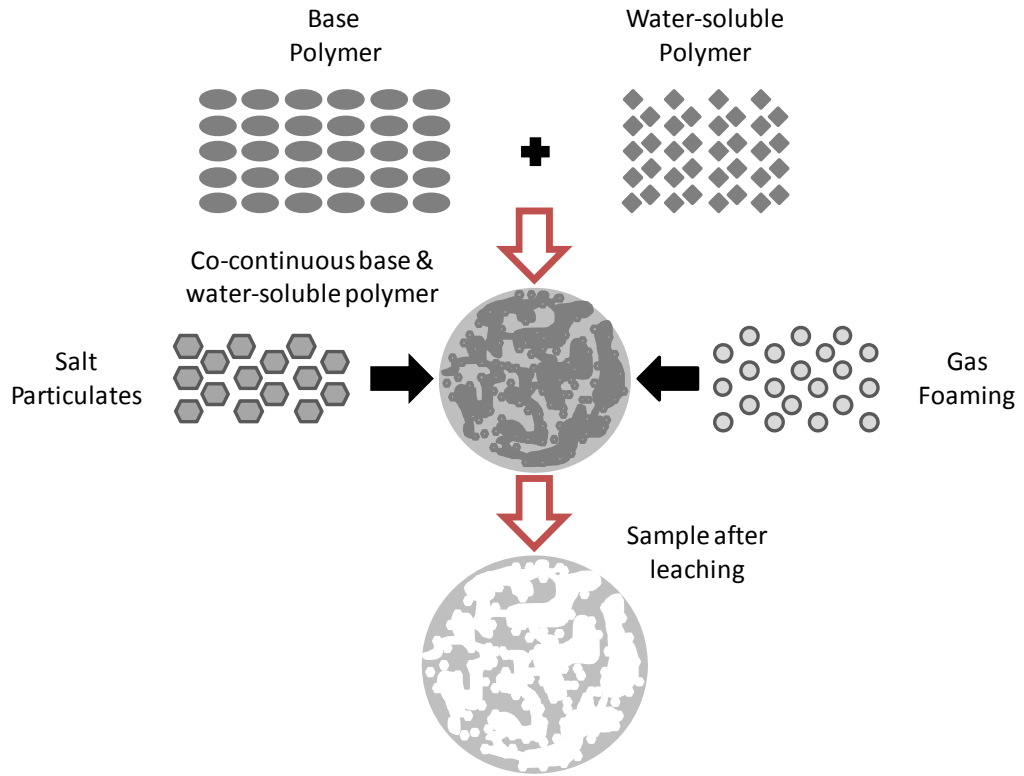


Figure 2.3 Schematic for creating porous structure with using sacrificial fillers

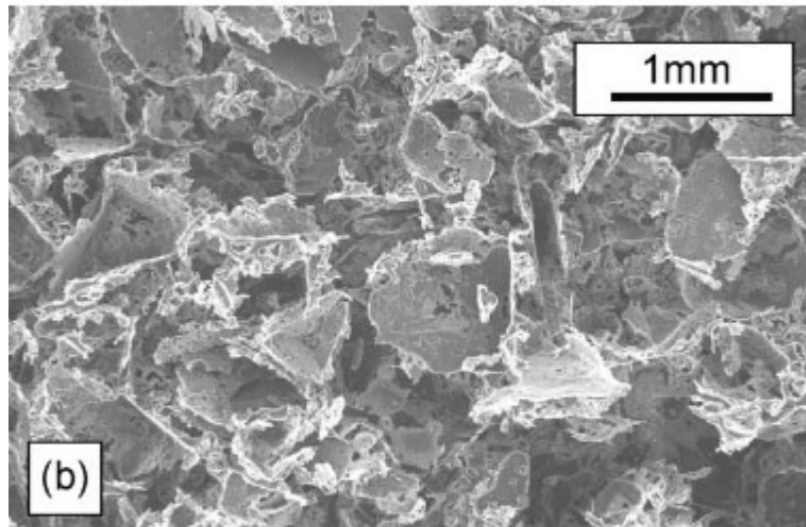


Figure 2.4 SEM picture of foamed porous structure by leaching of NaCl particulates [36]

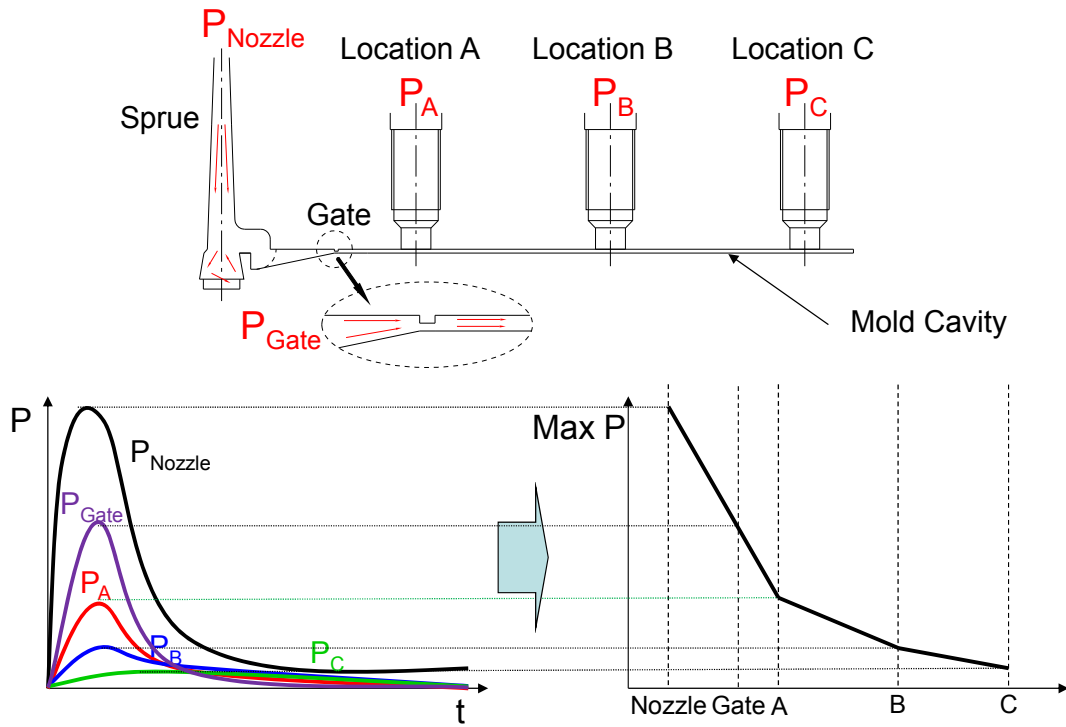
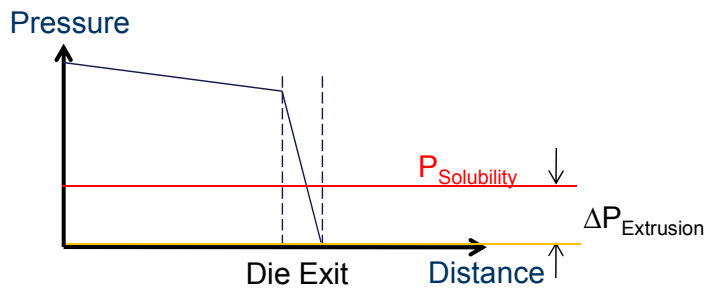


Figure 2.5 Measurement of cavity pressure profile [127]

Foam Extrusion (at steady state)



Foam Injection Molding

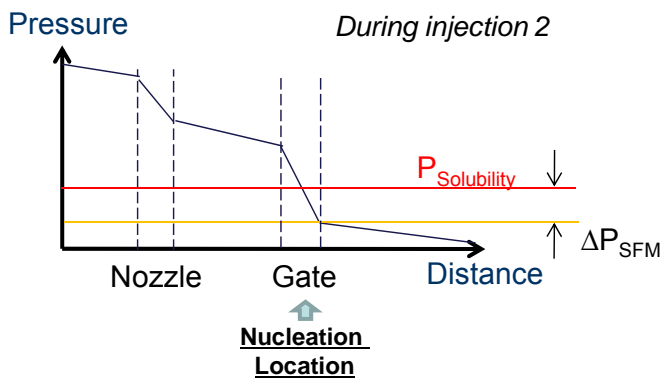
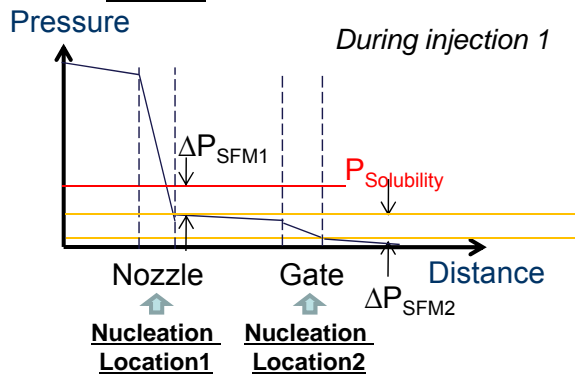
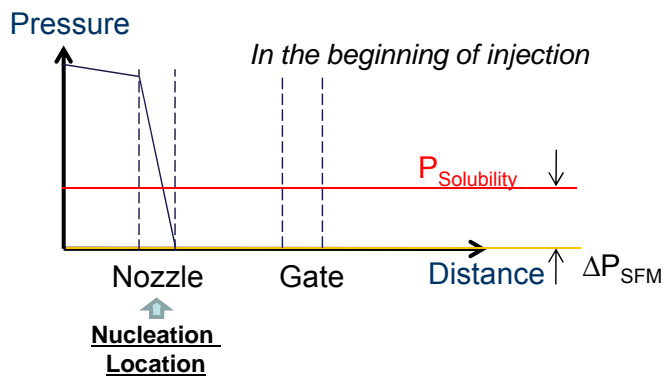


Figure 2.6 Pressure profiles in foam extrusion and FIM [127]

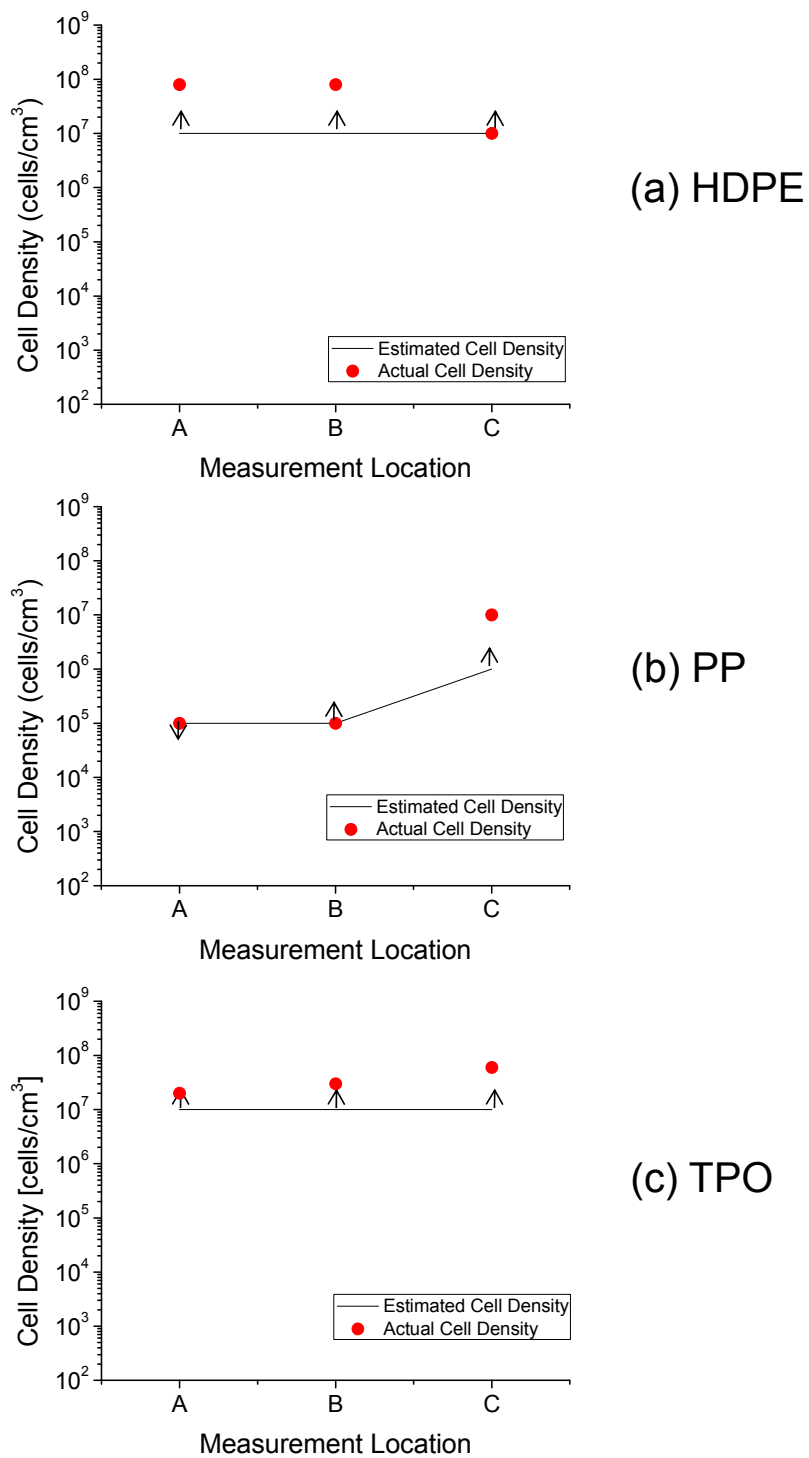


Figure 2.7 Comparison of estimated cell density from foam extrusion and actual cell density from FIM of (a) HDPE, (b) PP, and (c) TPO [127]

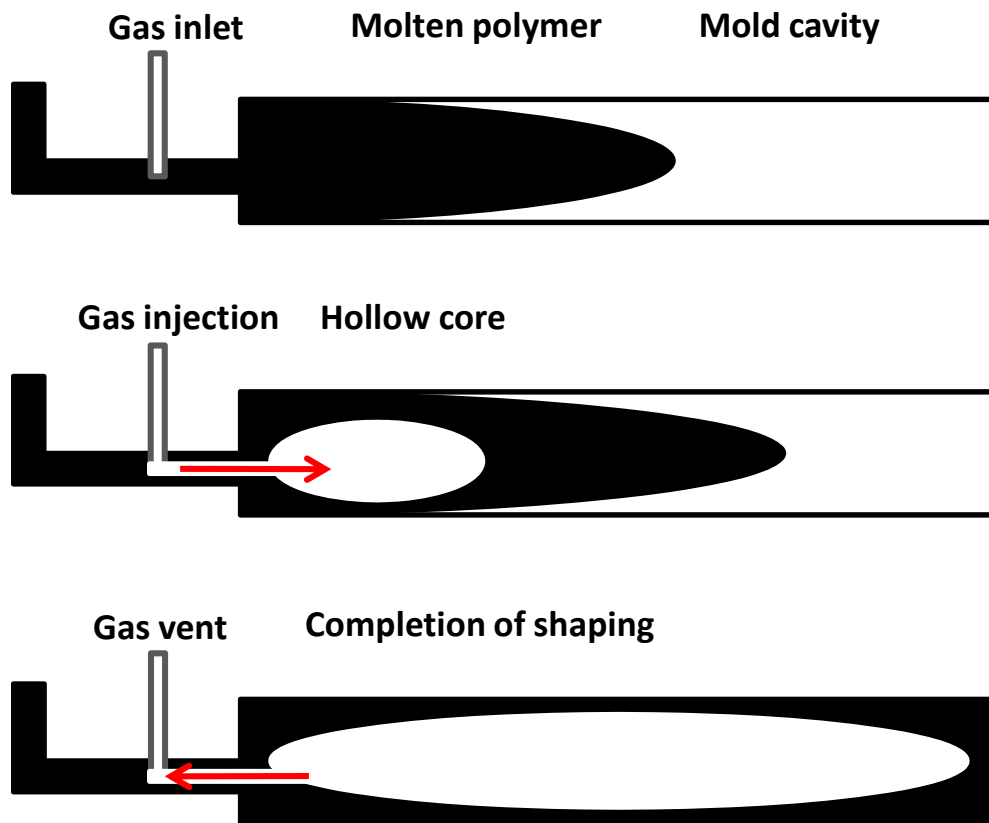


Figure 2.8 Schematic of conventional gas-assisted injection molding technology

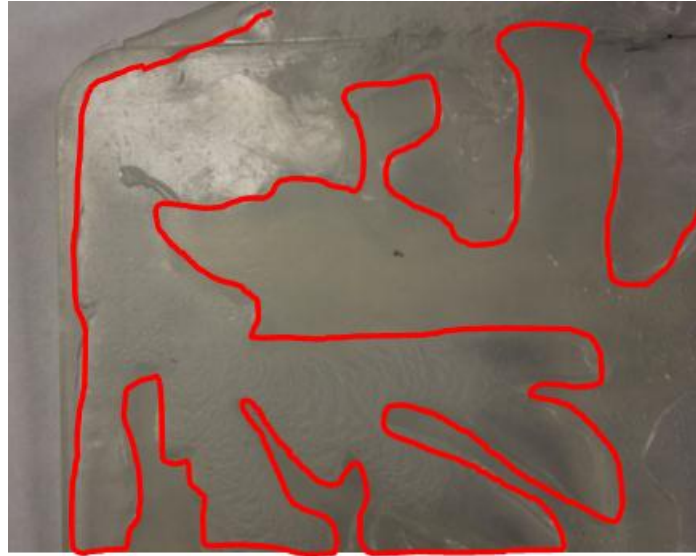
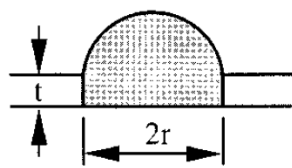
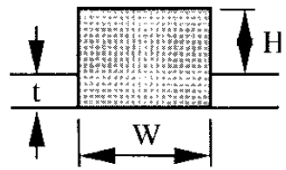


Figure 2.9 Fingering effect of GAIM TPU



$$R_{eq} = \sqrt{\frac{\frac{1}{2}\pi r^2 + 2rt}{\pi}}$$



$$R_{eq} = \sqrt{\frac{W(H+t)}{\pi}}$$

Figure 2.10 R_{eq} values of semi-circular and rectangular gas channels on thin plates [154]

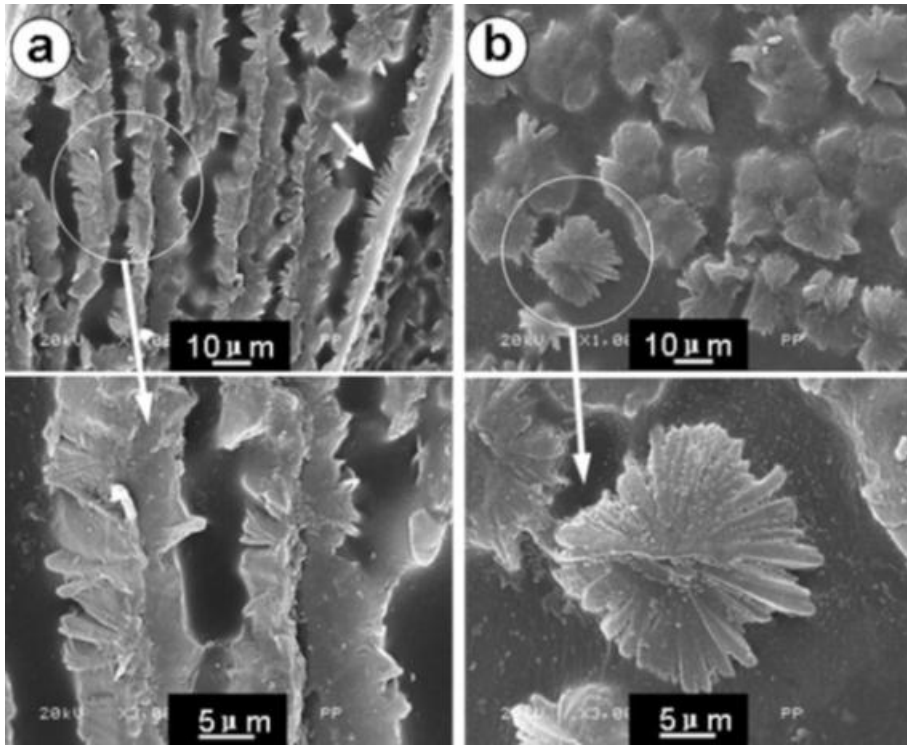


Figure 2.11 SEM pictures of etched GAIM PP at (a) skin layer and (b) near inner core

[164]

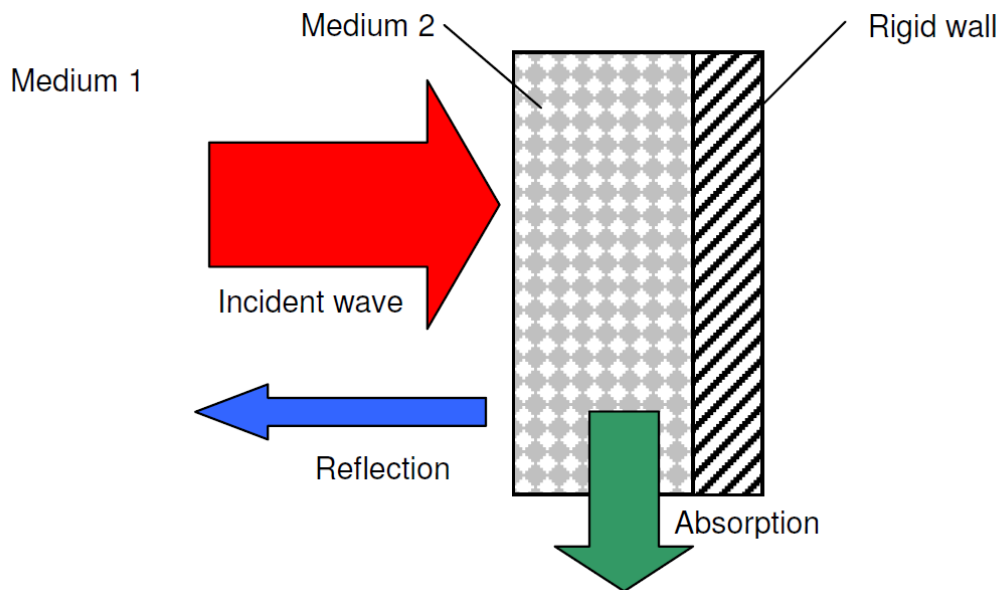


Figure 2.12 Acoustic functional mechanisms of a porous medium [167]

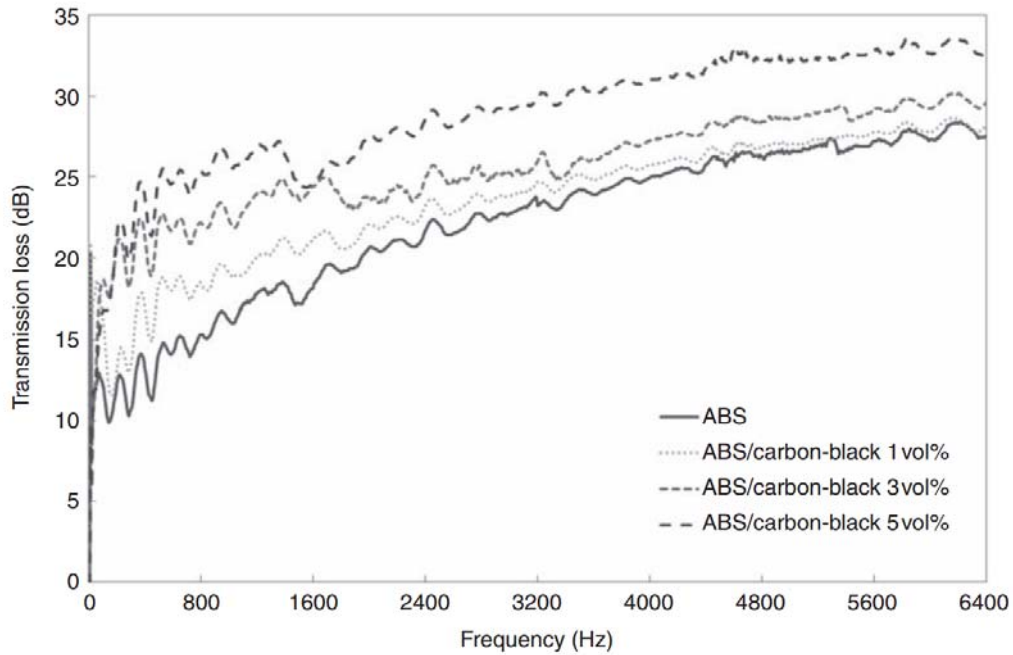


Figure 2.13 Transmission loss values of ABS and ABS/carbon-black composites with various carbon-black contents [173]

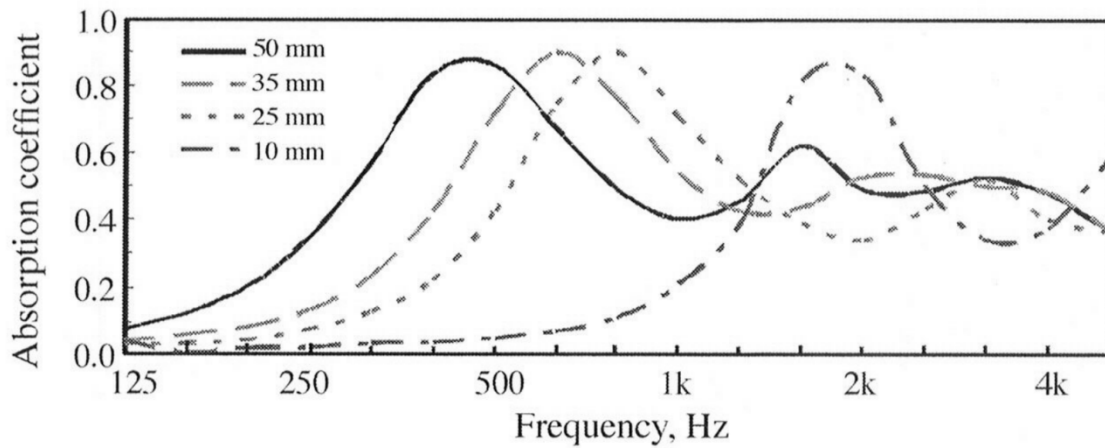


Figure 2.14 Acoustic absorption behavior of PP/PE blend foams with various thicknesses

[91]

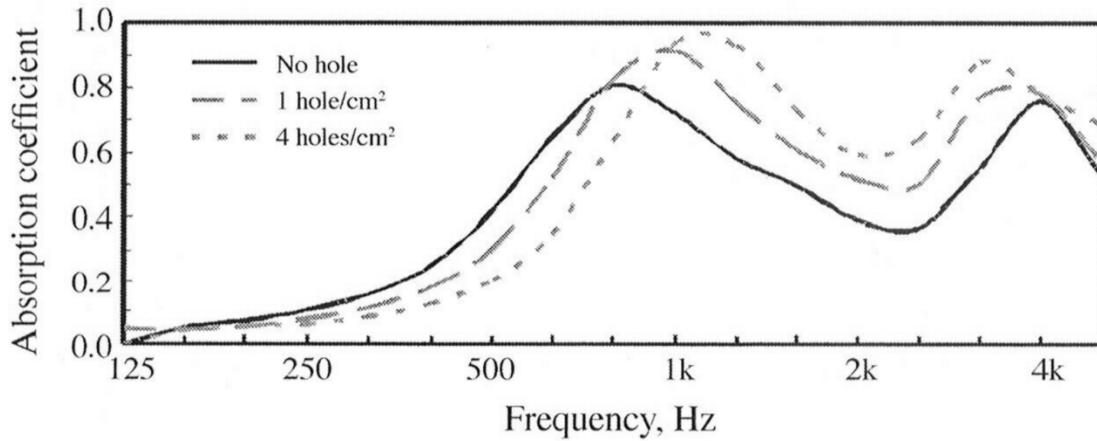


Figure 2.15 Acoustic absorption coefficients of PP/PE blend foams with different perforation density [91]

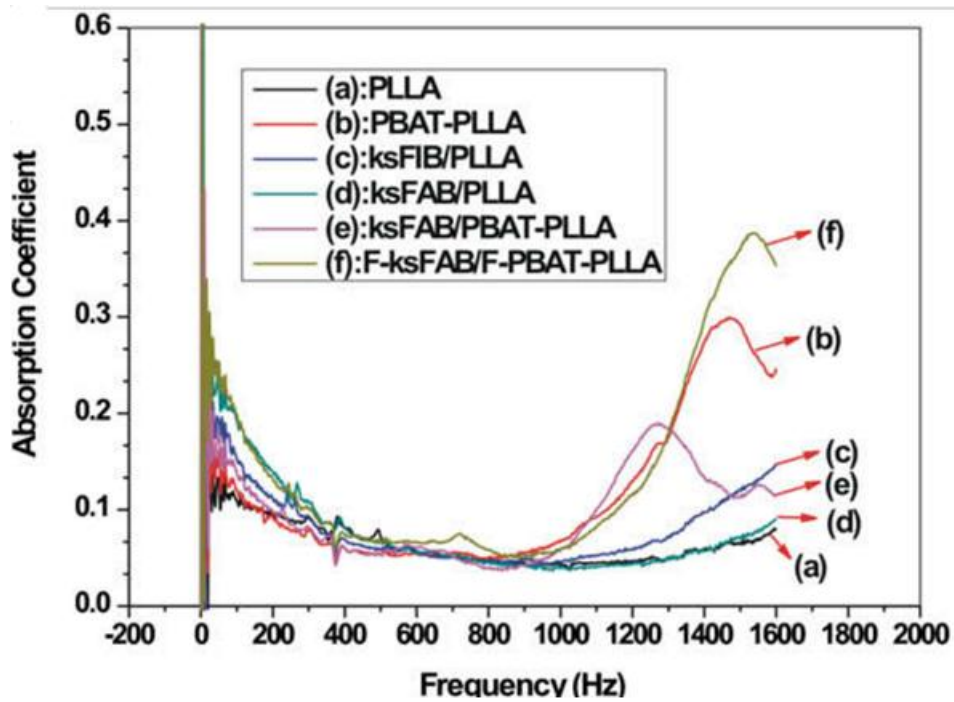


Figure 2.16 Acoustic absorption behaviors of various types of 3 mm-thick PLLA composites [176]

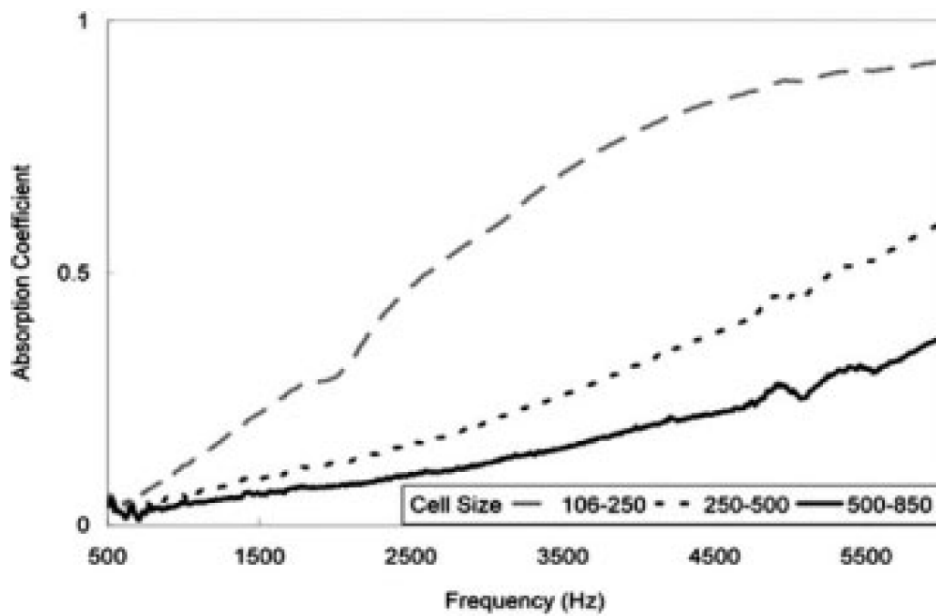


Figure 2.17 Acoustic absorption of 6.5-mm PP samples with different sizes of voids [31]

Chapter 3 Proposed Design of Gas-Assisted Foam Injection Molding Technology

3.1 Motivation

The proposed gas-assisted foam injection molding (GAFIM) was developed to strategically combine two already commercially available polymer processing technologies, GAIM and FIM, to manufacture a new foam structure that is able to outperform the conventional FIM parts for their acoustic properties. Furthermore, it is critical to overcome the existing limitation of FIM technology while maintaining the advantages from these two technologies when they are merged together.

3.1.1 Advantages of Gas-Assisted Injection Molding

The conventional GAIM technology can make several positive contributions, such as a larger void fraction, enhanced dimensional stabilities, lower clamping force, faster cycle time, and prevention of sink marks on the surface. A larger void fraction is possible because highly pressurized N_2 gas is able to penetrate into the injected polymer to create voids. Therefore, a cavity can be filled completely with the injection of a smaller amount of polymer material. Due to this void fraction, the material cost can be reduced as well. Since the polymer melt is highly pressurized within a cavity at the beginning of its cooling time, its dimensional characteristics (i.e., shrinkage and warpage) are enhanced

significantly with GAIM. Filling the cavity with gas equals to the injection of a smaller volume of material, which leads to a lower clamping force and faster cycle time by reducing the packing cycle dramatically. The sink marks can be removed by pressurizing the polymer melt in the cavity because the pressurized melt yields consistent contacts between the melt and the cavity wall during the cooling cycle.

3.1.2 Advantages of Foam injection molding

The foam injection molding technology has a number of advantages over the regular injection molding process as discussed in the previous chapter. The first main advantage is the reduction of material weight and material cost saving. Since 65 to 80 vol% of a full shot size is usually injected, in the case of low pressure FIM, this translates to a 35% to 20% of material cost savings. Secondly, the dimensional characteristics, such as shrinkage and warpage, of FIM products can be dramatically improved due to the elimination of residual stress by volume expansion. Thirdly, the reduction of cycle time can be achieved since the holding and packing phases become unnecessary and eliminated. Fourthly, the plasticization effect of the blowing agent decreases the melt viscosity of polymer, which can lead to other positive aspects: reduction in processing temperature, lower injection pressure, smaller tonnage for clamp force, better dispersion of filler, and minimum damages on fiber type fillers.

3.1.3 Synergistic Effects of the Proposed Gas-Assisted Foam

Injection Molding Technology

According to the previously mentioned literature, the existence of a hollow core or air gap in the plastic structure can improve acoustic performances [172]. As the

thickness of the hollow core increased, the overall acoustic absorption behavior improved. On the other hand, having foam layers also increased the acoustic absorption coefficients. Since these two different structures in plastic products can make positive contributions on their acoustic behaviors, the objective of the proposed gas-assisted foam injection molding is to create a polymer foam structure with a hollow core, which is a combined result of two manufacturing technologies, GAIM and the conventional FIM process.

The polymer structure that consists of the foamed layer and hollow core together can be obtained using the existing mold-opening technology. However, if conventional mold-opening is utilized with existing FIM technology to create such a structure, this will be classified as a 'passive' manufacturing strategy because the existence of a hollow core will be heavily depend on material properties such as melt strength and other processing parameters such as processing temperature and mold temperature. Furthermore, for each polymer and gas combination, it will require considerable amounts of trial-and-error type of experimental studies because there is no commercial computer software package that accommodates the foaming done by mold opening technology. In addition, a relatively large degree of mold opening is required to yield a hollow core in the structure. If the degree of mold opening is not large enough, then the structure would only consist of a solid skin layer and a foam layer. Consequently, one can only have indirect and 'passive' control over the resultant plastic structure when mold opening technology is employed to manufacture the proposed foam structure. In order to achieve a polymer structure with both the foamed layer and hollow core, the proposed GAFIM technology can be implemented. Unlike mold opening technology, GAFIM will be categorized as a 'pro-active' manufacturing strategy because it can guarantee the production of a hollow core

within the structure by the penetration of highly pressurized gas, and the degree of foaming can easily be controlled by adjusting the processing parameters of GAIM.

When the GAIM and FIM technologies are merged together strategically, several synergistic characteristics can be achieved. When the proposed GAFIM technology is employed, a number of advantages can be provided over the conventional GAIM and FIM processing technologies. First and foremost, the injection and the foaming stages of regular FIM process will be completely decoupled since the injection will be completed with the gas penetration of GAIM. During the gas injection period, the polymer/gas matrix within the cavity will be remained as highly pressurized. Then, rapid depressurization will be followed, which will also initiate the primary foaming. Second, higher cell nucleation and uniform foam structure can be obtained because of the decoupling mechanism and other characteristics that are provided by GAFIM technology. Those characteristics are additional shear and extensional energies, higher number of crystallites, etc. The roles of these characteristics and the details of foaming mechanisms will be discussed later in this thesis.

Third, the filling and cooling time can be further reduced when compared to the conventional FIM process because the filling phase is completed by additional high pressure gas injection. When the high pressure gas penetrates into the polymer/gas matrix, it travels significantly faster speed than the molten polymer matrix flow. Therefore, the overall filling time can be reduced. Since the relatively heavier foamed section that normally would take a long time to cool becomes a gas cavity, the cooling time can be noticeably reduced. Since the cooling time takes the majority of cycle time in general, the cycle time can be reduced significantly as a result.

Forth, it is possible to improve the surface quality of foamed samples. In the case of regular FIM, the surface quality is deteriorated by leaving flow swirl marks on the surface. Since the cell nucleation and growth continue to occur as the polymer/gas matrix travels within the cavity, the flow swirl marks are generated on the surface and the surface swirl marks become more severe as the flow length increases. In the case of GAFIM, however, the nucleated cells do not have to travel because the foaming takes place after the filling is completed. Therefore, the surface quality can be enhanced by minimizing flow swirl marks.

Fifth, the GAFIM technology can strategically place high void fraction sections without using the existing mold opening technique. The main drawback of existing mold opening technique is that the overall thickness of foam structure has to be increased considerably. In addition, the part design is limited with the mold opening because the mold can be opened in only one direction. Since a hollow core and foamed layers will be formed where the gas penetrates in the case of GAFIM, however, very high void fraction regions can be obtained in those gas penetration regions. The rest of foamed sample will have relatively lower void fraction. Depending on where the gas channels are located, high void fraction regions can be strategically located. Therefore, this can be utilized to achieve overall high void fraction without increasing the part thickness.

Sixth, the residual stress of polymer matrix can be significantly reduced. The FIM and GAIM technologies are known to decrease the residual stress and provide good dimensional stabilities. The proposed GAFIM technology will further reduce the residual stress, and thus it will enhance the dimensional stability of product more than when the existing FIM and GAIM technologies are utilized separately.

Last, the GAFIM technology can provide an acoustical advantage by producing the structure that consists of both foamed layers and a hollow core. In addition, the proposed GAFIM technology is able to provide a number of technological advancements over the existing GAIM and FIM technologies. The aforementioned overall research motivation and the advantages are summarized in Figure 3.1.

3.2 Fundamental Foaming Principles of the Proposed Technology

3.2.1 Coupled Nature of Conventional Foam Injection Molding Technology

In the conventional injection molding process, there are four major stages for one complete cycle, such as filling, holding (or packing), cooling, and ejection. In the case of the conventional FIM process, the foaming stage is added to replace the holding stage in general. Since the conventional FIM usually injects a short shot volume of the polymer/gas matrix into the atmospheric pressure cavity, foaming begins as soon as the polymer/gas matrix escapes from the main nozzle. Thus, the filling and foaming take place simultaneously [127]. As exhibited in Figure 3.2, bubbles are nucleated immediately after the polymer/gas matrix travels from the nozzle to the cavity by a large amount of pressure drop with fast pressure drop rate. As the foamed polymer/gas matrix travels through the cavity, the initially nucleated bubbles grow as well. At the end of filling, some bubbles are excessively overgrown and cause severe cell coalescences, especially at the end of cavity. Therefore, a non-uniform cellular morphology is obtained.

According to Lee's study, this foaming behavior primarily depends on two characteristics of the polymer/gas matrix, the time and the void fraction setting [127]. The time represents how long it takes for the polymer/gas matrix to completely fill the cavity. In most cases, therefore, the time is generally dictated by the injection flow rate. When the injection flow rate is slow, there is more time for the already nucleated cells to grow in the cavity as it is well described in Figure 3.3. Cell growth becomes the predominant foaming mechanism in determining the final foam structure. This cell growth dominant foaming then increases the degree of cell coalescence. In contrast, excessive cell growth can be minimized if the injection flow rate is fast. This process setting provides less amount of time for cell growth, which leads to cell nucleation becoming the dominant foaming mechanism. Therefore, the fast injection flow rate is preferred for uniform foam structure in general.

The void fraction setting is a term that represents the amount of volume the expanded volume of polymer/gas matrix is supposed to compensate so as to completely fill the cavity. If 70% of the shot size is injected, for example, 30% is its void fraction setting. If the void fraction setting is small, there is not enough volume for the nucleated cells to expand. This increases the cavity pressure dramatically, which might also increase the critical radius of nucleated cells and thus, promote cell collapse. Hence, low cell density can be obtained as shown in Figure 3.4. If the void fraction setting is excessively high, on the other hand, foaming behavior becomes the cell growth dominant mechanism because the initially nucleated cells have to travel a further distance before they reach the end of cavity, which means the cells have a longer time to grow. As cell size increases, the chance of cell coalescence also increases, which deteriorates the

quality of the overall foam structure.

Although Lee has developed several strategies to achieve a more uniform foam structure based on the analyses of cavity pressure profiles, these manufacturing strategies are focused on achieving a uniform cellular morphology throughout the structure rather than overcoming the inherited coupled mechanism of the filling and foaming phases.

3.2.2 Decoupling of the Filling and Foaming Mechanism

As aforementioned in the previous section, the motivation for the proposed GAFIM technology was to overcome the inherited coupled nature of the filling and foaming phases. The proposed technology decouples the filling and foaming stages by employing separate processing techniques to complete each phase independently. The filling of the cavity is completed by the implementation of GAIM as described in Figure 3.5 prior to the foaming stage. Once filling is completed, foaming takes place due to the depressurization of the polymer/gas matrix within the cavity.

Since the filling and foaming phases are completely decoupled and independent from each other, the foaming behaviors will be dramatically varied from those of conventional FIM technology. However, the final foam structures of proposed GAFIM technology are expected to be affected by the void fraction setting and the degree of gas penetration, because it determines whether the cavity is highly pressurized to decouple the filling and the foaming phases or not. Therefore, two different foaming behaviors are anticipated depending upon the void fraction setting – a high void fraction setting resulting a low cavity pressure and an appropriate void fraction setting to highly pressurized cavity with GAIM.

3.2.2.1 Low Cavity Pressure Case

If the void fraction setting is excessively large, the injected polymer/gas matrix is not able to fully fill the cavity by GAIM. The cavity cannot then be pressurized by N₂ gas from GAIM. Nonetheless, GAIM can still provide additional extensional strains and shear stresses to the polymer/gas matrix. It is expected that the addition of extension and shear energies will yield more oriented, polymer molecular chains and lead to form the higher number of crystallites and a higher cell density structure, as exhibited in the previously discussed literature [164-166].

3.2.2.2 Highly Pressurized Case

When the void fraction setting is appropriately set, the injected polymer/gas matrix should be able to completely fill the cavity by GAIM. The matrix within the cavity is then highly pressurized, and this pressurization will collapse the initially nucleated cells. This collapsing of initially nucleated bubbles is the critical step to decouple the filling and the foaming phases. Foaming will occur when the polymer/gas matrix is depressurized by the sprue-break or other pressure release mechanism. This depressurization is uniform within the cavity, which will lead to a uniform and consistent final foam structure throughout the cavity. Because of the additional extensional and shear energies, the foam structure of highly pressurized case also expects to obtain higher cell density and highly uniform morphology as aforementioned for the low cavity pressure case.

3.2.2.3 Foaming Mechanisms

The decoupling of GAFIM technology is expected to provide several advantages in the aspect of foaming. First, the additional shear and extensional energies applied by

GAIM can promote more cell nucleation in homogeneous nucleation mechanism according to the results of foaming studies in the past. Wong et al. investigated the effect of shear and extensional energies on the foaming behaviors of polystyrene in the visualization batch foaming set-up [178, 179]. When additional shear was introduced to the samples, the cell density values increased by about one order of magnitude according to Figure 3.6, and earlier cell nucleation was also observed [178]. In addition, providing extensional strain on the samples resulted in a cell density several orders of magnitudes higher than the static samples as shown in Figure 3.7 [179]. Applying additional extensional strain and extensional strain rate increased the local tensile stress of polymer/gas matrix as:

$$\sigma(t) = E\varepsilon(t) + \eta \frac{d\varepsilon(t)}{dt} \quad \text{Equation 3.1}$$

This increase in local tensile stress increased the negative difference of local pressure, $-\Delta P_{local}$, and it reduced the critical radius based on the critical radius equation:

$$R_{cr} = \frac{2\gamma_{lg}}{P_{bub,cr} - (P_{sys} + \Delta P_{local})} \quad \text{Equation 3.2}$$

Furthermore, a higher degree of super-saturation was achieved as the homogeneous nucleation rate (J_{hom}) increased in the equation below, exhibited as:

$$J_{hom} = N \sqrt{\frac{2\gamma_{lg}}{\pi m}} \exp\left(-\frac{16\pi\gamma_{lg}^3}{3k_b T_{sys} (P_{bub,cr} - (P_{sys} + \Delta P_{local}))^2}\right) \quad \text{Equation 3.3}$$

Therefore, the introduction of GAIM to the polymer/gas matrix during the foaming process is expected to still increase the cell density.

Second, the micron-sized crystallites formed by GAIM are expected to be utilized

as preferred heterogeneous nucleation sites. According to the previous studies, various types of semi-crystalline polymers formed micron-sized crystallites when GAIM technology was implemented [164-166]. Higher degree of crystallinity was obtained at the region near the hollow core (i.e., gas path) than the near skin region. It means that the gas penetration was able to provide enough shear and extensional energies to orient the polymer molecules and to form micron-sized crystallites during the gas penetration phase. Based on the past study, the degree of crystallinity was dominantly influenced by the gas injection pressure [166]. Therefore, the implementation of GAFIM is expected to promote higher degrees of both homogeneous nucleation and heterogeneous nucleation.

Third, the nucleation timing of the primary foaming will be very consistent throughout the part because the entire part will experience the identical rapid depressurization stage, which triggers the primary bubble nucleation. In other words, the on-set cell nucleation timings at different cavity locations will be nearly identical, unlike the various timings and locations of conventional FIM technology.

Fourth, higher degree of crystallinity provided by GAIM can increase the melt strength of the polymer matrix during the foaming phase. The increased melt strength of the polymer matrix will prevent the excessive cell growth and make the cell nucleation to become predominant foaming behavior.

Fifth, the cell coalescence can be minimized because the cell growth will be minimized by the increased melt strength and the cells will not have to travel due to the decoupling mechanism. If the cells do not have to travel with the polymer flow, their shapes will not be affected by the polymer flow field and the chance of cell coalescence

will be minimized.

Therefore, the implementation of GAFIM can utilize these advantages on the foaming mechanism by completely decoupling the filling and foaming phases. Due to the advantages, uniform cellular structure with high cell density and small cell size is expected to be manufactured.

3.3 System Implementation of the Proposed Technology

3.3.1 Schematic of the Proposed Technology

The most significant difference of the proposed technology from the conventional FIM process is the decoupling of the filling and foaming phases as described previously. Figure 3.5 shows how the proposed technology takes place step by step. First, a short shot volume of molten polymer/gas matrix is injected into a cavity. Then, high pressure N₂ gas is injected into the cavity and completes the filling phase by pushing the polymer/gas flow fronts. After the filling phase is completed, a high pressure of injected N₂ gas is maintained for a certain period of time. Due to this pressurization, the polymer/gas matrix is exposed to the high pressure as well. Once this high pressure is released suddenly by either sprue-break or other means of ventilation, a rapid pressure drop of the polymer/gas matrix provides the required thermodynamic instability for foaming. During this foaming stage, cell nucleation and growth occur towards the inner hollow core as arrows point in the figure; whereas these foaming mechanisms follow the polymer/gas flow direction in the case of conventional FIM technology. Not only the gas penetration or gas injection region experiences this foaming mechanism but also the non-gas injection, which represents the majority of parts, experiences the identical foaming mechanism because

the entire polymer/gas matrix within the cavity is exposed to the equal pressure profile during the decoupled filling and foaming stages.

3.3.2 Required Equipment for the Proposed Technology

3.3.2.1 Gas-Assisted Injection Molding System

In order to successfully implement the proposed technology, it is absolutely necessary to have a very precise control over the critical processing parameters of GAIM, such as the gas injection delay time, the gas injection pressure, and the gas injection duration. In general, the filling phase of the polymer or polymer/gas matrix takes less than a few seconds. Therefore, an adequate GAIM control system for this technology should be integrated to the existing FIM system to exchange the necessary electrical signals, so the gas injection delay time can be accurately controlled with respect to the start of the polymer or polymer/gas injection cycle. In addition, it should be able to execute various pre-programmed gas injection profiles in order to investigate the effect of the gas injection pressure, because this was a predominant factor that changed gas penetration behavior as well as polymer crystalline morphology based on the aforementioned literature [164-166].

3.3.2.2 Implementation of Gas Channels in a Cavity

As discussed in the previous chapter, the utilization of gas channels in GAIM can provide a number of advantages, such as increase in gas penetration length, lower polymer injection pressure, lower clamping force, and uniformly distributive packing. Since the nominal part thickness is only 3.2 mm, the implementation of gas channels is highly necessary for this relatively thin part application. In order to increase the

efficiency of GAIM and ensure the formation of a hollow core, the implementation of gas channels in the cavity is necessary for this research study. A semicircular shape is preferred because it can minimize the possibility of fingering during the GAIM process according to the literature [154]. Since the existing cavity has a wide and thin plaque, multiple gas channels will be implemented as well. The dimension of gas channels is determined later based on the following proposed design guidelines by Dier and Goralski [84]:

- Gas channels that run parallel to each other require careful consideration because gas can migrate from one to another;
- Gas channels should have an appropriate size with respect to the nominal wall thickness; and
- Gas channels must avoid sharp corners and right-angle changes.

The design and dimensions of the actual gas channel will be further explained in the next chapter.

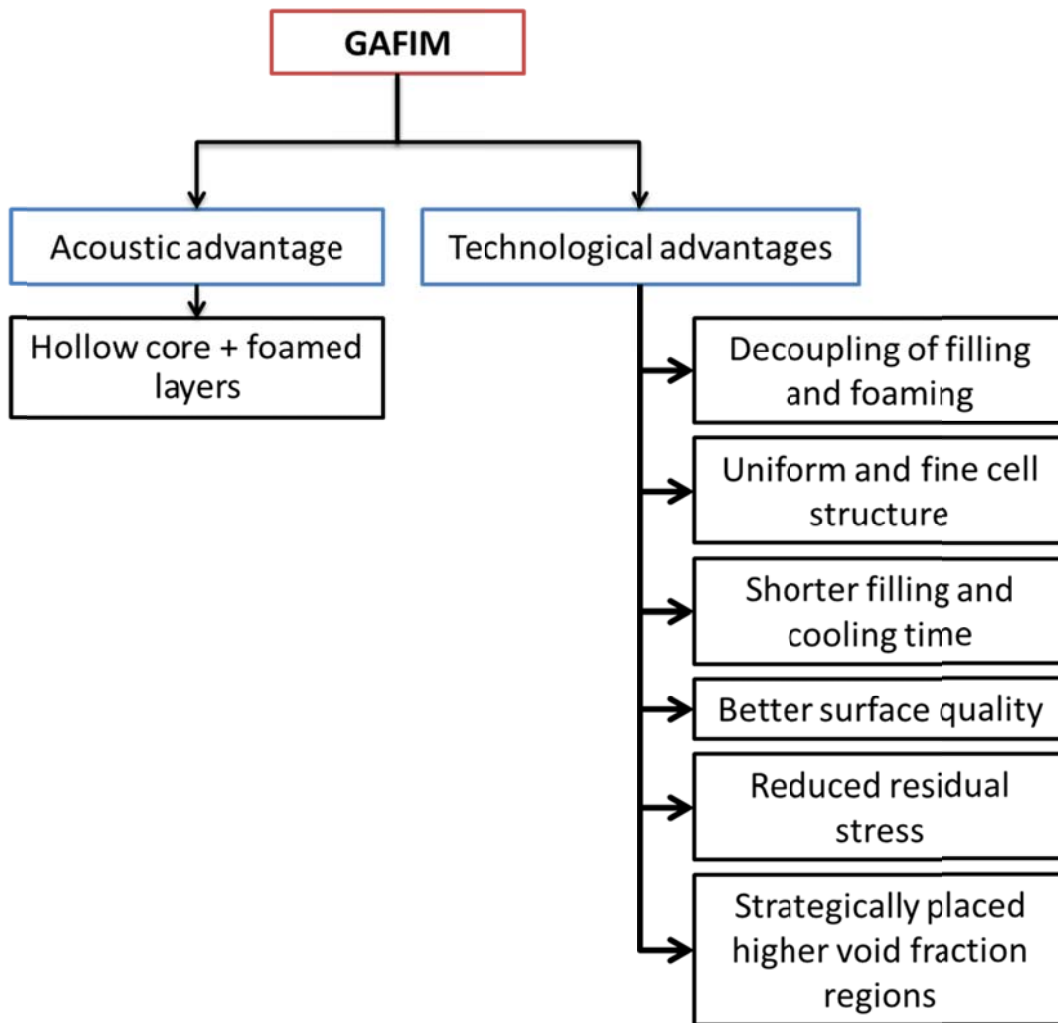


Figure 3.1 Technological innovations for the proposed GAFIM

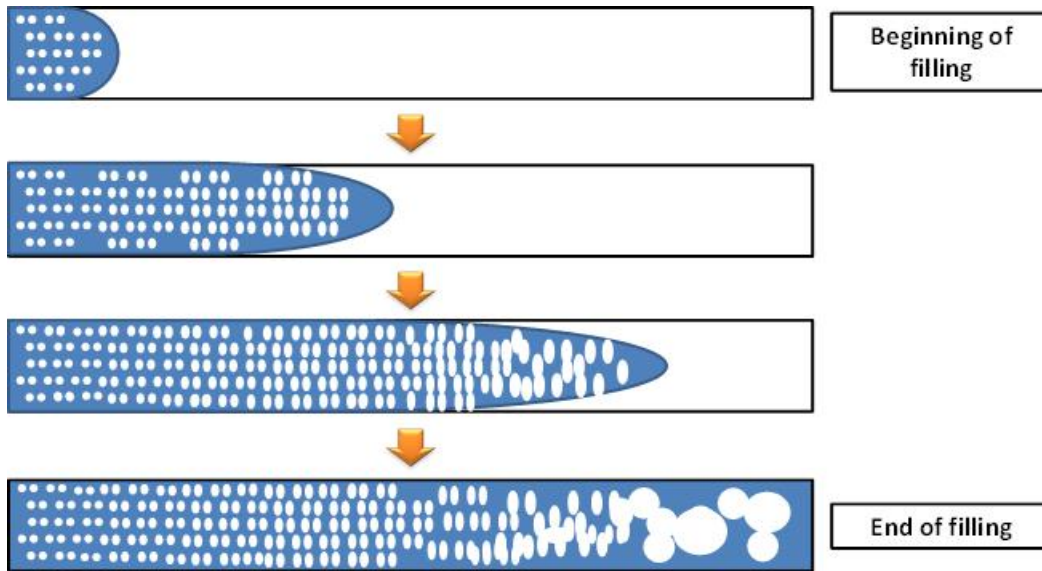
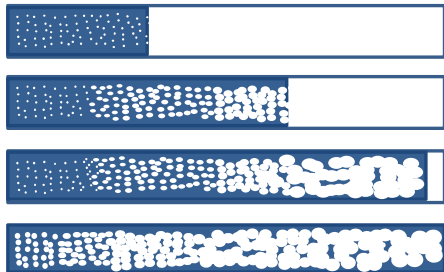


Figure 3.2 Foaming mechanisms of conventional foam injection molding

Low Injection Speed

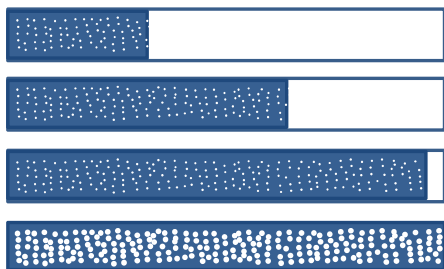


Excessive Cell Growth During Injection



Cell Coalescence During Injection

High Injection Speed



No Excessive Cell Growth During Injection



No Cell Coalescence During Injection

Figure 3.3 Effect of injection flow rate on the final cell structure [127]

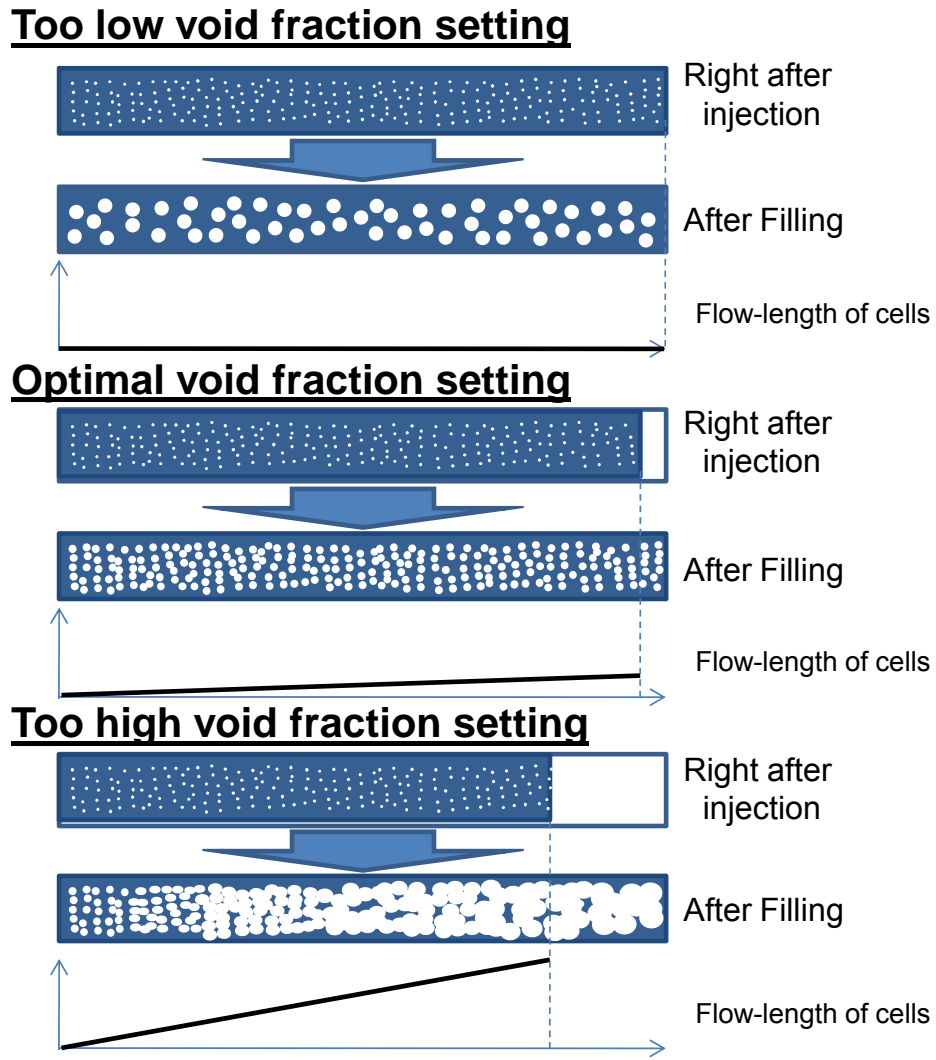


Figure 3.4 Effect of void fraction setting on the final cell structure [127]

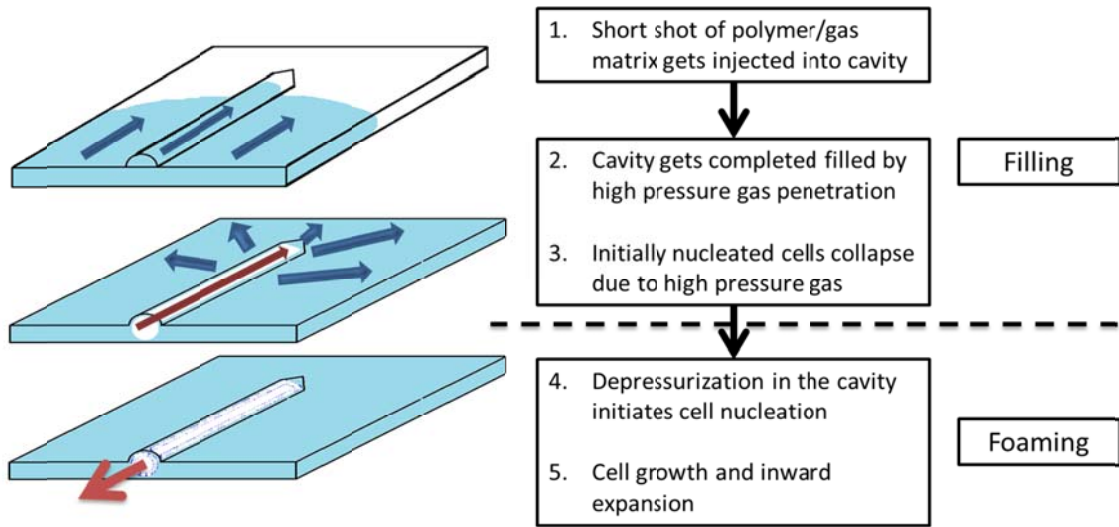


Figure 3.5 Schematic of the proposed gas-assisted foam injection molding technology

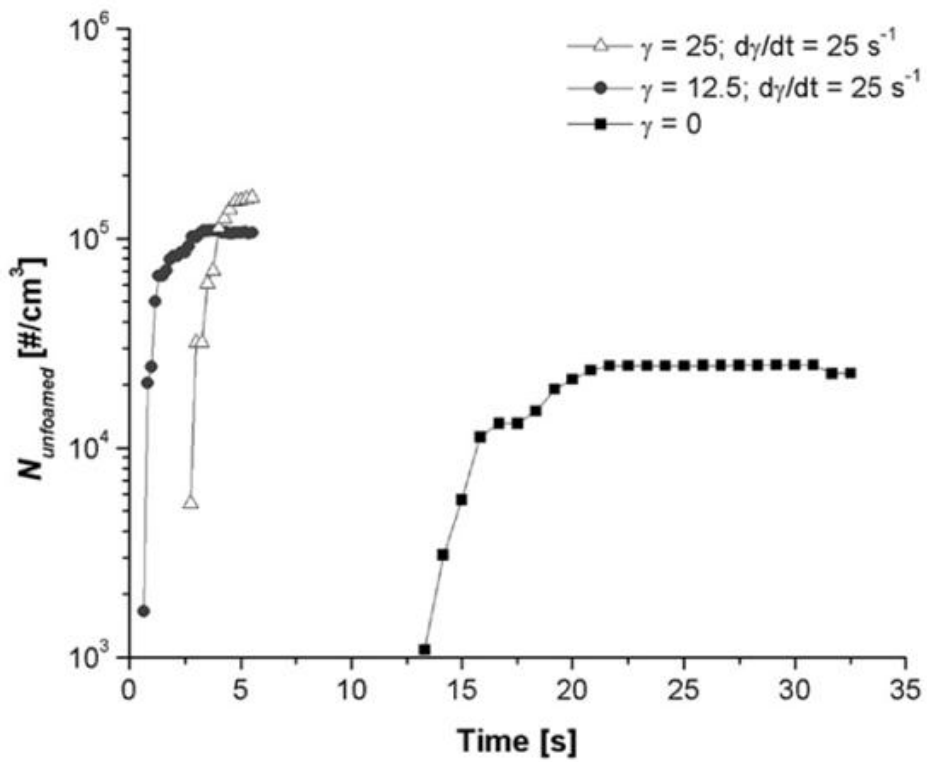


Figure 3.6 Effect of additional shear on cell density [178]

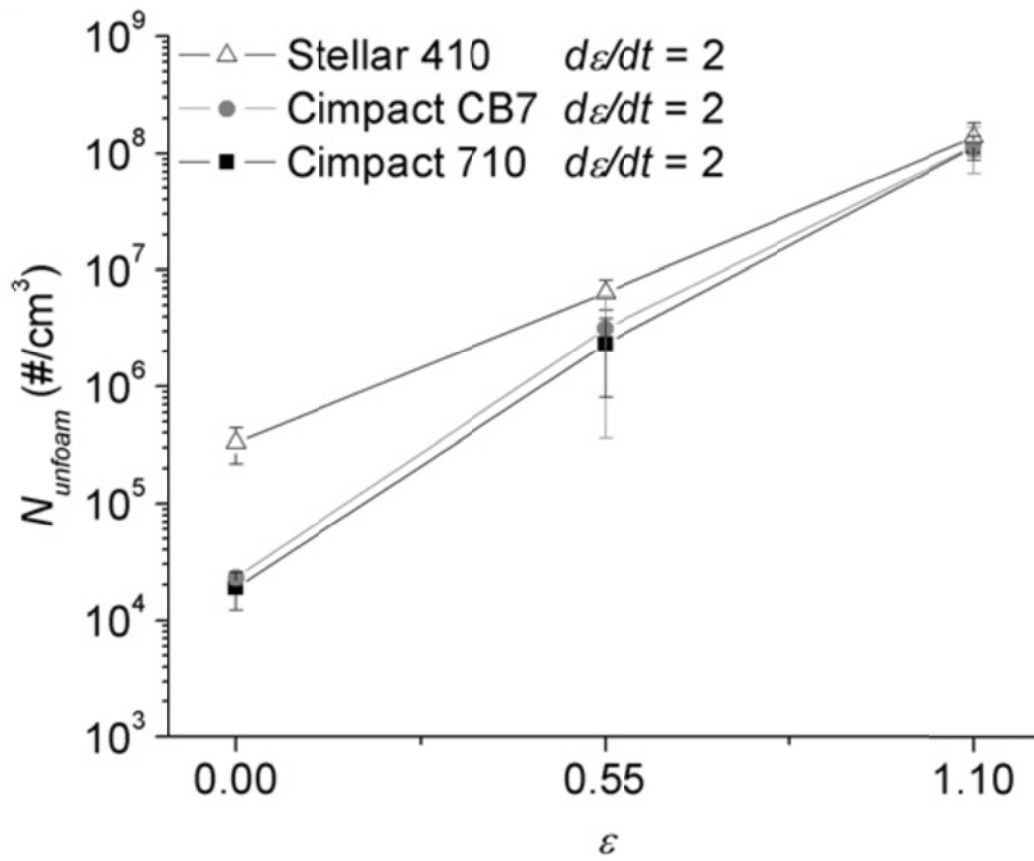


Figure 3.7 Effect of extensional strains on cell density [179]

Chapter 4 Experimental Studies of Gas-Assisted Foam Injection Molding Technology

4.1 Introduction

This chapter describes the actual experimental studies of GAFIM, so it first explains the details of common experimental materials and set-ups. Then, it discusses about the experiments with the processing variables of GAIM and the significance of the findings. Furthermore, the extensive experimental studies of FIM and GAFIM will be discussed to elucidate the foaming mechanisms of GAFIM technology.

4.2 Experimental Materials

Thermoplastic polyurethane (TPU) being used in all experiments in this chapter was Pellethane[®] 2355-75A from Lubrizol Advanced Materials Inc. and its physical properties are summarized in Table 4.1. TPU was selected because it has an excellent foaming capability and its highly flexible nature is very favorable to achieve high acoustic absorption coefficient.

The physical blowing agents used for the foaming experiments were CO₂ and N₂ from Linde Canada Ltd. For GAIM experiments, N₂ from Linde Canada Ltd. was employed to inject into the cavity.

4.3 Experimental Set-up

This section describes the manufacturing equipment for all the experiments in detail. In order to manufacture foam samples, two different FIM machines, an 80-ton advanced structural foam molding machine and a 50-ton Arburg injection molding machine, were utilized. For GAIM technology, a commercial 2-channel nitrogen control unit (NCU) was implemented.

4.3.1 Advanced Structural Foam Molding System

An 80-ton injection molding machine, TR80EH from Sodick Plustech Inc., was modified to an advanced structural foam molding (ASFM) machine [180-183]. As the schematic of ASFM in Figure 4.1 shows, a gear pump and an accumulator were added to the conventional FIM machine platform in order to provide a continuous extrusion and mixing process for the polymer/gas matrix. By decoupling the extrusion and molten polymer conveying processes, an independent and precise pressure control of the extrusion barrel became possible and this advantage enables an operator to ensure gas dissolution with the molten polymer inside the barrel by maintaining the barrel pressure significantly higher than the solubility pressure of gas. The maximum shot size is 108 cm³ and the maximum injection flow rate is 400 cm³/s.

In order to inject the physical blowing agent into ASFM, a high precision syringe pump, 260D syringe pump from Teledyne Isco, was employed. Its maximum outlet pressure is 51.7 MPa and the maximum volumetric flow rate is 107 ml/min.

4.3.2 Arburg Injection Molding Machine with MuCell[®] System

A 50-ton ALLROUNDER 270C from Arburg GmbH, shown in Figure 4.2, was

also utilized to manufacture the samples for the experimental studies. The maximum shot size of the Arburg 270C is 106 cm^3 and its maximum injection flow rate is $100 \text{ cm}^3/\text{s}$. This injection molding machine was retrofitted to accommodate the gas injection function of the MuCell[®] system (Trexel Inc.).

The MuCell[®] system is a commercially available equipment that meters and injects PBAs in their supercritical fluid (SCF) forms directly into the barrel of the injection molding machine [184-186]. The schematic of the MuCell[®] system setup is exhibited in Figure 4.3. It pressurizes the SCF using a set of high pressure pneumatic boosters and injects the SCF into the barrel through a pneumatic valve gate. The processing parameters are as follows: the delay time for SCF injection, the SCF flow rate, the SCF delivery pressure, and the SCF injection time. The MuCell[®] system needs to be electronically integrated with the injection molding machine for a successful and fully automatic process. In the actual system setup, the SCF flow rate and the SCF delivery pressure can be controlled directly from the MuCell[®] system; whereas the delay time for SCF injection and the SCF injection time are the functions of the Arburg 270C system.

4.3.3 Gas-Assisted Injection Molding System

As mentioned above, a 2-channel NCU from Bauer Compressors Inc. was utilized to effectively execute the GAIM process. This NCU provides the freedom to program up to five gas injection pressure profiles per cycle by varying the gas injection delay time, the gas injection pressure, duration of each stage, and the pressure change rate. The maximum gas injection pressure can be limited by the maximum pressure of the N_2 source, but the system can handle up to 34.47 MPa ($= 5000 \text{ psi}$). Its maximum pressure change rate is 24.13 MPa/sec ($= 3500 \text{ psi/sec}$).

4.3.3.1 Implementation of Gas Channel

As mentioned previously, the implementation of gas channels is crucial for the successful adaptation of the proposed GAFIM technology. The original cavity design was a simple plaque shape, which is exhibited in Figure 4.4, and the sample dimensions were 111.76 mm (width) x 134.62 mm (length) x 3.2 mm (thickness).

Since the original cavity had a relatively wide and thin plaque shape, it was determined to cut two channels parallel to the polymer flow direction. In addition, the semicircular shape was adopted to minimize the possibility of the fingering phenomenon. The diameter of the semicircular gas channel was determined based on the recommended design guidelines by Dier and Goralski [84] and the nominal wall thickness, which was 3.2 mm. As a result, the diameter of the semicircular gas channels became 0.25" (=6.35 mm), which was equal to 2 times the part nominal thickness. Since there was one main runner through which the polymer travels from the nozzle to the cavity, one short gas channel was designed and divided into two gas channels to maximize the void fraction. The modified cavity with two gas channels is exhibited in Figure 4.5 and the actual picture of modified cavity is shown in Figure 4.7. In addition, Figure 4.8 shows the drawing of new sample design with dimensions.

4.3.3.2 Methods of Gas Injection

For all the experiments in this chapter, two methods of gas injection were implemented for the GAIM process. First, gas injection was conducted through the main nozzle of the ASFM system. In order to accommodate this gas injection method to the nozzle of the existing ASFM equipment, an extra nozzle extension part had to be machined. The gas injection hole was drilled to the main nozzle and it was located behind

the main shut-off valve to prevent gas backflow to the main shot pot. In addition, a spring-loaded check valve was attached to the gas injection hole to prevent polymer back flow when the gas was not injected; the check valve is shown in Figure 4.9. This ‘through nozzle’ gas injection system schematic is exhibited in Figure 4.10. However, this gas injection method was a coupled design because the same nozzle was shared to serve two functions, injection of polymer/gas matrix and injection of N₂ for GAIM. The functional requirement (FR) and design parameter (DP) analysis was conducted and its result is described in the following equation.

$$\begin{pmatrix} \text{Injection of polymer – gas matrix} \\ \text{Injection of N}_2 \text{ for GAIM} \end{pmatrix} = \begin{bmatrix} X \\ X \end{bmatrix} (\text{Main Nozzle}) \quad \text{Equation 4.1}$$

Therefore, the gas injection method was changed to a decoupled design as shown below.

As an effort to decouple the polymer/gas matrix injection and N₂ gas injection for GAIM, a gas pin was implemented in the cavity for independent and direct gas injection into the cavity. The gas pin was located at the corner where the main gas channel was split as indicated in Figure 4.5. In order to verify the design, another FR-DP analysis was carried out with the new gas injection method as described below, and it was clear that the design became decoupled by using a direct gas injection method via gas pin.

$$\begin{pmatrix} \text{Injection of polymer – gas matrix} \\ \text{Injection of N}_2 \text{ for GAIM} \end{pmatrix} = \begin{bmatrix} X & O \\ O & X \end{bmatrix} \begin{pmatrix} \text{Main Nozzle} \\ \text{Gas Pin} \end{pmatrix} \quad \text{Equation 4.2}$$

Once the gas injection method was optimized, all the experiments using Arburg and MuCell[®] systems utilized this gas-pin method to inject the highly pressurized N₂ gas directly into the polymer/gas matrix within the cavity.

4.3.4 Moldflow[®] Simulation Study

In this chapter, Moldflow[®] 2013 version from Autodesk Inc. was utilized to simulate and verify the experimental results of both GAIM and FIM. Although Pellethane[®] 2355-75A was actually utilized in all the experiments, Estane[®] 58134 from Lubrizol Advanced Materials Inc. was employed for the simulation studies. The reason for this was Pellethane[®] 2355-75A was not listed as a material candidate in the material database of Moldflow[®]; and Estane[®] 58134, among other TPU resins in the database, had the most similar material properties as Pellethane[®] 2355-75A. The processing parameters that were utilized in Moldflow[®] will be described in the section 4.5.3.

4.4 Experimental Procedure

4.4.1 Manufacturing of Foams

Prior to every experimental study, the TPU pellets were dried at 60 °C in an oven for more than 8 hours in order to eliminate the moisture that might have been accumulated within the TPU during the storage.

Once the TPU pellets were dried, they were put into the hopper of the injection molding machine. The foam samples were then manufactured by either the FIM or the GAFIM process. For all the experimental studies, the mold temperature was maintained at 30 °C and the rest of the processing conditions will be described in the section 4.5 in detail for each experiment.

4.4.2 Foam Structure Characterization

In order to evaluate a foam structure, three evaluation criteria (i.e., the foam

density, the cell density, and the average cell diameter) were employed and measured usually at three different locations throughout the injected samples. The foam densities were measured using a standard water displacement method as per ASTM D792-00.

The cell density was calculated according to the micrograph obtained by a scanning electron microscopy (SEM). The samples were either fractured or cut in appropriate sizes and coated with a thin layer of platinum by using a sputter coater. Then, the morphologies of samples were observed using SEM, JSM-6060 from JEOL, and the cell density values were calculated based on the SEM micrographs and the following equation:

$$\text{Cell Density} = \left(\frac{n}{A} \right)^{\frac{3}{2}} \times \Phi \quad \text{Equation 4.3}$$

where n is the number of bubbles in the micrograph; A is the measured area of the micrograph; and Φ represents the expansion ratio. The expansion ratio was calculated based on the measured foam density.

The average cell diameter was measured based on the SEM images. The image analyzing software was utilized to measure the diameters of bubbles in that observed foam structure and the average diameter values, along with the calculated standard deviation, were reported.

4.4.3 Acoustic Characterization

In this research study, two types of acoustic properties were evaluated: acoustic absorption coefficient and transmission loss over a frequency range from 100 to 6300 Hz

using impedance tubes as per ASTM E1050. The testing specifications and detailed discussions will follow in the next chapter.

4.5 Effects of Processing Parameters of Gas-Assisted Injection Molding Technology

A series of extensive experimental studies have been carried out to investigate the effects of the processing variables of GAIM on the gas penetration behaviors as an effort to maximize the void fraction. Based on the literature review, the most critical processing variables of GAIM were the gas injection delay time [163] and the gas injection pressure [164-166]. Therefore, the effects of the gas injection delay time and the gas injection pressures were studied prior to the simultaneous utilization of GAIM with FIM technology and the experimental results were compared with Moldflow[®] simulation results as well. These GAIM experimental studies shared the fixed processing parameters as described in Table 4.2.

4.5.1 Effect of Delay Time

In this experiment, the effects of the gas injection delay time on the gas penetration behaviors were investigated. The gas injection delay time starts with the beginning of injection of the polymer/gas matrix. When determining the gas delay time, it is important to ensure the continuation of the polymer flow motion during the filling phase by GAIM. If the delay time is too early, gas can escape through the polymer melt. Gas cannot penetrate into the polymer melt effectively if the delay time is too late because the cooling rate of the polymer melt is very fast within the cavity. Therefore, a set of experiments was carried out to study the effect of the gas injection delay time.

In terms of the injection molding machine, ASFM was employed and the ‘through nozzle’ gas injection method, described in Chapter 4.3.3.2, was utilized. The injection molding processing conditions described in Table 4.2 were applied, and the gas injection delay time was varied from 0.5 to 1 sec. The gas injection delay times were relatively short because the gas had to travel through a spring-loaded check valve and push the polymer melt in the main nozzle to reach the polymer melt in the cavity. The other GAIM processing conditions are provided in Table 4.3.

As exhibited in the experimental results in Figure 4.11, GAIM TPU samples with a 0.5-sec delay were able to achieve a higher degree of gas penetration. As a result, the samples with a 0.5-sec delay could fully fill the cavity and obtained a higher void fraction. The samples with a 1.0-sec delay did not completely fill the cavity because the polymer melt at the cavity end (near Location C) was more solidified, so N₂ gas from GAIM could not push the molten TPU as effectively as it was able to when the delay was only 0.5 sec.

Figure 4.12 shows the cavity pressure profile during the filling phase for the 0.5-sec gas injection delay time case, and the pressure was measured at three different locations in the cavity, i.e., Near Runner, Location A, and Location C, as described in Figure 4.5. As indicated in the figure, the solid line is the set gas injection pressure profile by NCU. The polymer injection started around 239 sec and was completed at 241.2 sec, and that is why the pressures at Near Runner and Location A started to decrease at 241.2 sec. Within the next 0.5 sec, the pressures at both locations became zero. During this initial polymer injection stage, the pressure at Location C was maintained at almost zero because the polymer flow filled the cavity partially and did not reach Location C. For the next 0.8 sec, the pressure at all three locations increased very

rapidly up to around 8.27 MPa because N₂ gas of GAIM penetrated into the already injected TPU and filled the rest of the cavity completely. The gas injection pressure profile indicated that the first stage of GAIM did not actively participate in the secondary TPU filling because it took nearly 2 sec for N₂ gas to travel through the nozzle and the runner. Therefore, only the second stage of GAIM was able to push the TPU flow and fill the cavity completely.

It was observed that the second stage of GAIM came into play 0.5 sec later than the completion of the short shot injection of the polymer material. On the other hand, in the case of the 1.0 sec delay time, the identical second stage of GAIM was applied roughly 1.0 sec later than the completion of the polymer injection. In other words, the polymer melt was stopped and solidified for nearly 1.0 sec before the additional pressure from the N₂ gas was applied. During this 1.0 sec, TPU became rigid enough to deteriorate the efficiency of GAIM. Therefore, 0.5 seconds of the gas injection delay time led to the maximum gas penetration length by filling the entire cavity successfully.

4.5.2 Effect of Gas Injection Pressure Profile

In order to investigate the effect of the gas injection pressure, two sets of experiments were conducted. The fixed processing parameters, exhibited in Table 4.2, were implemented for these experiments as well. The first set of experiments simply aimed to compare the effect of the gas injection pressures on the void fraction and the gas penetration behavior. The second set of experiments aimed to investigate the polymer melt behavior inside of the cavity when the gas injection pressure profiles and their durations were varied together.

In the first set of experiments, the gas injection pressures were varied from 5.17 to 13.79 MPa as described in Table 4.4. The rest of the GAIM processing conditions are explained in the same table. According to Figure 4.13, the gas penetration behaviors enhanced as the gas injection pressure increased. This trend was identical to the results described in the literature [164-166]. In the cases of the 5.17 and 10.34 MPa samples, the injected N₂ was not able to fully fill the cavity; however, the cavity was fully filled when the gas injection pressure of 13.79 MPa was utilized.

The second set of experiments investigated the polymer melt behavior within the cavity when the gas injection pressure profiles were varied. When compared to previous experiments, the third gas injection stage was introduced for these experiments and its duration was varied from 10 to 30 sec. In an effort to analyze the polymer melt behavior, the cavity pressure profiles were utilized.

Figure 4.14 shows the cavity pressure profile when the duration of the third gas injection stage was 10 sec. During the first and second gas injection stages, the cavity pressure profile was identical to the previous experimental result exhibited in Figure 4.12. After the second gas injection stage was completed, the cavity pressures reduced to approximately 5 to 5.5 MPa and the pressure values were maintained for the remainder of the third gas injection stage. After the third gas injection stage was completed, the cavity pressures started to decrease slowly because of the cooling phase. In order to validate the consistency of this trend, the duration for the third stage was prolonged to 30 sec for the next experiment. The cavity pressure profile for this experiment is exhibited in Figure 4.15 and the cavity pressures were maintained at 5 to 5.5 MPa during the entire third gas injection stage. After the third gas injection stage was completed, the cavity pressures

started to decrease as observed in the previous experiment. Therefore, once the cavity was completely filled, the introduction of the third gas injection stage was able to pressurize the polymer melt within the cavity for a relatively long time.

4.5.3 Simulation Study Using MoldFlow[®]

In the previous section, the effects of the gas injection pressures and different pressure profiles on the gas penetration behaviors have been investigated, experimentally. This part of the study employed Moldflow[®] software from Autodesk Inc. to compare the simulation results to the actual experimental results.

The first set of simulation analysis examined the effect of the gas injection pressures on the TPU filling phase. In order to compare the simulation results with the actual experimental results, the identical processing conditions from the experimental studies were employed in Moldflow[®] and they are shown in Table 4.6. Furthermore, the evaluated gas injection pressures were 5.17, 10.34, and 13.79 MPa. Figure 4.16 illustrates how much the cavity is filled with TPU when the gas injection pressures were changed. Although the gas injection pressure increased close to three times, the polymer filling behaviors did not improve significantly. For all three cases, the degrees of filling from the actual experimental samples were significantly higher than those from the simulation studies. For instance, 13.79 MPa of gas injection filled the cavity entirely in the experimental study; whereas the simulation results exhibited a considerable amount of cavity volume as unfilled. Figure 4.17 shows the voids created by N₂ gas during the GAIM process. Similar to the actual experimental samples, the simulation results also show non-uniformity of the gas penetration behavior in the gas channels. N₂ gas penetrated a longer distance in one channel than in the other channel; and the fingering

effect was more pronounced as the gas injection pressure was increased. Based on the simulation results, the gas voids were connected to the unfilled region of cavity, which meant that gas escaped through the polymer melt in the cavity. In addition, these indicated that the software overestimated the cooling rate of injected TPU than the actual experimental rate, and that was why the GAIM process was not as effective in the simulation study. In all three gas injection pressure cases, consequently, the actual experimental study exhibited dramatically enhanced the gas penetration and the cavity filling behaviors than the simulation results from Moldflow[®].

The second set of the simulation study aimed to investigate the effect of different gas injection pressure profiles on the TPU filling behaviors. As discussed in the previous section, two gas injection pressure profiles, explained in Table 4.5, were utilized for the simulation analysis. Figure 4.18 exhibits the gas voids created by different GAIM pressure profiles and the introduction of the third gas injection stage did not enhance the filling behaviors. The primary reason for this is the overestimation of the polymer cooling rate and gas paths being interconnected to the unfilled region of the cavity.

In an effort to determine the most dominant factor of the GAIM process in Moldflow[®] simulation, additional simulations were conducted, and the impact of shot size and melt temperature was investigated. The effect of the shot sizes is displayed in Figure 4.19; and complete filling was achieved with 87 vol% of the full shot. Since the actual sample of 75 vol% shot size was fully filled with the identical GAIM processing conditions, there was a 12% of discrepancy observed between the simulation and the actual experimental results. In terms of melt temperature, the simulation result showed that the gas was not able to penetrate into the polymer matrix at all when 190 °C was

applied as the melt temperature. The unfilled portion of the cavity was quite significant even when the temperature was increased from 190 °C to 220 °C. On the other hand, when the temperature was further increased from 220 °C to 227 °C, the efficiency of GAIM increased significantly, and the cavity was finally filled completely. Since the melt temperature became such a dominant processing parameter, it was realized that the melt viscosity was the most critical characteristic in determining the gas penetration behavior of Moldflow[®] GAIM studies.

In order to investigate the efficiency of Moldflow[®], the identical processing conditions were applied for both experimental and simulation studies, and their results were compared. It was observed that the simulation underestimated the pressurization effect of gas on the polymer melt and overestimated the cooling behavior of TPU in the cavity. Further simulation studies were conducted to investigate the effects of melt temperature and shot size, and the increase in melt temperature had the most significant impact on the degree of filling once the temperature was higher than the melting temperature to a certain degree. Therefore, the simulation logics of Moldflow[®] seemed to be highly dependent on the temperature effect than the other processing conditions for the GAIM technology simulation.

4.6 Low Cavity Pressure Case of the Proposed Technology

This set of experimental studies has been carried out in order to investigate the effect of GAFIM technology when the cavity was not fully pressurized due to excessively high void fraction setting. As mentioned in Chapter 3, the additional extensional and shear stresses to the melt are provided by N₂ gas from GAIM to induce a higher degree of

cell nucleation by reduction of the critical radius, R_{cr} , and increase of nucleation rate, J_{hom} . In addition, these extensional and shear energies would promote higher degree of heterogeneous nucleation via aligning the polymer molecular chains and forming higher number of crystallites.

Furthermore, it is required to investigate whether the other advantages of GAFIM in foaming are still applicable or not when the cavity pressures are low. In order to validate this hypothesis, the following GAFIM experiments were conducted with two different PBAs, CO₂ and N₂.

4.6.1 Experiment with CO₂

In this experimental study, CO₂ was utilized as a PBA for the proposed GAFIM technology. In order to investigate the effects of GAFIM technology, FIM experiments were carried out first and then GAFIM experiments were conducted with the identical manufacturing conditions. The results of each group of experiments were then compared and carefully analyzed.

For the injection molding machine, ASFM was employed, with the fixed processing conditions of ASFM listed in Table 4.2. Regarding the GAIM process, N₂ gas was injected through the main nozzle of ASFM as described in Figure 4.10; the fixed GAIM processing parameters are described in Table 4.7. The void fraction settings were intentionally large to avoid completely filling the cavity by expansion of the polymer/gas matrix from both GAIM and foaming. The void fraction settings were experimental variables, and they were 35 and 40 vol%. In other words, their shot sizes were 65 and 60 vol%, respectively.

In order to evaluate the foaming behaviors, the cross-sections of the gas injection regions at two different locations, Location A and Location C (as indicated in Figure 4.5), were observed by using SEM. Since the cavity was not fully pressurized, the gas paths were not created, even in the gas injection regions. As a result, the gas injection regions obtained nearly identical cellular morphology as the non-gas injection regions and the effects of GAFIM technology was more pronounced at the gas injection region. Thus, the gas injection regions were discussed extensively in the low cavity pressure case.

Figure 4.21 shows the cellular morphologies from both FIM and GAFIM experiments when the void fraction setting was 35 vol%. In the case of the FIM samples, the foam structures had a lower cell density and larger average cell size than the ones from the GAFIM samples at both locations. At Location C, especially, a largely coalesced cell was observed in the middle which verified that severe cell coalescence occurred during the FIM process. Due to a slow injection flow rate of $24 \text{ cm}^3/\text{s}$, it took approximately 2 seconds for the polymer/gas matrix to arrive at Location C. In other words, the initially nucleated cells had about 2 seconds to grow freely before they reached their final destination, and the cells were able to grow even more to a certain degree since the melt temperature at the core region was cooled very slowly. Furthermore, the TPU/gas matrix at the center region experienced the least amount of shear and extensional energies, which resulted in a lower degree of crystallinity. Because of these circumstances, the overall foaming mechanism became cell growth dominant.

When GAFIM was implemented, the foam structures at both locations significantly improved. The introduction of GAIM yielded a higher cell density with much reduced cell sizes as exhibited in Figure 4.21. At Location A, the cells were more

consistent and uniform in terms of their sizes than those of the FIM sample. Furthermore, the fine cell structure at Location C indicated that the addition of GAIM helped to resolve the inherited challenge of the conventional FIM process in a certain extent. Consequently, the predominant foaming mechanism became cell nucleation rather than cell growth. This change in foaming mechanism from cell growth to cell nucleation was the primary reason for approximately 10 times higher cell density values for both void fraction settings as displayed in Figure 4.22. Due to the excessively high set void fraction, the adaptation of GAFIM was not able to completely pressurize the cavity. The main reason for this deteriorated gas penetration behavior was because the injected N₂ gas escaped through the polymer melt and minimized the efficiency of GAIM. This phenomenon was similar to what was observed with the earlier Moldflow[®] simulation results when the void fraction setting was excessively high.

4.6.2 Experiment with N₂

As an effort to further verify the hypothesis, another experimental study was carried out; and N₂ gas was employed as the PBA for this study. In this experimental study, the Arburg injection molding machine was utilized, and MuCell[®] was employed to provide PBA into the injection molding machine. In terms of processing conditions, the identical conditions as the previous CO₂ experiment were applied. However, the void fraction setting was fixed to 35 vol% and the PBA content was 0.3 wt%. In terms of the GAIM process, the gas injection method was changed from ‘through nozzle’ to ‘gas pin in the cavity.’ Thus, N₂ gas from GAIM was injected through the gas pin, which was located as shown in Figure 4.5.

The cellular morphologies at three different locations of the FIM and GAFIM

samples are exhibited in Figure 4.23. In general, the foam structures of FIM had significantly larger cell sizes with a lower cell density compared to previous experiments with CO₂. In particular, at Location C, a very large cell in the middle that had a diameter larger than 7 mm was formed as a result of cell growth dominant behavior, because the filling and foaming mechanisms were coupled in the conventional FIM process. Furthermore, a number of cells with diameters larger than 1 mm were observed at Location A and B. Consequently, it was concluded that cell growth was the predominant foaming mechanism for the FIM samples.

On the other hand, the GAFIM samples achieved dramatically improved foam structures with smaller cell sizes and higher cell density values at all three locations. As it was observed from the previous experiments with CO₂, the predominant foaming mechanism changed from cell growth to cell nucleation by implementing GAIM. As a result, the GAFIM samples achieved one order of magnitude higher cell density than the FIM samples as shown in Figure 4.24 throughout the different locations of cavity.

4.6.3 Foaming Mechanism Analysis

The cavity pressure profiles were plotted against time for both FIM and GAFIM when the cavity was not completely pressurized in order to investigate their foaming mechanisms (Figure 4.25). In the case of FIM sample, the maximum cavity pressures at different locations were lower than the solubility pressure during the injection and cooling phases. This shows that the cells were nucleated as the polymer/gas matrix travelled from the nozzle and the prematurely nucleated cells continued to grow until the molten TPU matrix solidified. Since the temperature of core region was considerably higher than that of the near skin region, the cells at the core region were significantly

larger than those at the near skin region. Due to the higher shear energy at near skin region, more TPU molecules were highly oriented and formed micron-sized crystallites. These resulted in smaller cells and higher cell density in these sub-skin regions at all three observed locations in the cavity.

When the GAFIM was implemented, the cavity pressure profiles changed dramatically as displayed in Figure 4.25. Although 13.79 MPa of N₂ gas was injected for GAIM, the cavity pressures increased to only around 4.83 MPa since the gas penetration behavior by GAIM was not effective. The gas escaped through the flow end due to the excessively high void fraction setting. During gas injection, the pressures at all four locations were maintained at 4.48 MPa for few seconds. On-set timings of cell nucleation and the pressure drop rate values at all four locations were very close to each other. Besides these two traditional characteristics, the pressure drop rate and the pressure drop, GAFIM also enabled TPU molecules to highly orient by applying additional shear and extensional energies, especially at the core region where the injected gas travelled with the least amount of flow resistance. These highly oriented molecules became easier to crystallize and the formed micron-sized crystallites were utilized as preferred nucleation sites for heterogeneous nucleation. Since the pressure drop rate was relatively small as well as the magnitude of pressure drop, the additional shear and extensional energies were dominant factors, which yielded the uniform and finer cellular morphology was achieved with the implementation of GAFIM. Furthermore, the results confirmed the previously discussed hypothesis that additional extensional and shear energies by GAIM could yield a cell nucleation dominant foaming mechanism by reducing the critical radius and increasing the nucleation rate [178, 179].

4.7 Highly Pressurized Case of the Proposed Technology

The previous experimental study was focused on investigating the effect of GAFIM technology on the predominant foaming mechanisms and final cellular morphologies when the cavity was not pressurized effectively. In this section, the research aimed to investigate the effect of GAFIM technology on the foaming behaviors when the cavity was completely pressurized at a high pressure.

For this experimental study, the Arburg injection molding machine was employed for the sample manufacturing and the MuCell[®] system was implemented again for the PBA injection. The processing conditions for these two systems are listed in Table 4.8. The shot size was increased to 80 vol% from 60-65 vol% of the previous partial filling case in order to ensure the complete filling of the cavity by additional GAIM. Since the cavity would be completely filled, the polymer/gas matrix would be highly pressurized for the remainder of the gas injection time. During this pressurization period, the initially nucleated cells would be collapsed. The primary foaming would then occur once this pressurization is terminated by sprue-break. This manufacturing cycle of GAFIM technology is briefly described in Figure 3.5. Since foaming can be dominantly determined by the characteristics of GAIM process, the pressure of the polymer/gas matrix during this pressurization step would be very critical. Therefore, the effect of these gas injection pressures was carefully investigated in the following experimental studies.

In order to determine the effects of GAFIM technology on the final foam structure, the foam properties were measured and evaluated at two different regions that were categorized as non-gas injection region and gas injection region based on Figure 4.26.

The gas injection region was referred to the gas channel where the highly pressurized gas was directly penetrated along to the existing polymer/gas matrix. It is expected that the effect of GAFIM would be more pronounced in this gas injection region because the gas flow was highly directional in this region. Since the majority of foamed sample is still non-gas injection region, however, it is critical to determine the effectiveness of GAFIM technology on the non-gas injection regions as well. For both types of regions, the foam characteristics were measured at three different locations (i.e., Location A, Location B, and Location C) depending on the flow length from the sprue to the flow-end as exhibited in Figure 4.26.

4.7.1 Experiment with Low Gas Injection Pressure

In the first experiment, the effect of low gas injection pressure was determined when the gas injection pressure was 6.89 MPa. The rest of the GAIM processing conditions described in Table 4.9 were applied.

As it was discussed previously in Figure 3.5, the first step of GAFIM process was the injection of short shot of the polymer/gas matrix. Towards the end of this injection phase, the high pressure N₂ gas was injected to complete the filling of cavity. That was why the cavity pressures at all four cavity locations were increased to about 7.58 MPa at 2 second as exhibited in Figure 4.27. Then, the cavity pressures were maintained at 7.58 MPa uniformly for 3 seconds until the depressurization stage. The rapid depressurization was occurred via sprue-break and the primary foaming occurred during this stage since the cavity pressures became significantly less than the solubility pressure. The on-set timings of cell nucleation at four different locations were very close to each other and the pressure drop rates at Near Runner, Location A, Location B, Location C were 31.72

MPa/sec, 10.7 MPa/sec, 113.12 MPa/sec, 89.54 MPa/sec, respectively. Once the foaming by depressurization was occurred, the foamed sample was cooled for the rest of cycle time.

Figure 4.28 exhibits SEM pictures of gas injection regions and non-gas injection regions of GAFIM samples. Due to the adaptation of gas channels, the maximum thickness of gas injection region was 6.4 mm. Meanwhile, the non-gas injection region had the nominal thickness of 3.2 mm. The gas injection region structures consisted of a solid skin layer, a foam layer, and an air cavity that was created by gas path. The existence of air cavity verified that the actual GAFIM technology was successfully carried out as proposed and expected. On the other hand, the non-gas injection foam structure only had a solid skin layer and a foam core. Further, the non-gas injection regions achieved thicker solid skin layers than the gas injection regions of the same sample.

Figure 4.29 compares the cellular morphologies at gas injection regions of FIM and GAFIM samples. The foam structure of FIM samples at gas injection region was very similar to that of GAFIM samples at non-gas injection region, consisting of the solid skin layer and the foam core. When the foam layers of both FIM and GAFIM samples at the gas injection regions were observed at higher magnification as shown in Figure 4.30, the cellular morphology was noticeably enhanced and became more uniform with respect to the flow length. In the case of FIM samples, the nucleated cells were severely deformed as the flow length was increased. However, the bubbles of GAFIM samples were able to maintain the spherical shapes. When the non-gas injection regions were examined at higher magnification as exhibited in Figure 4.31, furthermore, it was

observed that the implementation of GAFIM technology improved the foam structure at those regions as well.

Due to the employment of GAFIM technology, the cell density values at the gas injection regions as well as the non-gas injection regions were increased as illustrated in Figure 4.32. The cell density values of GAFIM samples at each region were approximately 10 times higher than those of FIM samples. At location C, especially, the average cell density at the non-gas injection region of GAFIM samples was nearly 100 times higher than that of FIM samples. When the gas injection and non-gas injection regions were compared, the cell density values of non-gas injection regions were nearly 10 times higher than those of gas injection regions.

As exhibited in Figure 4.33, the average cell diameters at the non-gas injection and gas injection regions of GAFIM samples were noticeably smaller than those of FIM samples. At the non-gas injection regions, the average cell diameter values were reduced by 22 to 64 % by the implementation of GAFIM technology. Meanwhile, the degree of reduction was from 35 to 67 % for the gas injection region samples. Consequently, it was clear that the innovative foaming mechanism of GAFIM technology was able to provide dramatically finer cellular morphology and supreme uniformity throughout its samples than the conventional FIM technology.

In terms of local foam density values of GAFIM samples as shown in Figure 4.34, the density values of gas injection regions were significantly lower than those of non-gas injection regions because of the air cavity within the gas injection regions. As aforementioned, the concept of strategic placements of higher void section (i.e., the gas

injection region) within the sample while the rest of sample being relatively lower void fraction region was verified. This design feature can be advantageous for final properties such as acoustics and mechanical. In addition, the foam density values of GAFIM samples were noticeably consistent to the density values of FIM since the density values of FIM samples varied nearly 20% with respect to the changes of flow length.

4.7.2 Experiment with High Gas Injection Pressure

Since the gas injection pressure was the predominant factor to determine the crystalline kinetics of the polymer matrix for the regular GAIM process, the gas injection pressure was increased to maximize the formation of crystallites at both gas injection and non-gas injection regions. Hence, the crystalline dominant heterogeneous nucleation would become the dominant foaming mechanism. Therefore, the gas injection pressure was increased from 6.89 to 13.79 MPa for the second experiment; the rest of GAIM processing conditions were identical to the previous experiment, as listed in Table 4.9.

Prior to the complete injection of TPU/gas matrix, 13.79 MPa of N₂ gas pressurized the cavity to the high pressure, which was approximately 14.48 MPa, as shown in Figure 4.35. Then, the high cavity pressures were maintained while 13.79 MPa of N₂ gas was being supplied for 3 seconds. Then, the pressures were released by the rapid sprue-break. The pattern of the cavity pressure profile for this experimental study was almost identical to that of the previous experiment, therefore, except the maintained cavity pressures during the gas injection stage. When the polymer/gas matrix was exposed to the high pressure, the initially nucleated bubbles were collapsed as described in the previous experiment. Then, the rapid depressurization was followed and the pressure drop rates at Near Runner, Location A, Location B, Location C were 22.72

MPa/sec, 8.57 MPa/sec, 215.65 MPa/sec, 182.72 MPa/sec, respectively. After the primary cell nucleation was occurred via the depressurization, the cavity pressures increased again slightly because of the foam expansion. The independent cell nucleation only became possible because the filling and the foaming stages were completely decoupled. Hence, the initially nucleated cells were collapsed and the primary foaming was induced by the rapid depressurization separately.

Figure 4.36 displays the gas injection regions of FIM and GAFIM samples with two gas injection pressures. As it was described in the previous experiment, the foam structure of GAFIM samples with 13.79 MPa of gas injection pressure shared the identical structures as the GAFIM samples with 6.89 MPa. As the gas injection pressure was increased, however, the bubbles became smaller and their sizes were more consistent according to Figure 4.37.

In the aspect of non-gas injection region that represents the majority of manufactured foam samples, the cellular morphologies of FIM and both GAFIM samples were exhibited in Figure 4.38. As the gas injection pressure was increased from 6.89 to 13.79 MPa, the number of large cells was noticeably reduced. In the cases of FIM and GAFIM with 6.89 MPa of gas injection pressure, there were number of the bubbles whose diameters were larger than few hundred micrometers throughout the part. On the other hand, in the case of 13.79 MPa of gas injection pressure, there were very few bubbles whose sizes were larger than few hundred micrometers while the rest of bubbles were very small, especially at Location A and Location C.

This finer cellular morphology of 13.79 MPa gas injection pressure case directly

translated to significantly higher cell density values. According to Figure 4.40, the cell density values of both gas injection and non-gas injection regions were higher than 10^8 cells/cm³. Thus, the cell density values of 13.79 MPa sample were higher than the other two cases (i.e., FIM and GAFIM with 6.89 MPa of gas injection pressure) at both gas injection and non-gas injection regions.

Additionally, the difference of cell density values between the gas injection and non-gas injection regions was minimized by the increase of gas injection pressure. For FIM and 6.89 MPa GAFIM samples, meanwhile, the differences between two regions were more than an order of magnitude. The non-gas injection regions of the FIM and 6.89 MPa GAFIM samples consistently achieved approximately 10 times higher cell density than the gas injection regions of two sample types. On the other hand, the difference between the gas injection and non-gas injection regions of 13.79 MPa GAFIM samples was almost negligible at all three cavity locations. Consequently, the increase of gas injection pressure yielded noticeably higher cell density and improved the uniformity as well.

As it was expected from the measured cell density values, the average cell sizes were dramatically reduced as the gas injection pressure was increased, as illustrated in Figure 4.41. For both gas injection and non-gas injection regions, the average cell diameters of 13.79 MPa gas injection pressure GAFIM samples were ranged from 26 to 41 μm at all three cavity locations. In the case of FIM samples, on the other hand, the average cell diameter values were increased as the flow length became longer because of the coupled mechanisms of filling and foaming phases. At the non-gas injection regions of FIM samples, especially, the average cell diameters were doubled, from 39 μm of

Location A to 81 μm of Location C. In the aspect of the average cell sizes, therefore, its uniformity throughout the foam sample was enhanced significantly by the increase of gas injection pressure.

As it was observed in Figure 4.34 and Figure 4.42, the differences of foam density values of GAFIM samples were due to the existence of air cavity at the gas injection regions. The regular FIM samples, however, obtained noticeably varied foam density values despite the lack of air cavity within the foam structure. Hence, the density variation was as large as 30% at certain locations of the cavity. Consequently, the implementation of GAFIM technology enhanced the overall quality of foam structure by providing consistent foam density.

The various cellular characteristics (i.e., cell density, average cell diameter, and foam density) were measured and compared between the FIM and GAFIM samples. Further, those characteristics were also evaluated between the gas injection and non-gas injection regions within the foam samples. As a result, the implementation of GAFIM technology and the increase of gas injection pressure provided positive contributions to the measured cellular characteristics and improved the uniformity within the foam samples. The foaming mechanisms of both FIM and GAFIM technologies will be extensively discussed and determined in the following section.

4.7.3 Foaming Mechanism Analysis

When the GAFIM technology was implemented, the foaming mechanism was completely changed from the existing FIM technology. Based on the literature review, two major factors that determine the overall quality of foaming were the magnitude of

pressure drop (i.e., the degree of super-saturation) and the pressure drop rates [127, 148]. These studies focused on optimizing the gate geometry and the processing parameters of FIM technology in order to take full advantages of these two characteristics. In order to result in uniform cellular morphology, the injection flow rate and the set void fraction were optimized to maximize the cell nucleation and minimize the cell coalescence. In the case of the existing FIM, injection and foaming are coupled because bubble nucleation is initiated as the polymer/gas matrix pressure became less than the solubility pressure by introducing a thermodynamic instability. Since this timing can be varied by the cavity pressure, the locations of nucleation vary from the gate to the inside of cavity [127]. Cell nucleation continues to occur during the injection phase and the nucleated cells keep growing as the polymer/gas matrix travel into the cavity. Therefore, cell growth of existing FIM heavily depends on the time that the nucleated cells are exposed before the polymer is solidified and the distance that the nucleated cells have to travel to fill the cavity. Although the processing conditions can be optimized, the inherited coupled mechanisms between the filling and the foaming phases of FIM cannot be simply overcome.

The proposed GAFIM resolved this technological challenge of conventional FIM by completely decoupling the filling and the foaming phases. In the case of GAFIM, the initial bubble nucleation behavior during the filling phase was identical to that of conventional FIM. Near the end of this filling phase, however, the highly pressurized N₂ gas was injected to complete the filling phase and the gas directly penetrated into the polymer/gas matrix within the cavity. When the cavity was completely filled while the gas was continuously applied, then the cavity pressures became significantly higher than

the solubility pressure. Because of this high pressure of polymer/gas matrix, the initially nucleated cells became collapsed. This was the most critical moment of the foaming process of GAFIM technology since the collapsing stage was what decoupled the filling and the foaming phases. Once the initially nucleated cells were collapsed, the primary cell nucleation was then induced via the depressurization stage, which was carried out by the sprue-break in this research study.

In order to verify the concept of cell collapsing via pressurizing the already foamed polymer/gas matrix with high pressure gas, a batch foaming visualization system was utilized [7]. The high pressure chamber was heated and maintained at the temperature of 220 °C, which was equal to the processing temperature of the FIM and GAFIM experiments. The N₂ gas was injected at 3.79 MPa, which was the solubility pressure of 0.3 wt% of N₂ at the processing temperature, and it was saturated for 30 minutes. As soon as the pressure was released, then the visualization system started recording. Once the gas was released as exhibited in Figure 4.43, the cells were nucleated by the pressure drop. Then, N₂ gas was injected at the pressure of 13.79 MPa back to the chamber and the initially nucleated cells started to get collapsed instantaneously according to the images at 3 second and 4 second. While the gas was supplied at 13.79 MPa continuously for the rest of experiment, all the initially nucleated cells were collapsed eventually at the end. Therefore, this visualization experimental result verified the decoupling concept of GAFIM technology that was described previously.

The decoupling by GAFIM technology provided three major advantages in the aspect of bubble nucleation mechanism. First, on-set timings of cell nucleation became fairly uniform throughout the different cavity locations. During the initial nucleation

stage, the nucleation timings and locations were varied but these initial bubbles were collapsed since the high pressure, considerably higher than the solubility pressure, was applied to the polymer/gas matrix in the cavity. When the cavity pressure was released uniformly, the on-set cell nucleation timings at different locations of cavity were all occurred within 0.2 seconds. This uniform on-set cell nucleation timing, after the complete filling, positively contributed to the uniform final cellular structure. The GCP technology pressurizes the cavity pressure so it becomes higher than the solubility pressure to reduce premature nucleation and excessive growth. The technology also decouples the filling and the foaming to some extent. Therefore, the foaming mechanisms of the GCP and the GAFIM were similar to each other. However, the GCP technology cannot decouple the filling and the foaming completely since the nucleated cells still have to travel uniform distances for expansion prior to foaming.

Second, the polymer/gas matrix was pushed by the high pressure gas as the gas was penetrated into the matrix. During this penetration phase, the additional extensional strains and shear stresses were provided to the matrix. The additional extensional strains and shear stresses caused the local pressure deviation to become larger, in which resulted in a larger degree of local super-saturation [178, 179]. The larger degree of local super-saturation reduced the free energy barrier for cell nucleation, which led to higher cell nucleation rate as it was discussed in Chapter 2. The higher cell nucleation rate contributed to the higher cell density of final foam structure.

Third, the molten polymer molecular chains became more oriented by the additional extensional strains and shear stresses. Since the TPU matrix consisted of soft segments and hard segments, especially, these hard segments with shorter chain length

were aligned and became more readily available for the crystallization by the additional strains and stresses. During the highly pressurized gas was injected and maintained for 3 seconds in the actual experiment, a high number of crystallites were formed. Once the cavity was depressurized, the crystallites actively participated in the cell nucleation mechanism as heterogeneous nucleation sites. Since the heterogeneous nucleation requires a significantly smaller amount of energy than the homogeneous nucleation, the heterogeneous cell nucleation dominant mechanism resulted in the higher cell nucleation rate as well as the higher final cell density.

According to the experimental results, the increase of gas injection pressure yielded the noticeable improvements at both gas injection and non-gas injection regions in terms of cell density, cell size, and foam density values. The reason for these improvements was because the higher gas injection pressure caused the formation of higher number of crystallites, which promoted higher degree of heterogeneous nucleation [164-166]. Consequently, the major cell nucleation mechanism of GAFIM technology was the crystalline induced heterogeneous nucleation.

Because of this crystalline induced heterogeneous nucleation, the non-gas injection regions were able to achieve higher cell density than the gas injection region. Since the thickness of non-gas injection region was nearly the half of the maximum thickness of gas injection region, the polymer/gas matrix at the non-gas injection region was significantly faster than that of gas injection region. This faster cooling rate yielded the higher crystallization rate and resulted in the higher number of crystallites in the non-gas injection regions. As a result, the cell density values at the non-gas injection regions became noticeably higher than those of the gas injection regions. When the gas injection

pressure was increased, however, the difference between the non-gas injection and the gas injection regions in terms of cell density values became almost negligible. Consequently, the increased gas injection pressure was able to provide very uniform foam structure.

The decoupled foaming mechanism of GAFIM technology provided advantages not only on the cell nucleation but also on the cell growth behaviors. First, the implementation of GAFIM technology provided the increased melt strength of polymer matrix because the delay of foaming reduced the temperature of polymer melt core at the moment of cell nucleation. In addition, the formation of large number of crystallites by the high pressure gas injection also contributed to the increase of melt strength. As a result of these combined effects, the increase of melt strength of polymer matrix prevented the excessive bubble growth during the foaming phase. This was the reason why the average cell sizes of GAFIM were significantly smaller and more uniform than those of FIM samples.

Second, the complete decoupling of filling and foaming phases eliminated the travelling of nucleated bubbles. In the conventional FIM process, the nucleated cells have to travel as they grow and they are exposed to high shear flow of polymer matrix as exhibited in Figure 3.2, Figure 3.3, and Figure 3.4. As a result, more cell coalescences are observed as the flow length of polymer/gas matrix is increased. This cell coalescence phenomenon is often the main reason for non-uniform foam structure along the flow length. When the bubble travel was eliminated by decoupling of filling and foaming phases, however, the nucleated bubbles experienced the minimum degree of deformation and maintained their spherical shapes during their growth stage. Therefore, the

decoupling mechanism enhanced the uniformity of cellular morphology along the flow length of sample. Consequently, the employment of GAFIM technology was able to provide more uniform cell structure despite the flow length of matrix via its decoupling mechanism.

Therefore, the GAFIM technology was able to provide these advantages in the aspects of foaming by overcoming the inherited coupled nature of conventional FIM. The GAFIM was able to produce more uniform and finer cellular morphology. Furthermore, it was observed that the gas injection pressure affected the foaming behavior of the GAFIM by inducing the higher number of crystallites which were effectively utilized as heterogeneous nucleation sites and increased the melt strength of polymer matrix.

4.8 Summary

In this chapter, a number of extensive experimental and simulation studies were discussed in detail. First, the actual experimental results and the simulation results of GAIM technology were examined as an effort to maximize the void fraction (i.e., the degree of gas penetration). Then, the research effort was focused on studying the effects of the proposed GAFIM technology. The GAFIM technology decoupled the filling and the foaming phases and provided a more preferred environment for the cell nucleation dominant foaming. The advantages were the uniform on-set cell nucleation timing throughout the entire sample, the larger degree of local super-saturation, and the higher number of crystallites as heterogeneous nucleation sites. The bubble growth behavior was also improved by the increased the melt strength and the elimination of bubble travel. Although the pressure drop rate and the pressure drop were two critical factors in the

conventional FIM, the gas injection pressure played the most critical role in the foaming mechanism of GAFIM because it determined the crystallization kinetics of polymer/gas matrix during the decoupled filling and foaming phases. Overall, the GAFIM was able to enhance the uniformity of the foam structure and to provide higher cell density values throughout the different locations of foam samples.

Table 4.1 Physical properties of Pellethane® 2355-75A

Physical Properties	Values
Density	1.19 g/cm ³
Melt Flow Index	28.0 g/10 min
Shore A Hardness	79.0 – 87.0

Table 4.2 Common fixed processing conditions of injection molding process for GAIM experiments

Processing Parameters	Values
Barrel Temperature	220 °C
Barrel Screw RPM	36 RPM
Barrel Back Pressure	10~16 MPa
Cooling Time	50 sec
Sprue Break Delay	5 sec
Injection Flow Rate	24 cm ³ /s
Polymer Injection Shot Size	75 vol%

Table 4.3 GAIM processing conditions for the delay time study

GAIM Processing Parameters	Exp. 4.1	Exp. 4.2
Gas Injection Delay Time [sec]	1.0	0.5
1 st Gas Injection Pressure Ramp [MPa/sec]	24.13	24.13
1 st Gas Injection Pressure [MPa]	13.79	13.79
1 st Gas Injection Duration [sec]	2.0	2.0
2 nd Gas Injection Pressure Ramp [MPa/sec]	6.89	6.89
2 nd Gas Injection Pressure [MPa]	10.34	10.34
2 nd Gas Injection Duration [sec]	1.0	1.0

Table 4.4 GAIM processing conditions for the gas injection pressure study

GAIM Processing Parameters	Exp. 4.3	Exp. 4.4	Exp. 4.5
Gas Injection Delay Time [sec]	0.5	0.5	0.5
1 st Gas Injection Pressure Ramp [MPa/sec]	24.13	24.13	24.13
1 st Gas Injection Pressure [MPa]	5.17	10.34	13.79
1 st Gas Injection Duration [sec]	3.0	3.0	3.0

Table 4.5 GAIM processing conditions for the gas injection pressure profile

GAIM Processing Parameters	Exp. 4.6	Exp. 4.7
Gas Injection Delay Time [sec]	0.5	0.5
1 st Gas Injection Pressure Ramp [MPa/sec]	24.13	24.13
1 st Gas Injection Pressure [MPa]	13.79	13.79
1 st Gas Injection Duration [sec]	2.0	2.0
2 nd Gas Injection Pressure Ramp [MPa/sec]	6.89	6.89
2 nd Gas Injection Pressure [MPa]	10.34	10.34
2 nd Gas Injection Duration [sec]	1.0	1.0
3 rd Gas Injection Pressure Ramp [MPa/sec]	6.89	6.89
3 rd Gas Injection Pressure [MPa]	6.89	6.89
3 rd Gas Injection Duration [sec]	10	30

Table 4.6 Fixed processing parameters for Moldflow[®]

Fixed Processing Parameter for Moldflow[®]	Values
Melt Temperature	220 °C
Mold Temperature	30 °C
Injection Flow Rate	24 cm ³ /s
Polymer Injection Shot Size	75 vol%

Table 4.7 GAIM processing parameters for CO₂ experiment

GAIM Processing Parameters	Values
Gas Injection Delay Time [sec]	2.0
1 st Gas Injection Pressure Ramp [MPa/sec]	24.13
1 st Gas Injection Pressure [MPa]	13.79
1 st Gas Injection Duration [sec]	3.0

Table 4.8 Common processing parameters for the pressurized case

Processing Parameters	Values
Processing Temperature	220 °C
Mold Temperature	30 °C
Injection Flow Rate	24 cm ³ /s
Polymer Injection Shot Size	80 vol%
N ₂ content	0.3 wt%
Cooling Time	40 sec
Sprue-break Delay Time	3.0 sec

Table 4.9 GAIM processing conditions for the pressurized case

GAIM Processing Parameters	Values
Gas Injection Delay Time [sec]	2.0
1 st Gas Injection Pressure Ramp [MPa/sec]	24.13
1 st Gas Injection Pressure [MPa]	13.79
1 st Gas Injection Duration [sec]	3.0

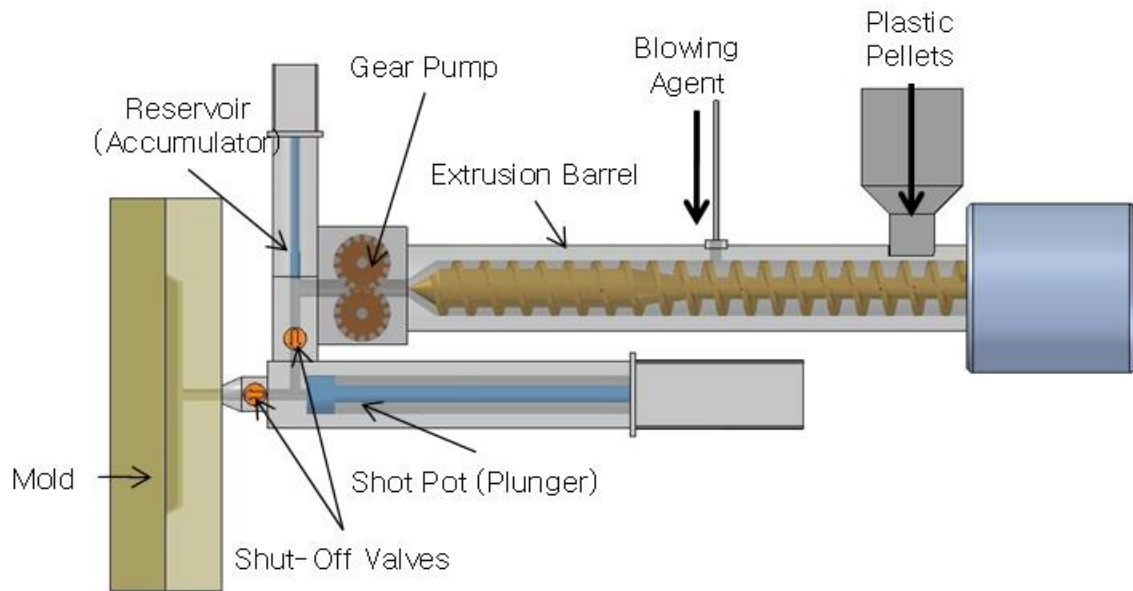


Figure 4.1 Schematic of advanced structural foam molding machine [75]



Figure 4.2 Arburg ALLROUNDER 270C [187]

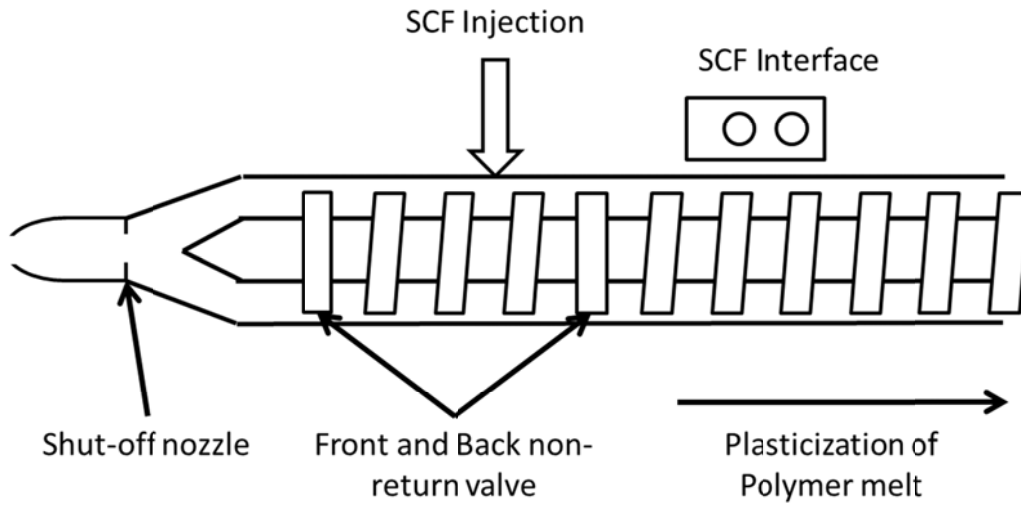


Figure 4.3 Schematic of MuCell[®] system setup

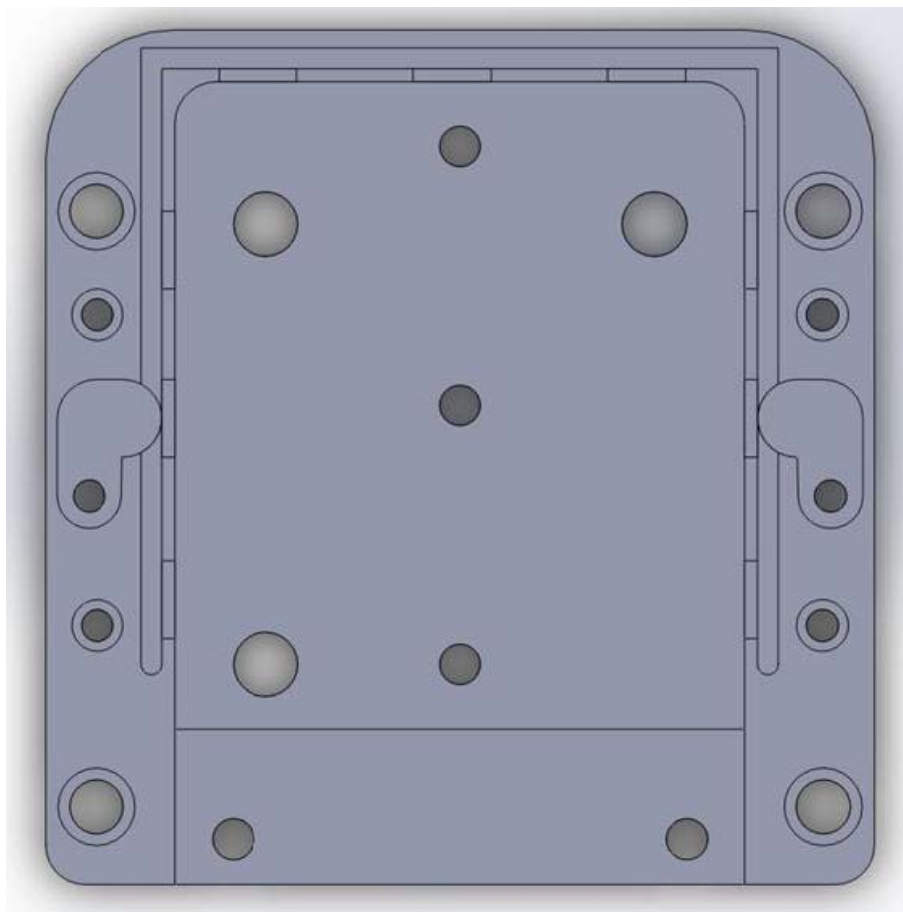


Figure 4.4 Original cavity drawing

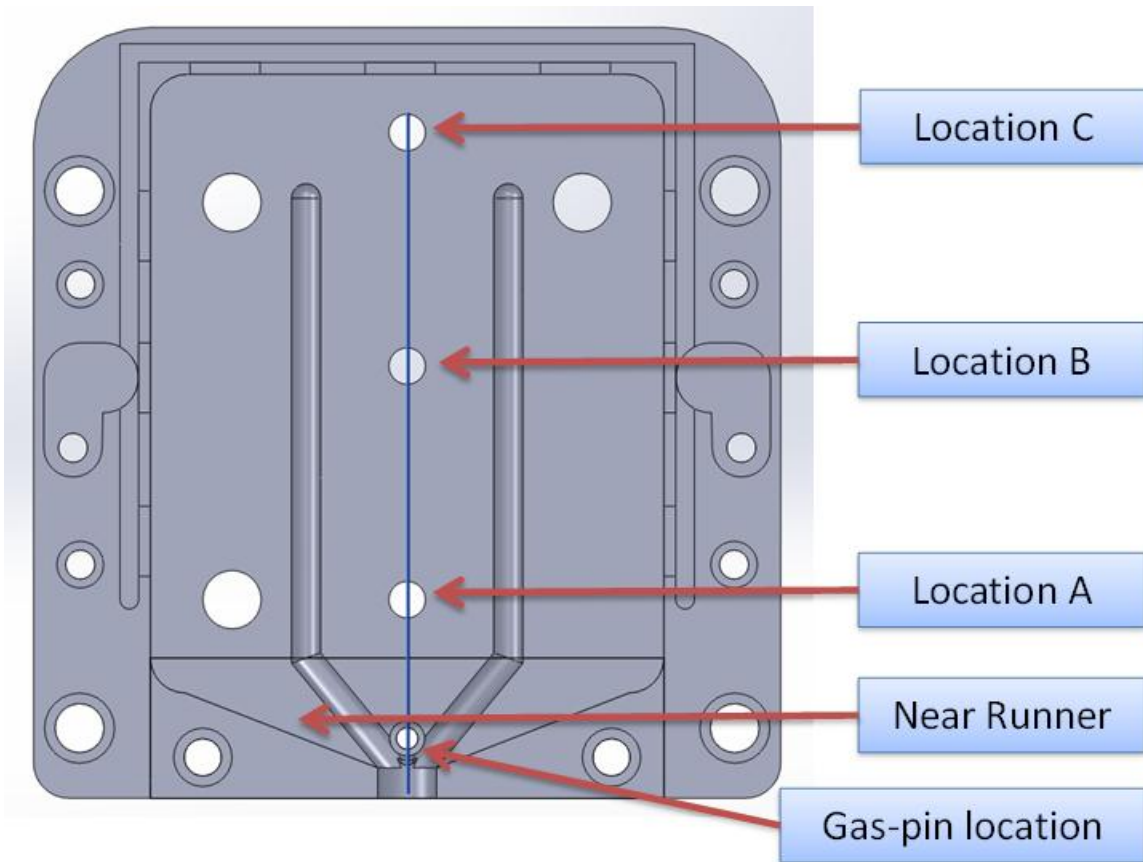


Figure 4.5 Modified cavity with gas channels and measurement locations

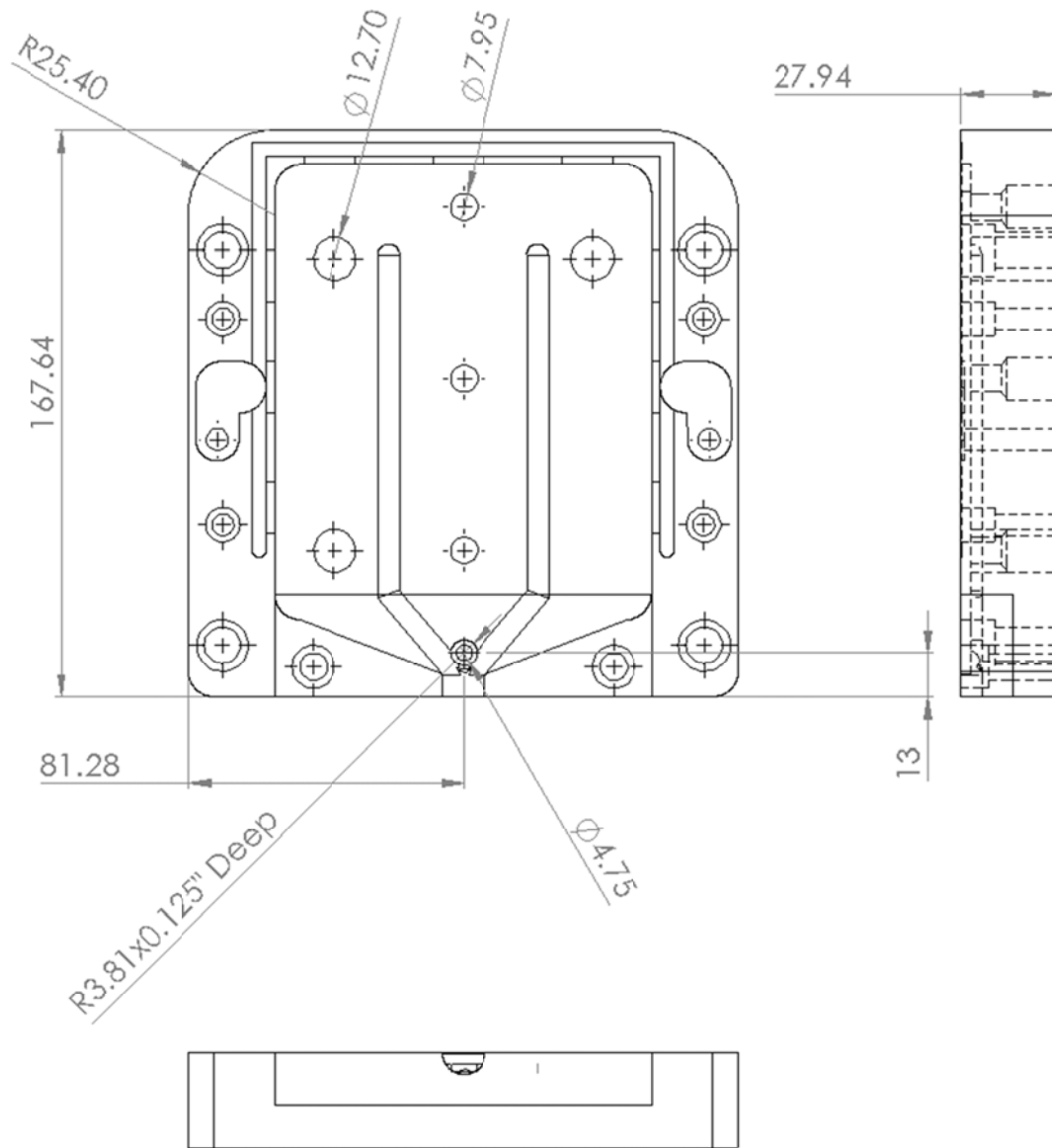


Figure 4.6 Engineering drawing of cavity with gas channels

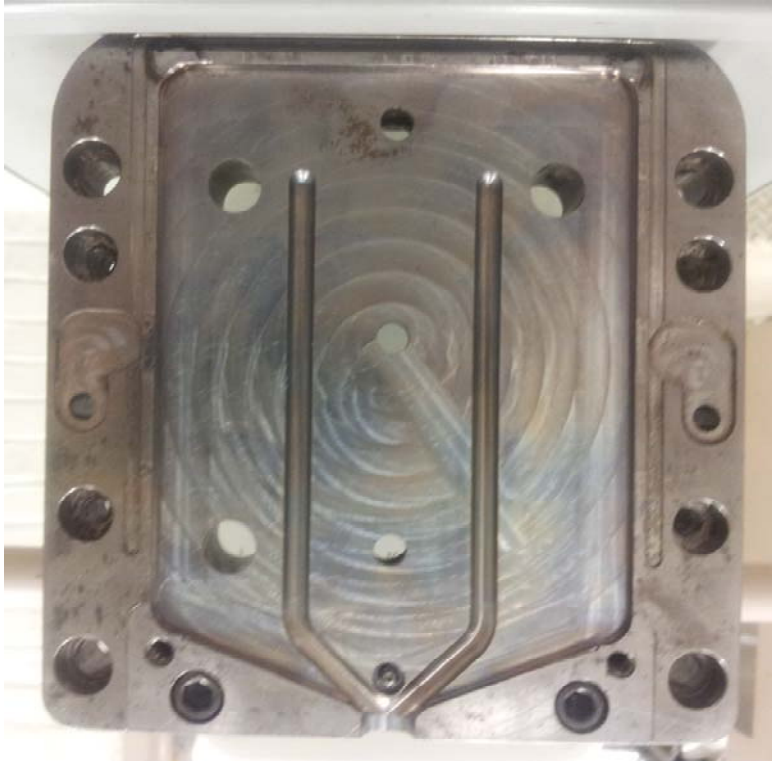


Figure 4.7 Picture of actual cavity insert with gas channels

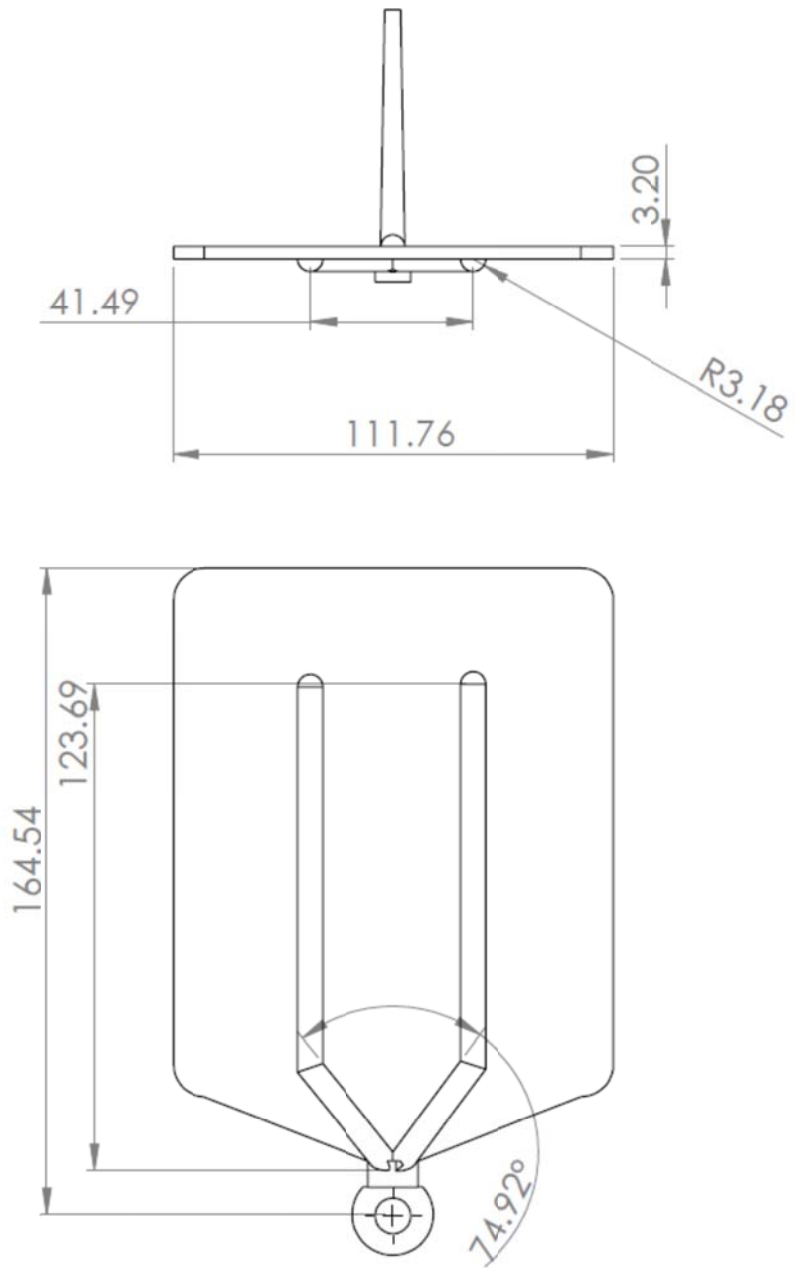


Figure 4.8 Drawing of sample part with gas channels

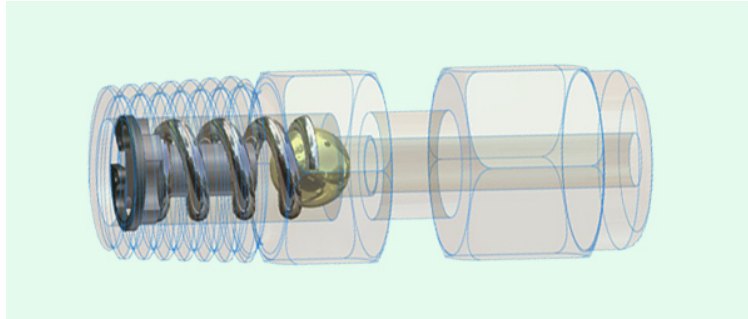


Figure 4.9 Spring-loaded check valve

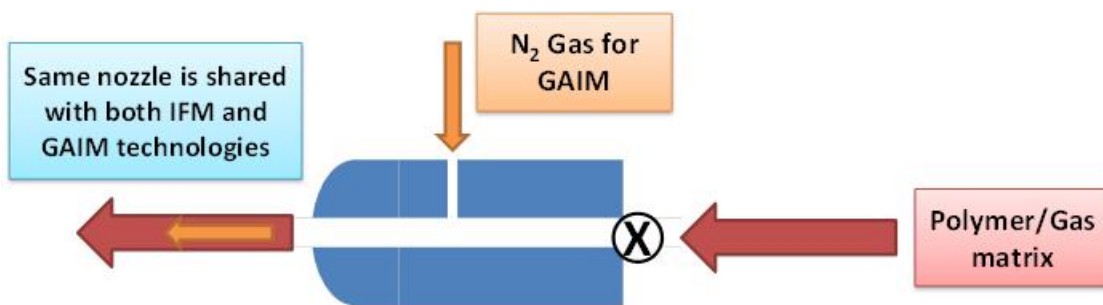


Figure 4.10 Schematic of 'through nozzle' gas injection system



Figure 4.11 Effect of gas injection delay time

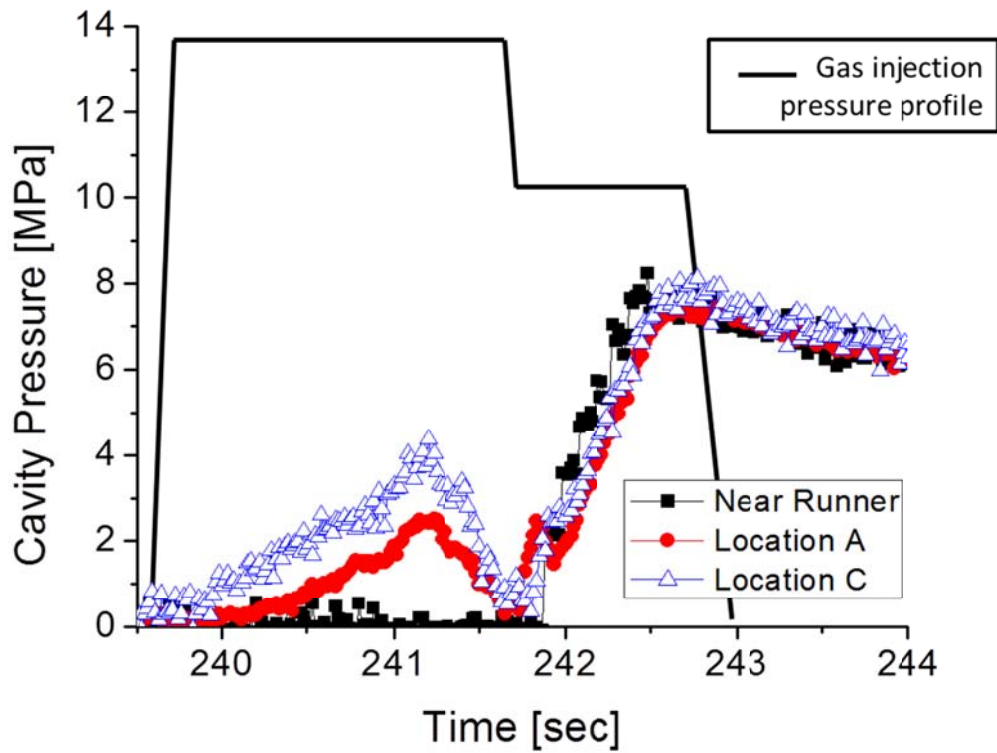


Figure 4.12 Cavity pressure profile when GAIM was applied



Figure 4.13 Effect of gas injection pressure

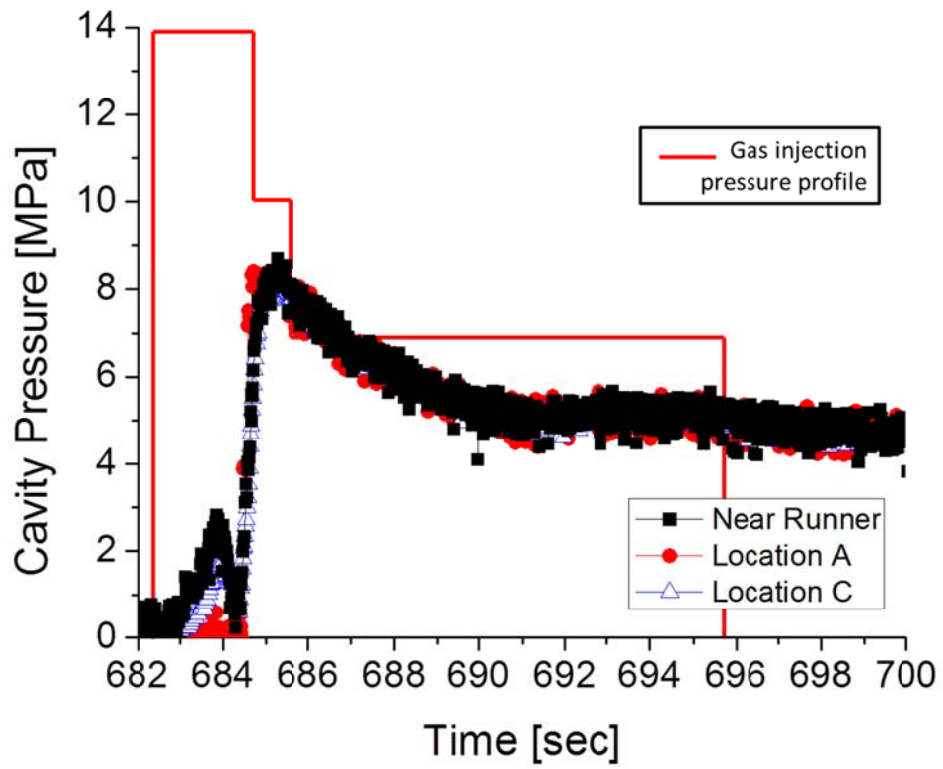


Figure 4.14 Cavity pressure profile of Exp. 4.6

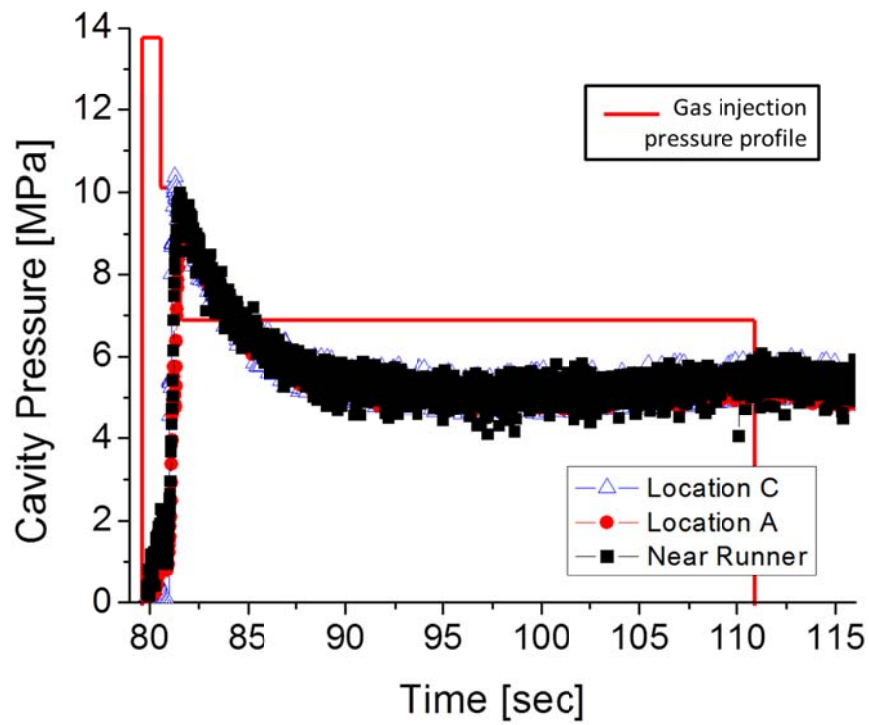


Figure 4.15 Cavity pressure profile of Exp. 4.7

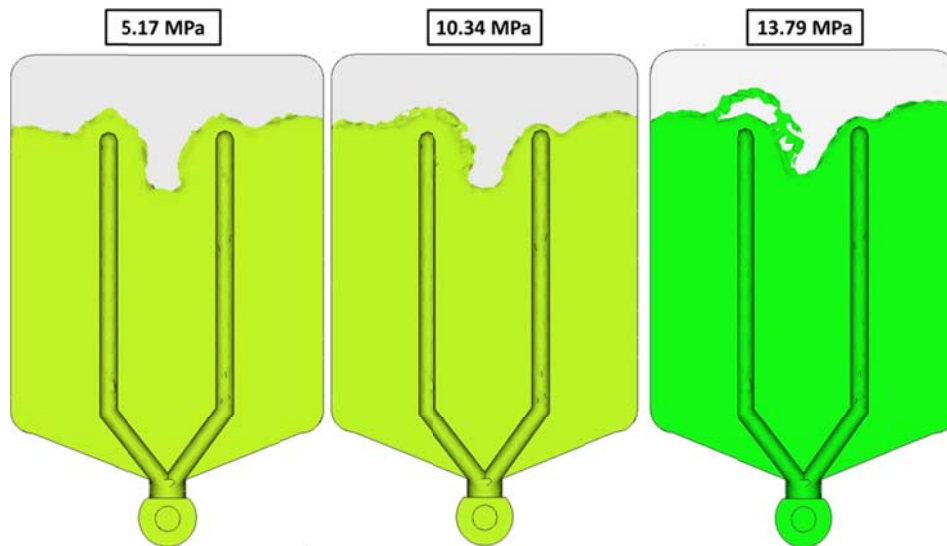


Figure 4.16 Filled polymer volumes by gas injection pressure changes based on

Moldflow[®]

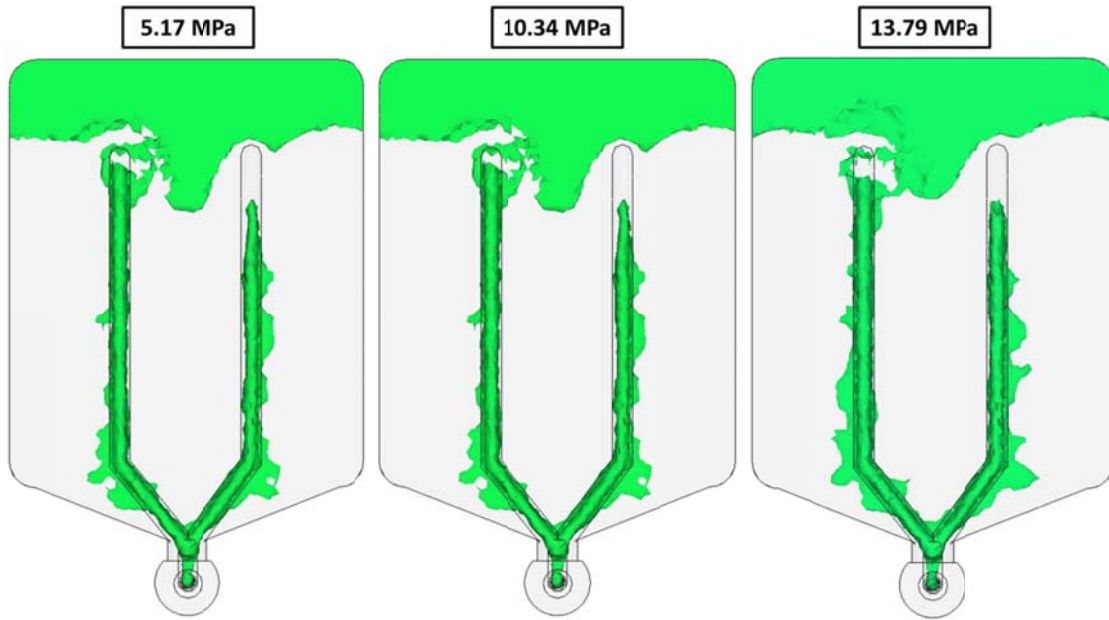


Figure 4.17 Voids created by GAIM based on Moldflow[®]

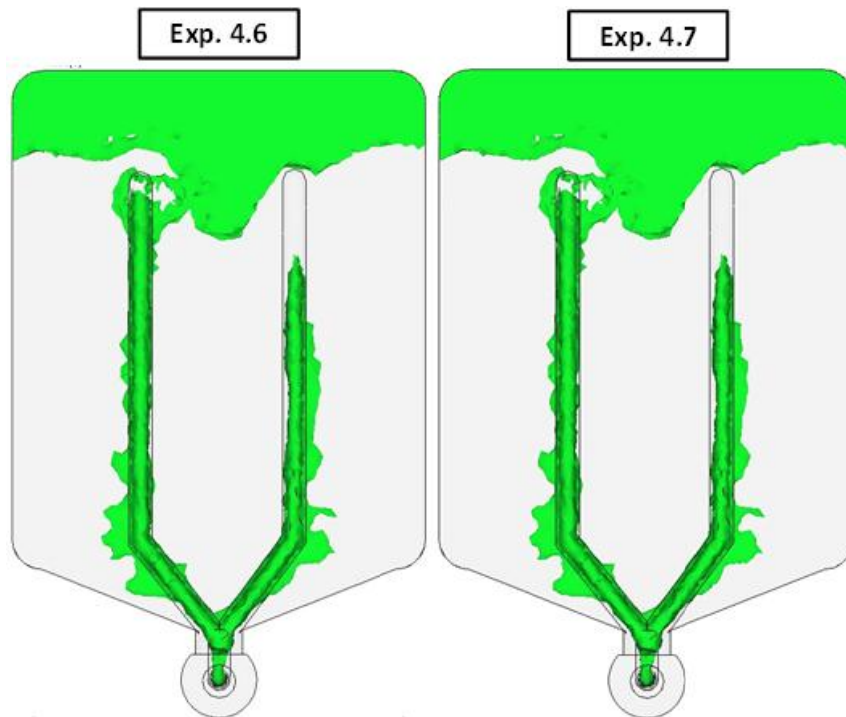


Figure 4.18 Gas voids from different GAIM pressure profiles

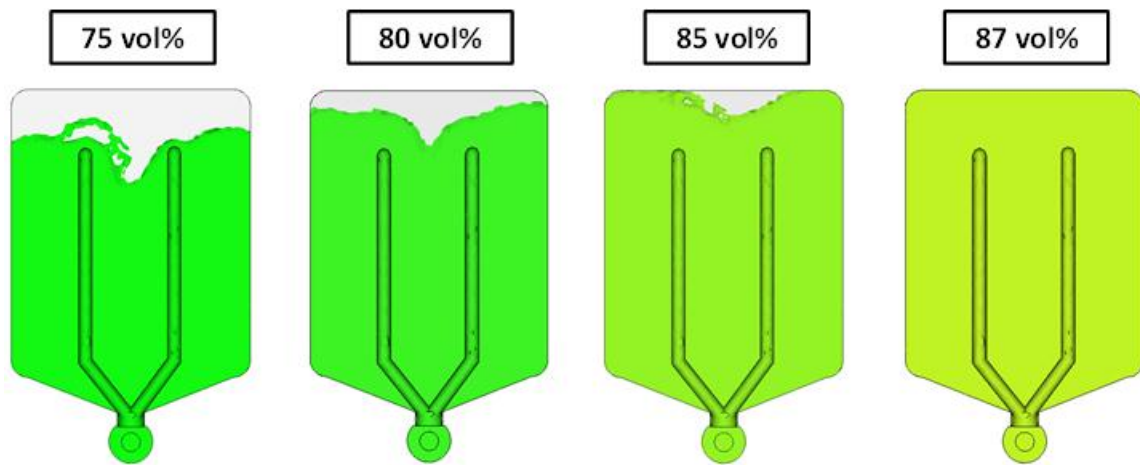


Figure 4.19 The effects of shot sizes on the degree of filling of GAIM samples

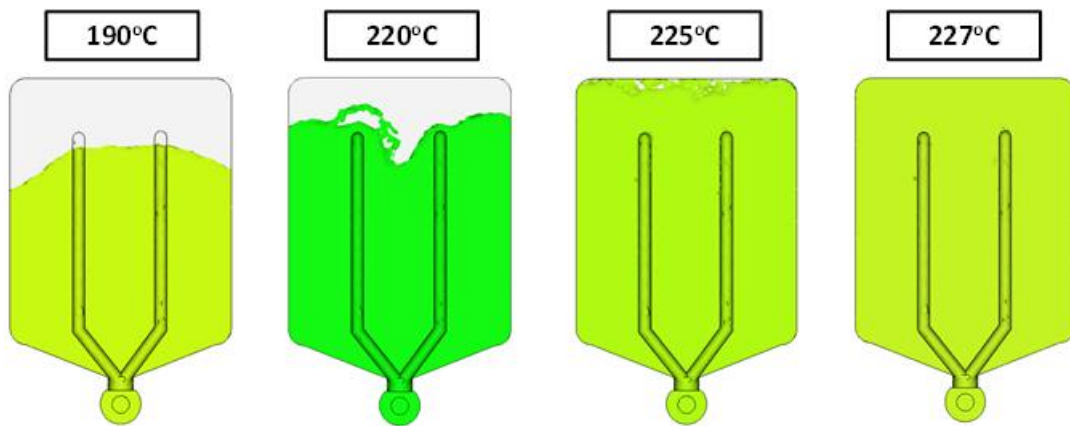


Figure 4.20 The effects of melt temperature on the degree of filling of GAIM samples

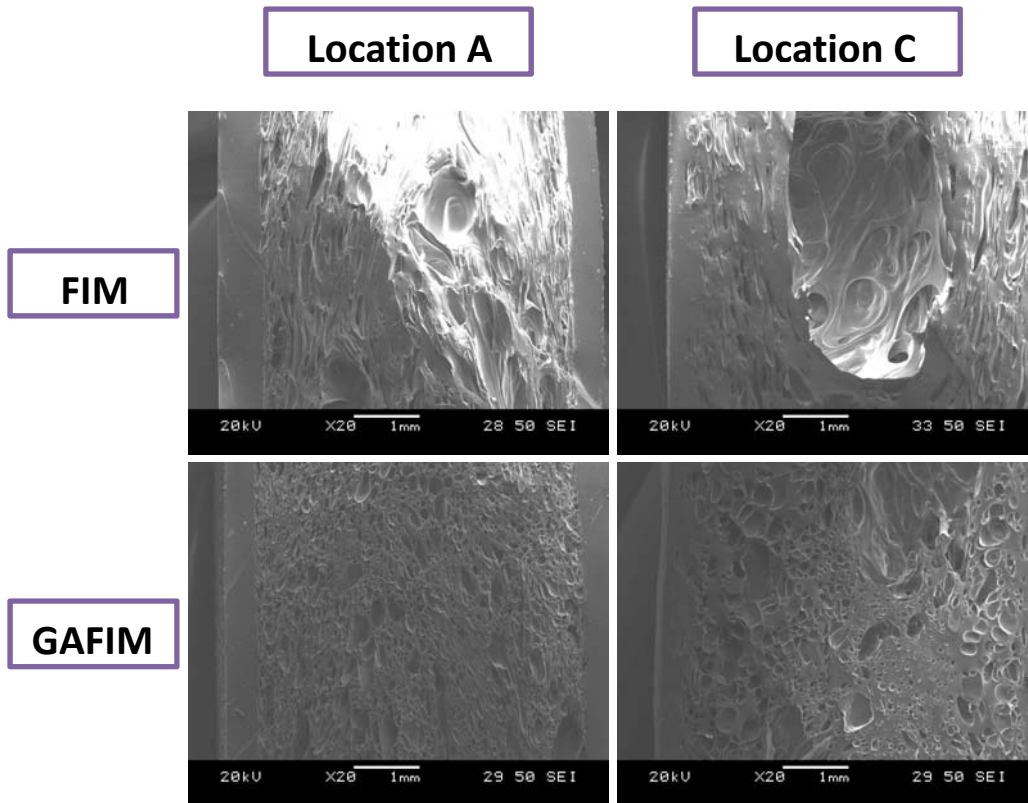


Figure 4.21 SEM pictures of FIM and GAFIM samples with 35 vol% of void fraction setting

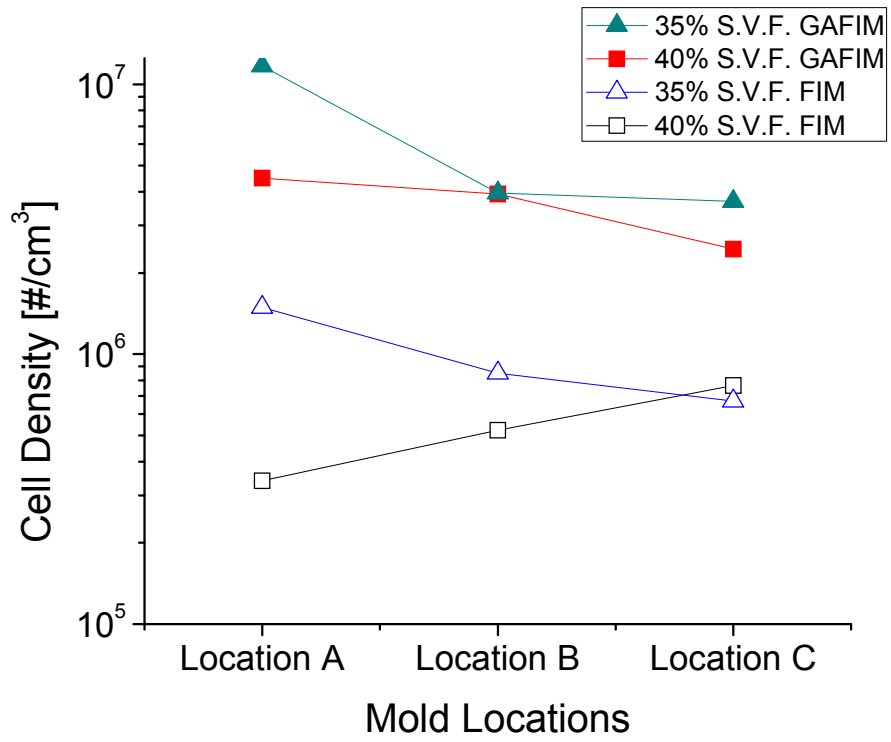


Figure 4.22 Cell density values of both FIM and GAFIM samples

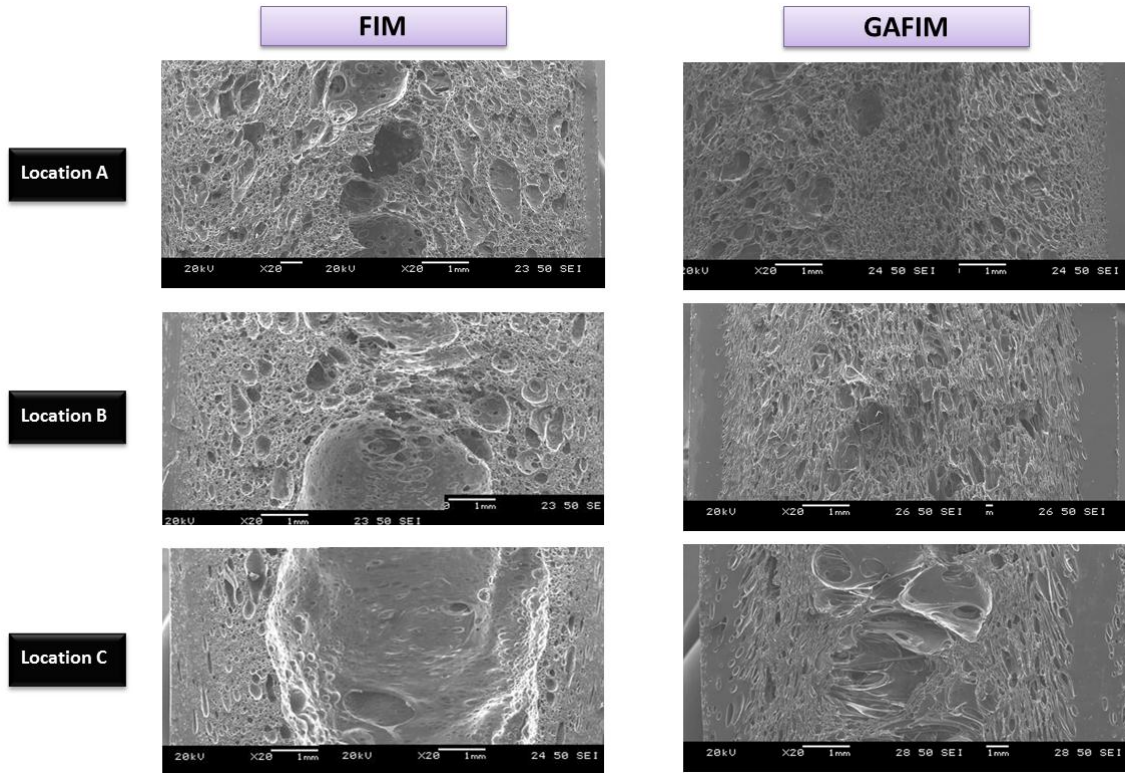


Figure 4.23 Cellular morphologies of FIM and GAFIM samples with N₂ as PBA

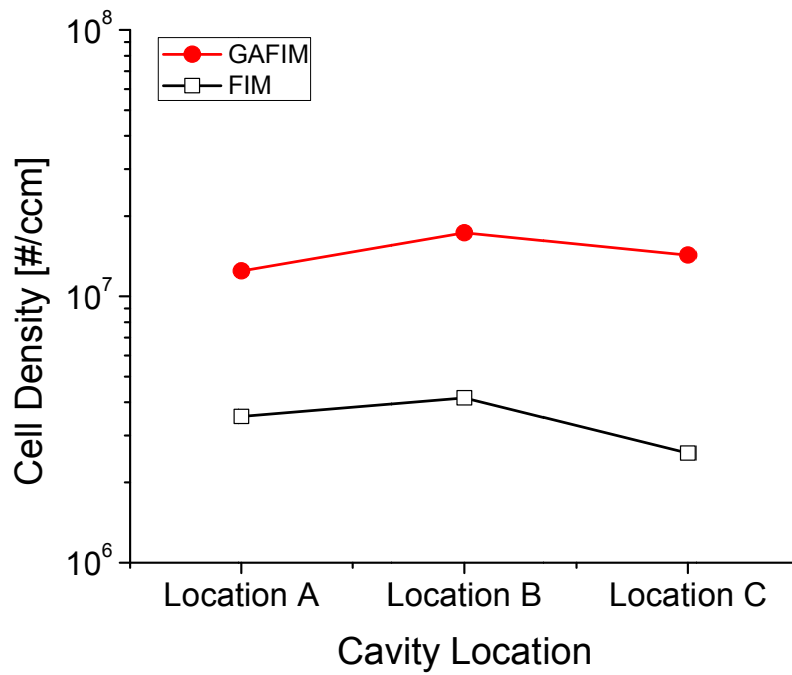


Figure 4.24 Cell density values of FIM and GAFIM at three different locations

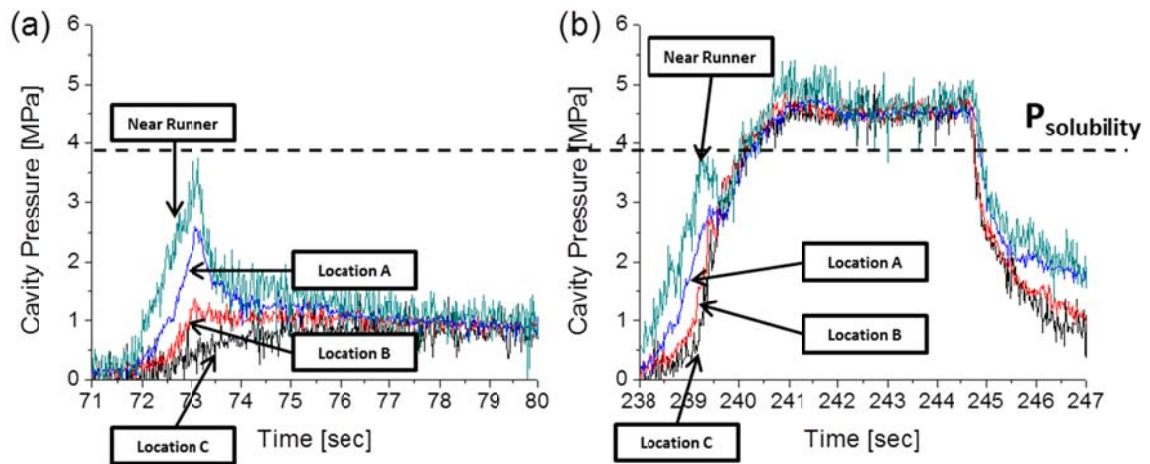


Figure 4.25 Cavity pressure profiles of (a) FIM and (b) GAFIM for 35 vol% void fraction setting and N_2 as PBA

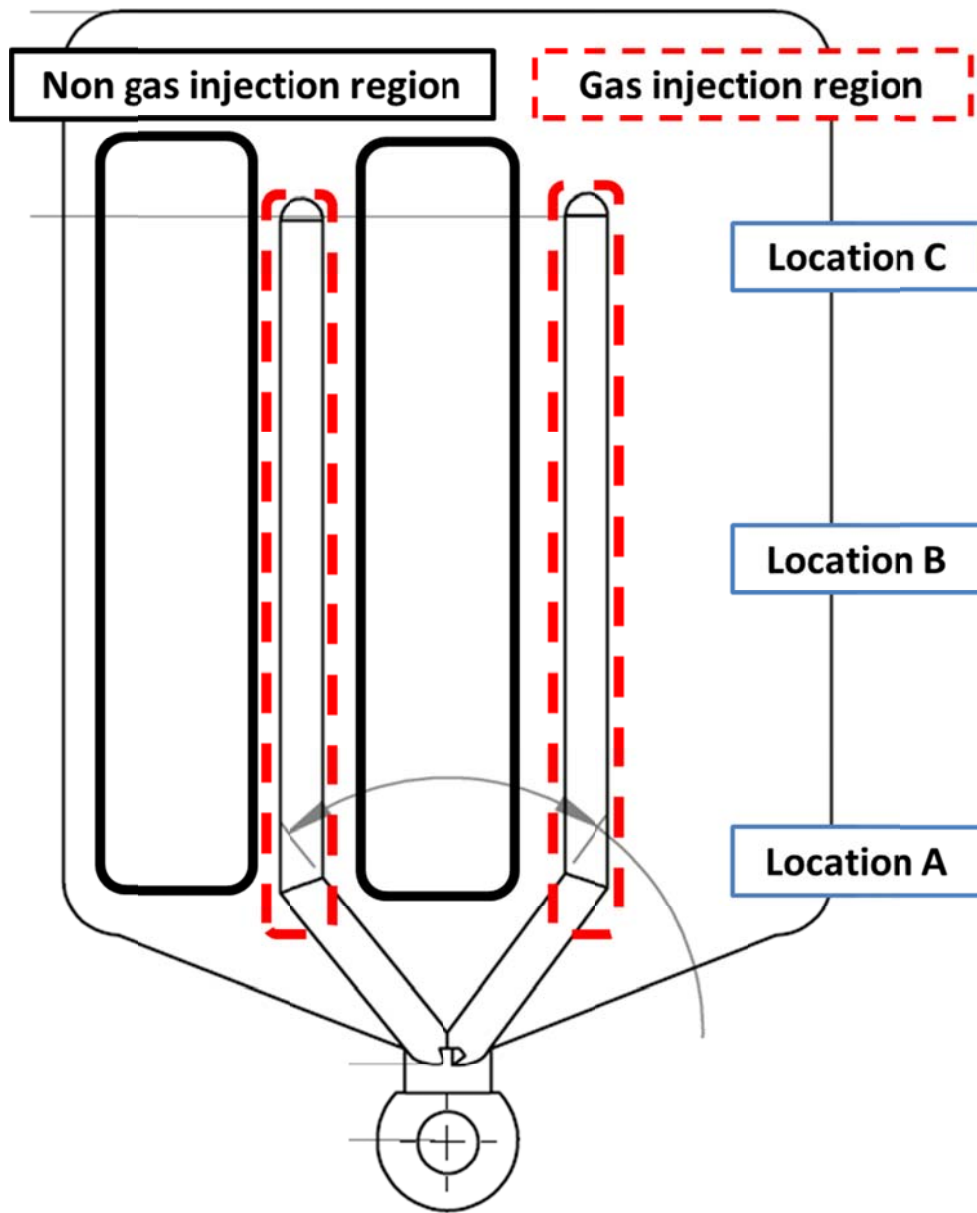


Figure 4.26 Measurement locations of non-gas injection and gas injection regions in a foamed sample

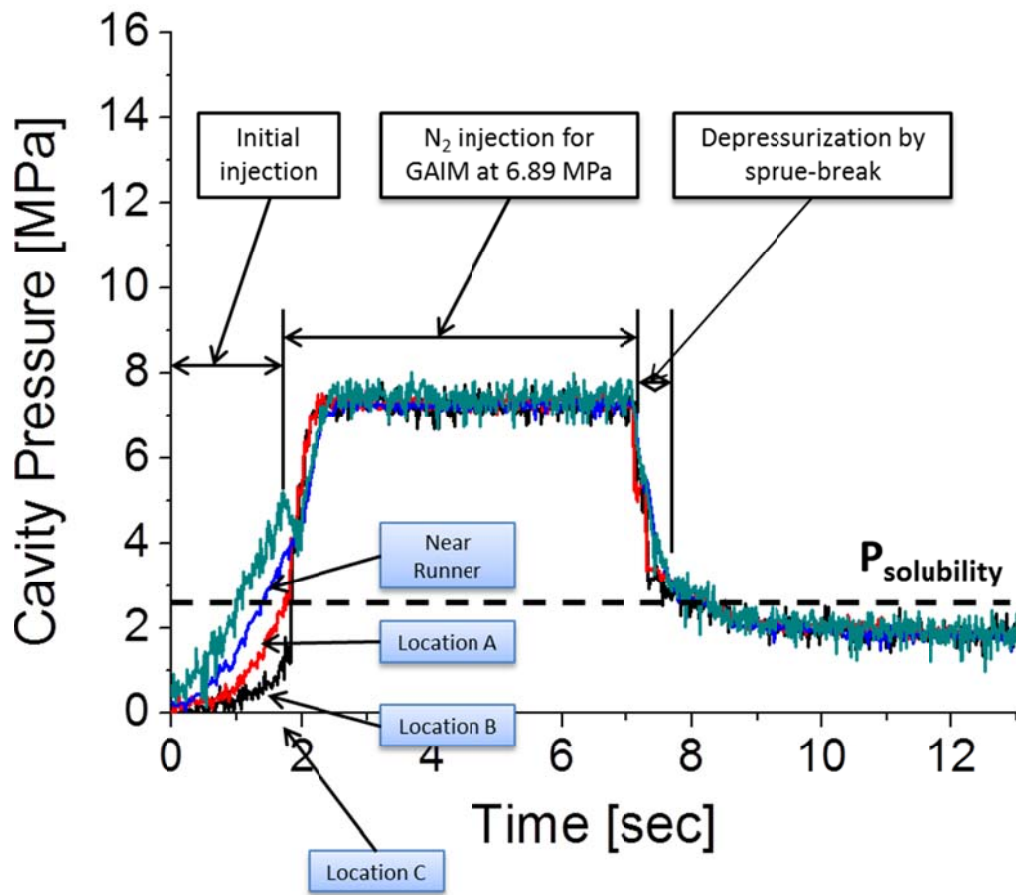


Figure 4.27 Cavity pressure profiles of medium GAIM pressure experiment

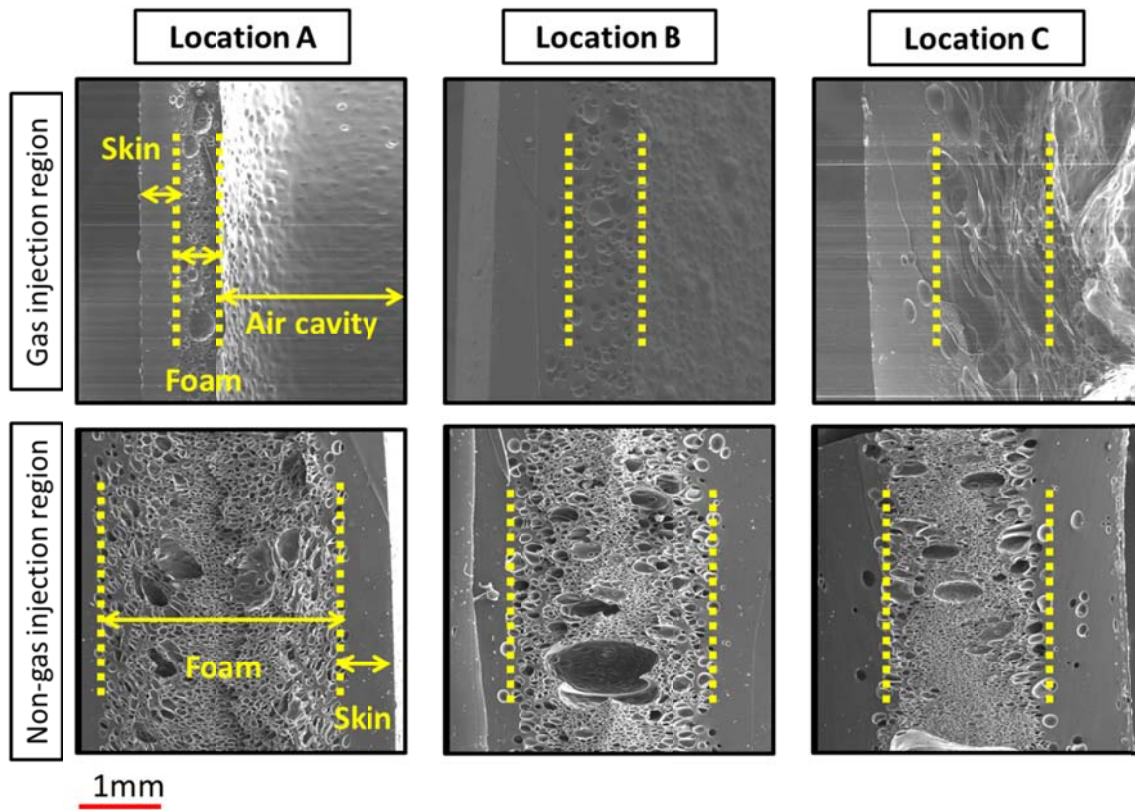


Figure 4.28 SEM images of gas injection (GI) and non-gas injection (NGI) regions of GAFIM sample

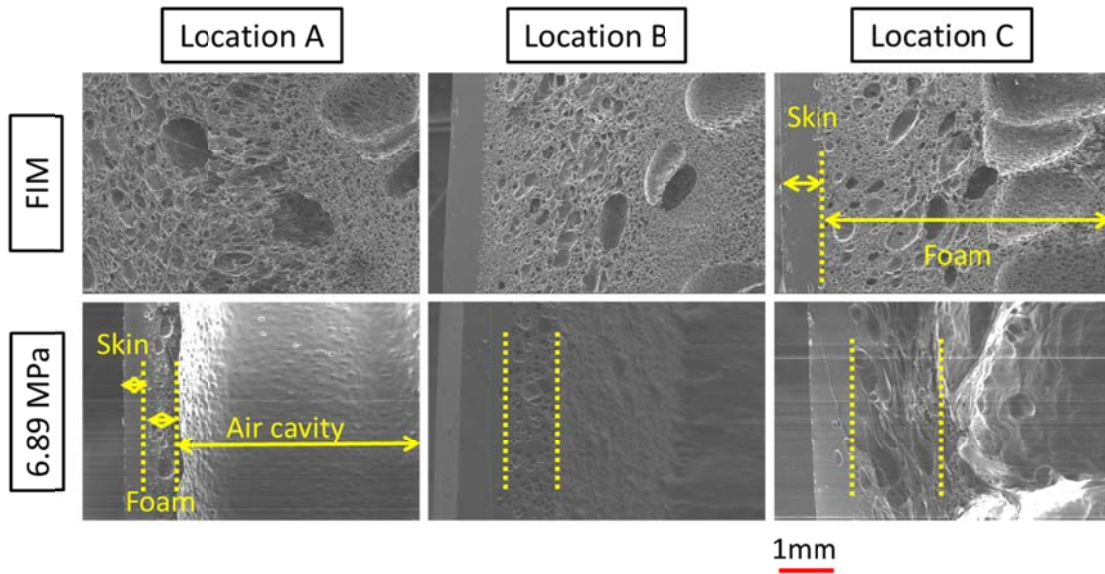


Figure 4.29 SEM pictures of FIM and GAFIM samples at gas injection (GI) regions

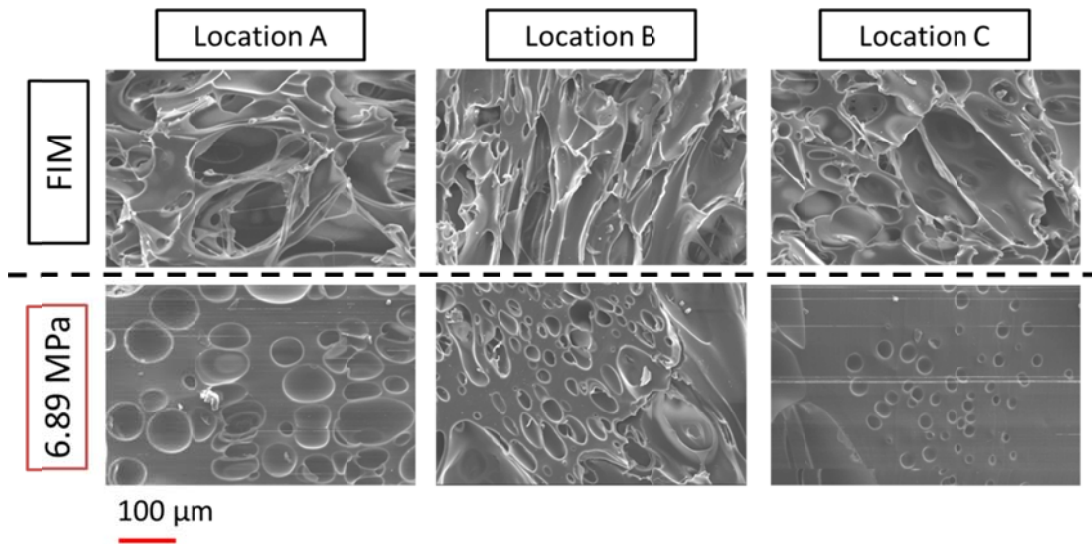


Figure 4.30 SEM pictures of both FIM and GAFIM (6.89 MPa of gas injection pressure) samples at gas injection regions

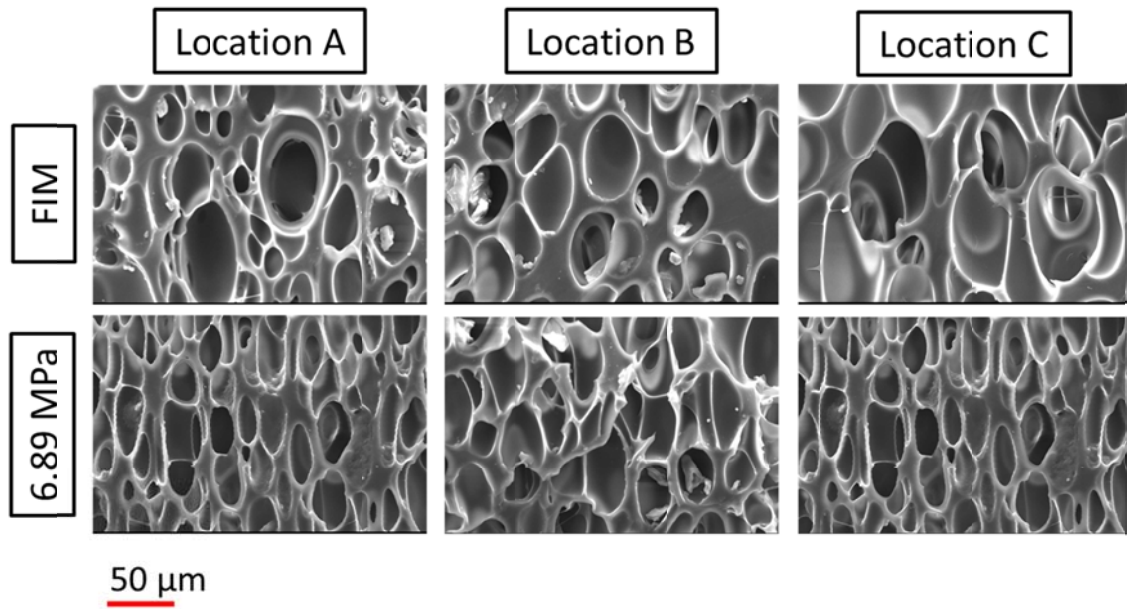


Figure 4.31 Magnified SEM images of both FIM and GAFIM samples at non-gas injection (NGI) regions

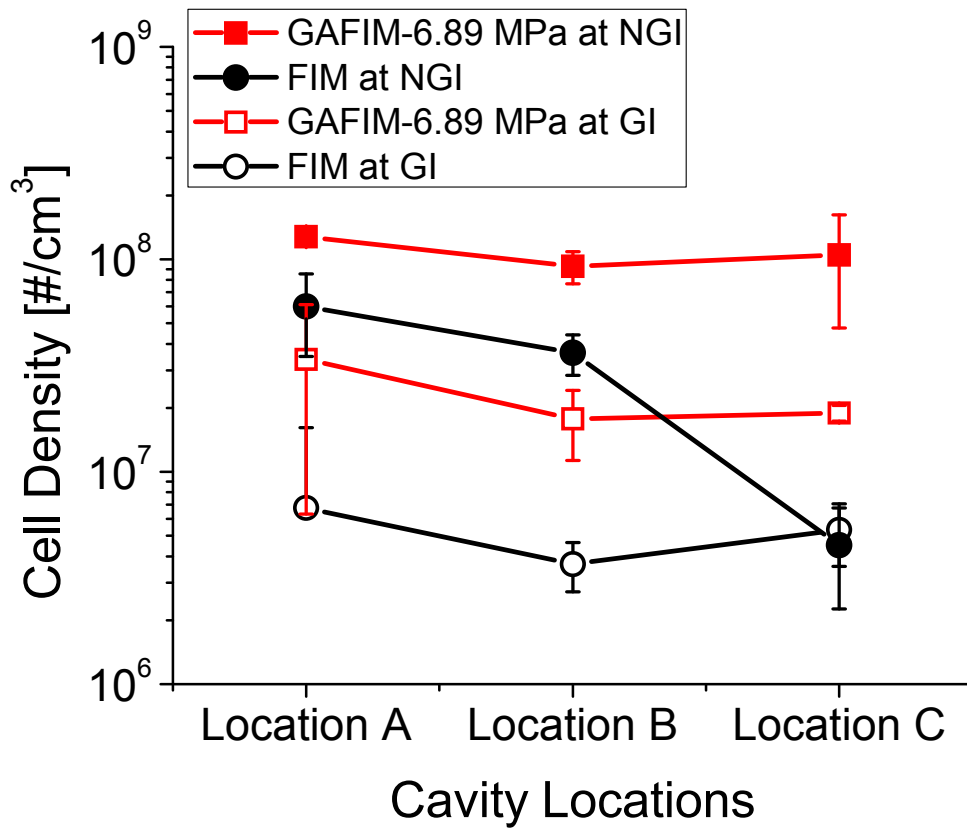


Figure 4.32 Cell density changes at both gas injection (GI) and non-gas injection (NGI) regions due to the implementation of GAFIM

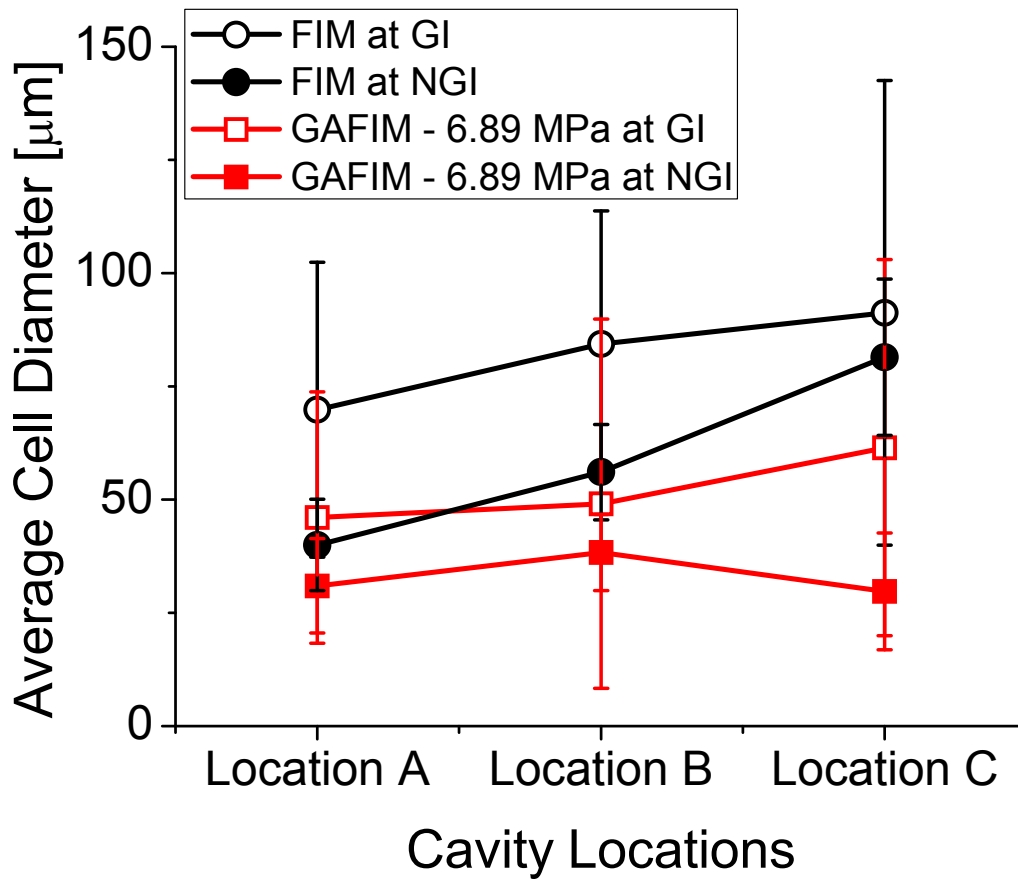


Figure 4.33 Average cell diameters at both gas injection (GI) and non-gas injection (NGI) regions of FIM and GAFIM samples

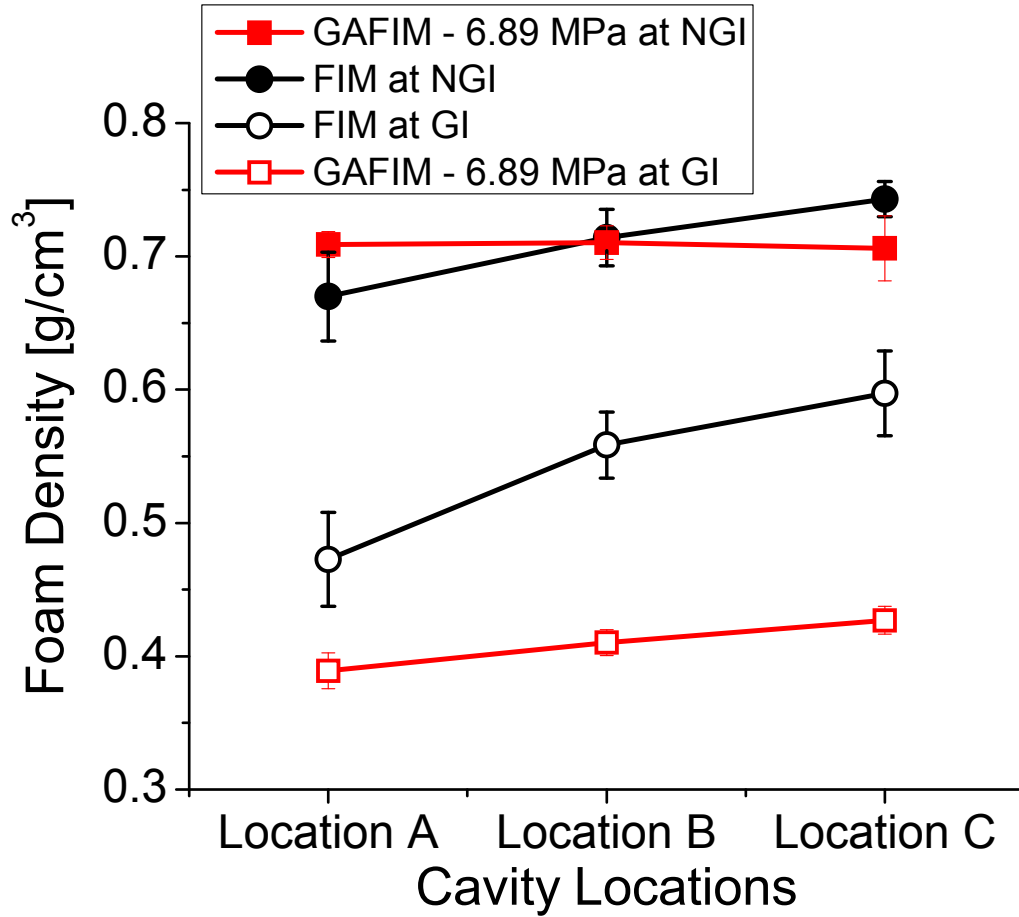


Figure 4.34 Average foam density values at gas injection (GI) and non-gas injection (NGI) regions of FIM and GAFIM samples

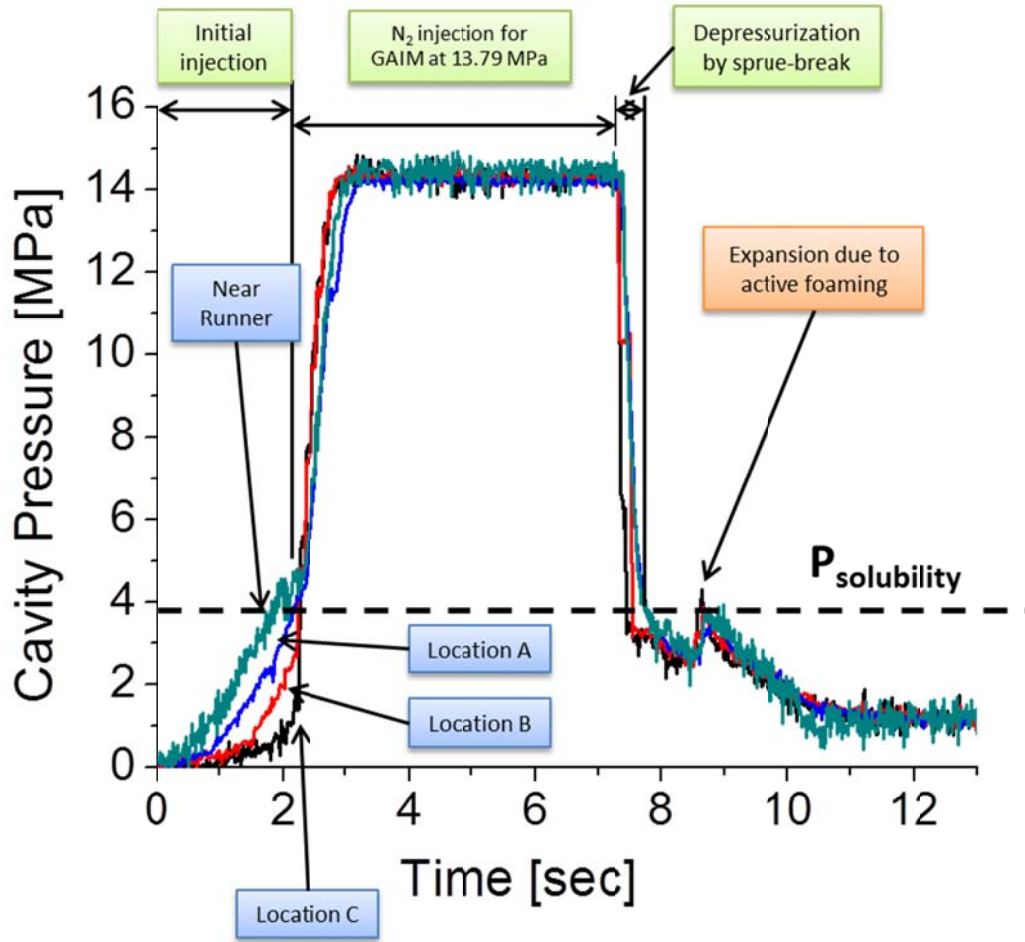


Figure 4.35 Cavity pressure profile of highly pressurized cavity case with 13.79 MPa of gas injection pressure

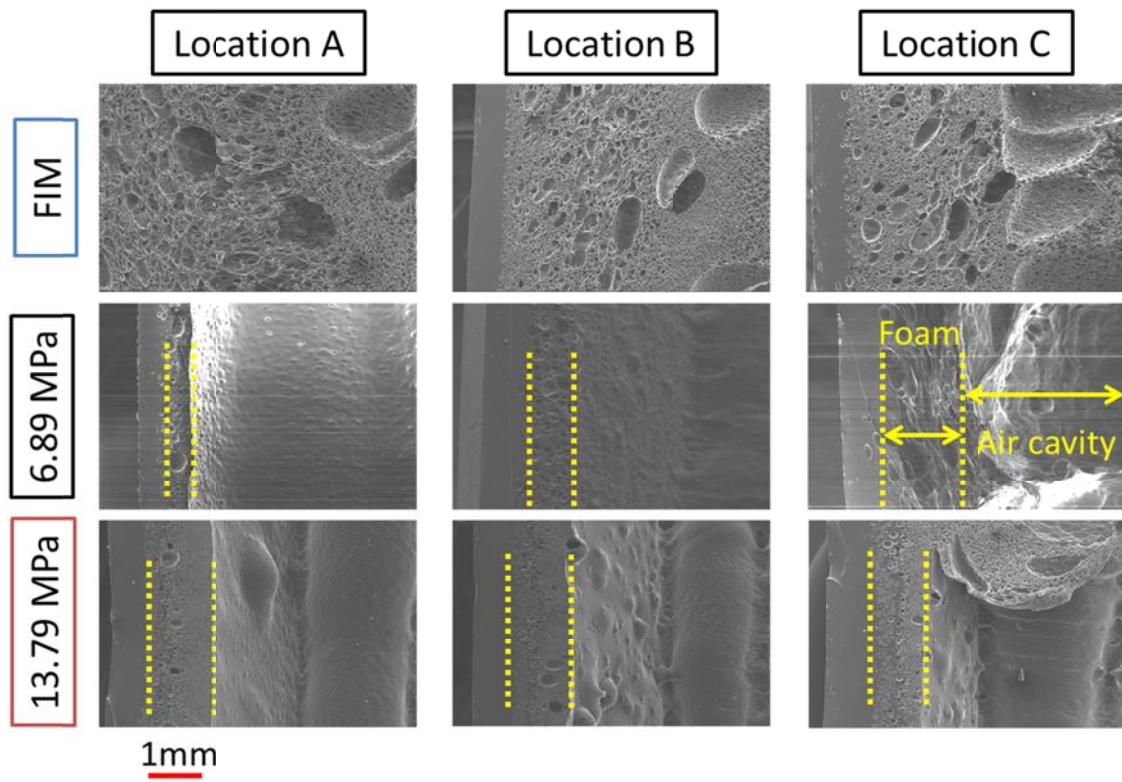


Figure 4.36 SEM pictures of gas injection (GI) regions for FIM and two GAFIM cases

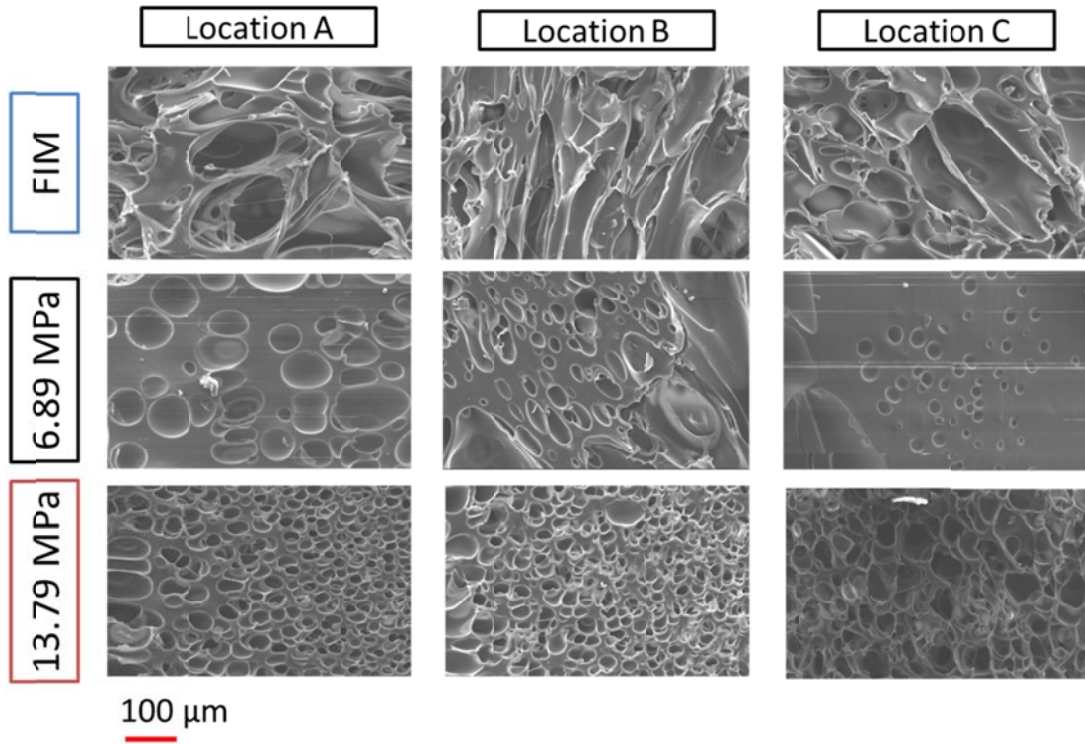


Figure 4.37 Magnified SEM pictures of gas injection (GI) regions for FIM and two GAFIM cases

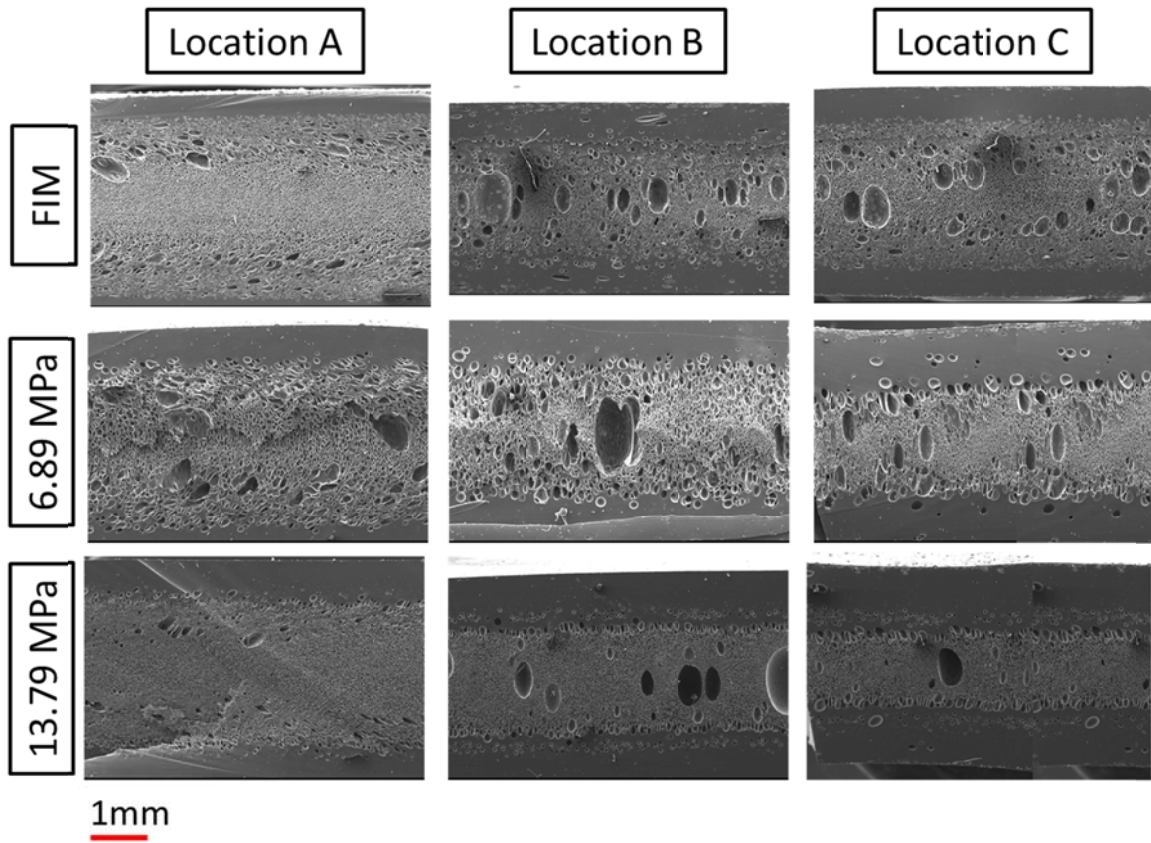


Figure 4.38 SEM images of non-gas injection regions (NIG) for FIM and two GAFIM cases

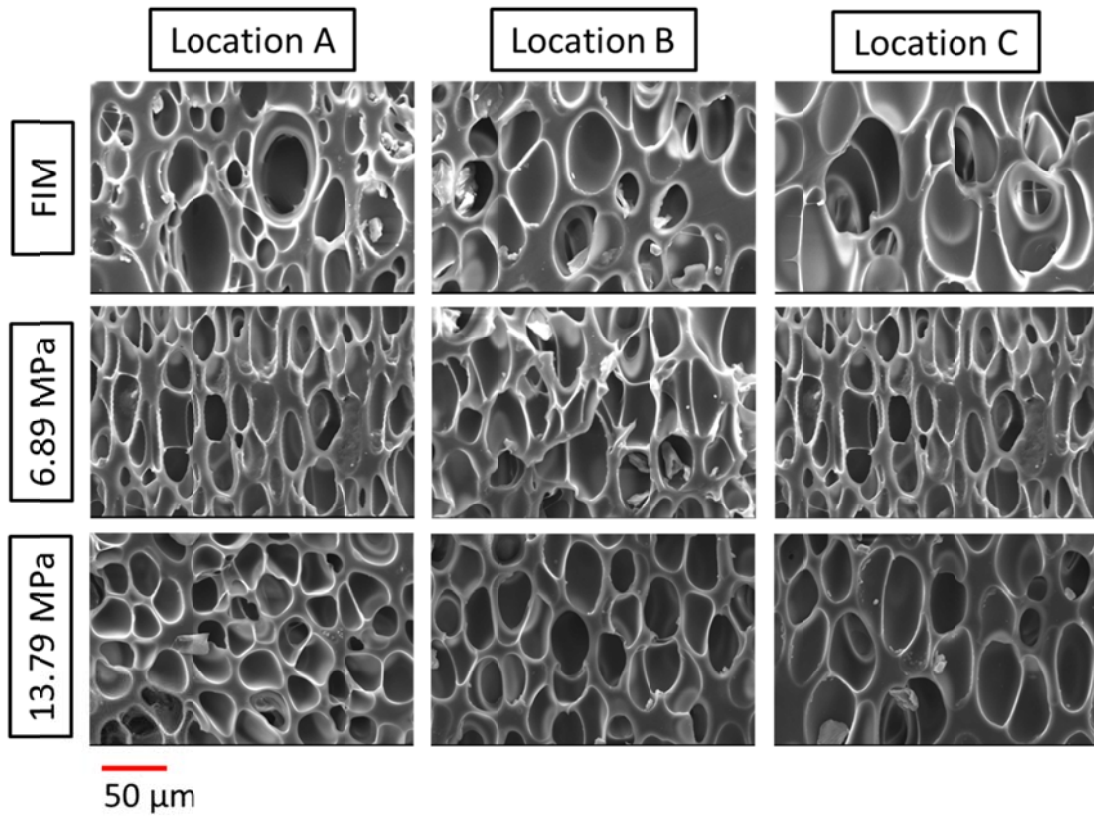


Figure 4.39 Magnified SEM images of non-gas injection (NGI) regions for FIM and both GAFIM cases

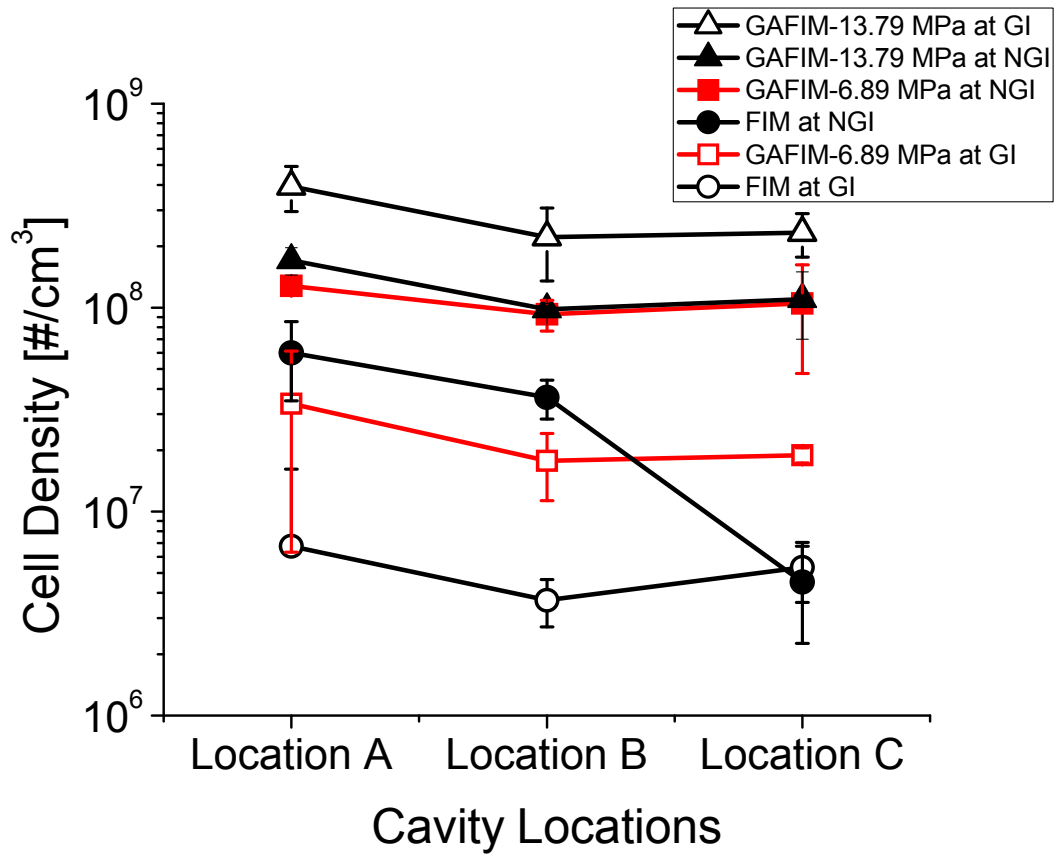


Figure 4.40 Cell density changes of gas injection (GI) and non-gas injection (NGI) areas due to the increase of gas injection pressure of GAFIM

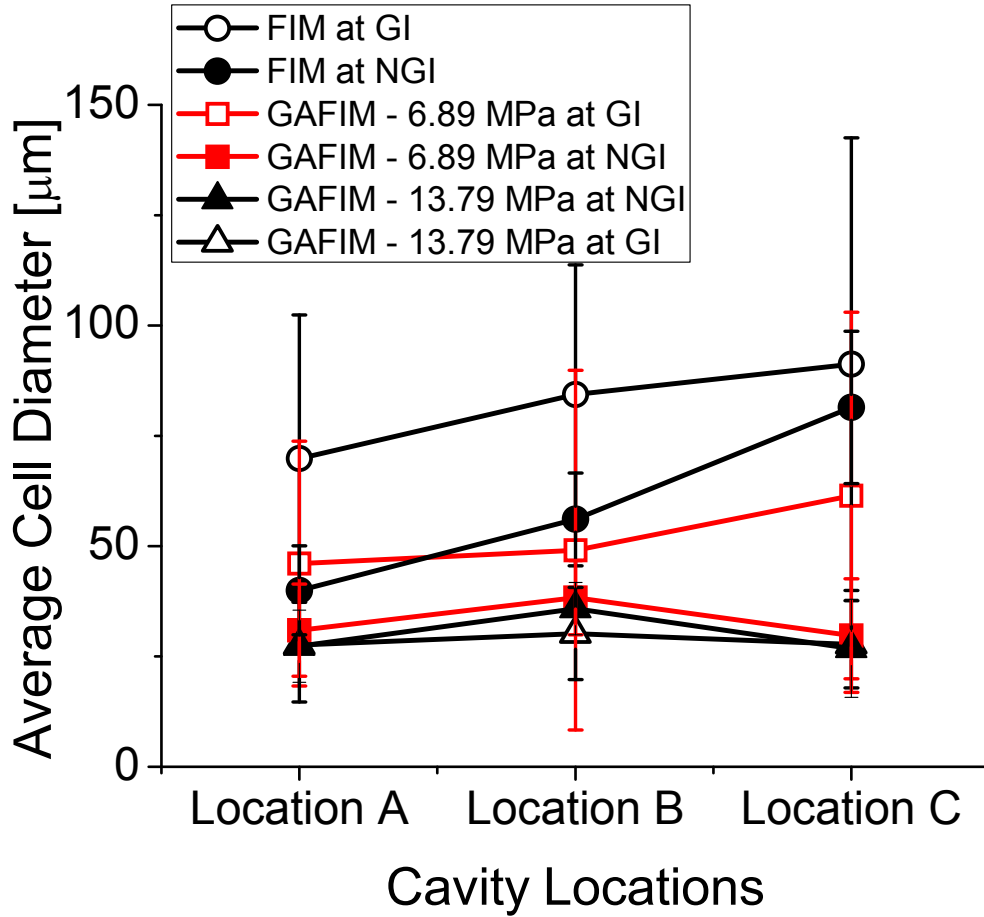


Figure 4.41 Average cell diameter values of gas injection (GI) and non-gas injection (NGI) regions for FIM and two GAFIM cases

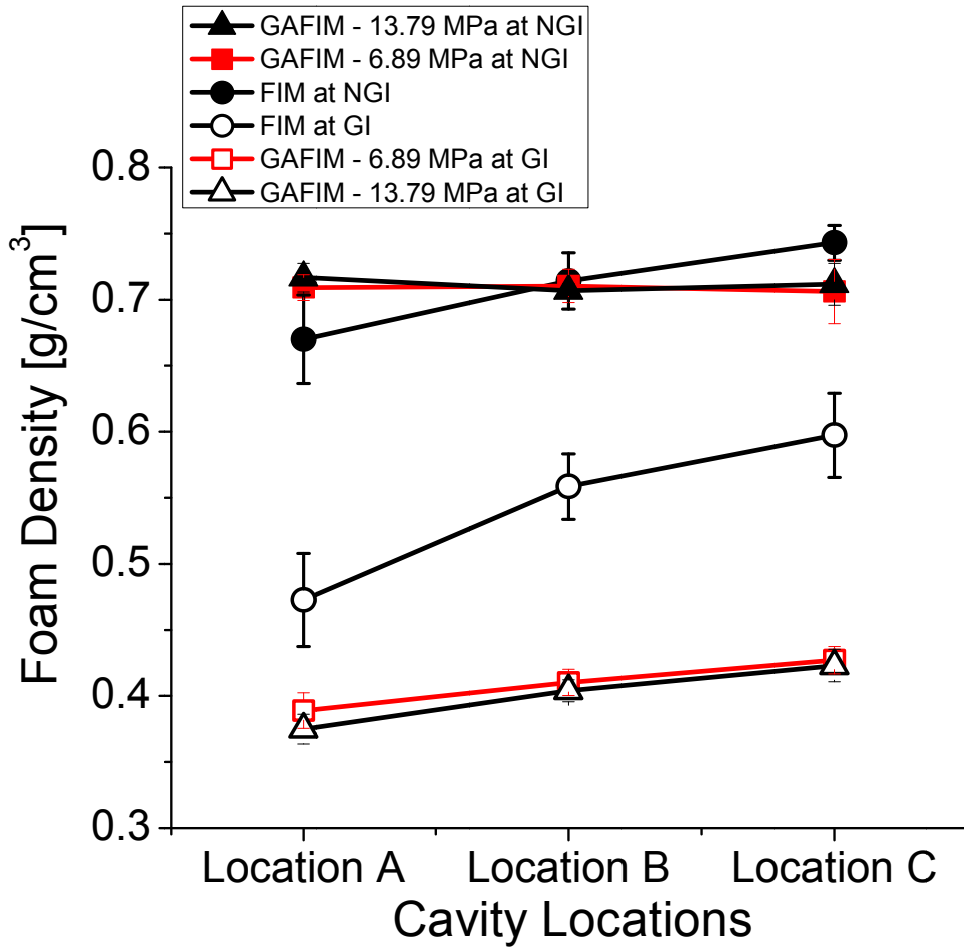


Figure 4.42 Average foam density values at gas injection (GI) and non-gas injection (NGI) regions of FIM and two GAFIM cases

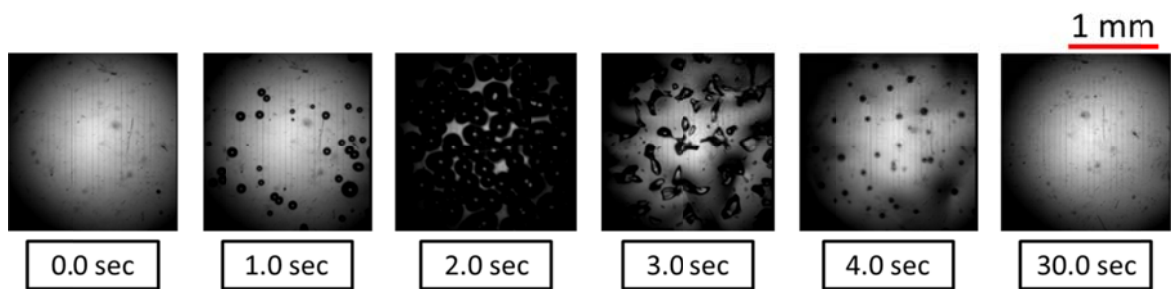


Figure 4.43 Images from the visualization batch foaming system with respect to time

Chapter 5 Acoustic Property

Characterization of the Manufactured

Foams

5.1 Introduction

In this thesis study, two acoustic functions were evaluated: acoustic absorption coefficients and acoustic transmission losses. The acoustic absorption coefficient represents the effectiveness of absorption of a normal acoustic wave that hits the tested sample at each measured frequency. The acoustic transmission loss represents the acoustic insulation behavior and also quantifies how much acoustic noise is being blocked by the tested sample.

In order to measure these two acoustic properties, a commercial impedance tube testing setup from BSWA was employed. The impedance tube testing setup had two different sizes of tubes, 100 mm and 30 mm, depending on the testing frequency range. For 100-mm diameter testing tube, the measuring frequency was from 100 to 1600 Hz. The 30-mm diameter testing tube was utilized to measure from 800 to 6300 Hz. The foam samples had to be cut into one or both sizes to measure the acoustic properties at the desired frequency range. All the acoustic tests using the impedance tube setting were conducted based on ASTM E-1050 test specification, and the testing configurations for absorption coefficient measurements are displayed in Figure 5.1 [188]. The impedance

tube testing setup for acoustic transmission loss measurements are exhibited in Figure 5.2 [188]. In particular, this thesis study focused on the acoustic properties at a lower frequency range, which is lower than 1600 Hz, because the sensitivity of human hearing is high from 250 to 2000 Hz of frequency [91].

5.2 Strategies to Improve Acoustic Properties of Injection

Foam Molded Samples

In this section, several strategies were attempted to improve the acoustic properties of the conventional FIM samples. The strategies utilized were perforation, mold opening, and the newly developed GAFIM technology. The effectiveness of each strategy was carefully examined based on the actual measurements of acoustic absorption and insulation properties via the commercial impedance tube system.

5.2.1 Perforation

In general, perforation is one of the existing strategies to enhance the acoustic properties of not only plastic products but also of other types of materials. This technique is often utilized on a rigid cover plate in front of the foam part in order to allow the acoustic wave to transmit into the foam structure [169]. Figure 5.3 shows the effect of the open area ratio of the rigid cover plate on the acoustic absorption coefficients of the entire structure, which consists of a 1 mm-thick rigid wall and a 20 mm-thick porous layer. As the open area ratio increased, the acoustic absorption coefficient behaviors improved; this trend agrees with the results from the literature. Therefore, the results show the importance of surface condition on the acoustic absorption behavior. However, the perforation is most likely to be carried out as one of the post manufacturing

techniques, which can increase the overall manufacturing cost and time considerably. Nonetheless, it is important to investigate the effects of perforation on conventional FIM thermoplastic samples as an effort to further enhance acoustic functionalities.

5.2.1.1 Effect of Manual Perforation

For this manual perforation study, the samples were prepared using the regular FIM process. After the sample manufacturing, the samples were manually perforated with a commercial electric drill and the acoustic properties were measured.

Kramschuster and Turng utilized PVOH within PLA matrix as a polymeric sacrificial domain in their study as one of the effective strategies to create porous structure [144]. In this experimental study, PVOH was also selected as a water-soluble sacrificial domain. Prior to be utilized in the FIM process, PVOH was compounded with its plasticizer, glycerin, using a twin-screw extruder and pelletized to make it easier to form a continuous matrix within the base polymer. The base polymer for this study was thermoplastic poly-olefin (TPO), Hifax TRC 779 from LyondellBasell. Then, the pelletized PVOH/glycerin and TPO were blended together, and the mix was utilized to manufacture the samples with using a 50-ton Arburg All-rounder 270C and MuCell[®] system. As the PBA, 5.0 wt% of CO₂ was employed. The rest of the processing conditions are displayed in Table 5.2. After the foam samples were manufactured, they were put into water for a long time to leach out the PVOH/glycerin matrix from the samples. The leaching of PVOH/glycerin was expected to create channel-like voids because PVOH/glycerin is solubilized in the water. This increased the chances of achieving a porous structure. Once the leaching process was completed, the samples were dried and perforated. The perforation was done with three different hole diameters, 5.5

mm, 3.1 mm, and 1.75 mm. The acoustic absorption coefficients were measured from 100 to 1600 Hz.

The perforated samples are shown in Figure 5.4, and the samples were perforated through the entire thickness of the samples. A consistent perforated area was maintained, although the perforated hole diameters were varied. The area was close to 240 mm², which was almost equal to approximately 3 % of total surface area. First, the perforated samples were utilized as rigid cover plates with the commercial polyurethane foam. The perforated samples had a thickness of 3.2 mm, and the polyurethane foam was 22 mm thick. As shown in Figure 5.5, the 22-mm polyurethane foam was able to only accomplish the maximum absorption coefficient of 0.6. After the addition of perforated samples as rigid cover plates, the acoustic absorption coefficients increased to 1. Thus, a nearly 80% of improvement was accomplished in terms of acoustic absorption behavior and this agreed with the results from the literature [169].

The acoustic absorption coefficients of perforated samples alone were measured, and the results are shown in Figure 5.6. Despite the previous results and different hole diameters, the perforated samples did not obtain any significant amount of acoustic absorption mainly due to two reasons. First, the overall structure had a relatively high elastic modulus since TPO was utilized as the main base polymer and its flexural modulus was 1650 MPa. Second, the total sample thickness was small, which was equal to 3.2 mm. It was very challenging to obtain effective acoustic absorption with relatively thin samples, especially at a lower frequency range [91, 176]. When the perforated samples were utilized as rigid cover plates again, followed by the foamed and leached TPO samples, the acoustic absorption behaviors improved as displayed in Figure 5.7.

Therefore, it was noticed that the perforated samples were only effective when they were utilized as rigid cover plates in front of another foam layer.

5.2.1.2 Effect of Perforation Roller

Since the previous results indicated that perforation was only effective when it was used as a cover plate structure followed by a foam structure, another strategy was employed to create a porous side on the surface. The perforation roller from Stewarts of America Inc., was utilized. It had 656 pins/in² and the tips of the pins were 2 mm away from each other. The roller was heated in the heating chamber at a temperature higher than 220 °C, which was significantly higher than the melting temperature of polypropylene (PP) and PVOH/glycerin, and it was rolled on the top surface of the FIM samples to create pores on only one surface. The hole diameter was close to 1 mm in average, and the hole penetration depth was close to 1 mm within the 3.2 mm of entire foam thickness.

In order to conduct FIM experiments, the 50-ton Arburg All-rounder 270C and MuCell[®] were utilized. In this experimental study, the effects of injection flow rates and shot sizes were investigated, as well as the effects of surface perforation on the final acoustic absorption properties. The corresponding variables are shown in Table 5.3. The fixed processing parameters were 10.0 wt% of CO₂, 200 °C of processing temperature, and 30 °C of mold temperature. In terms of materials, 50 vol% of PP, BE170 from Borealis, and 50 vol% of PVOH/glycerin, which was described in the previous section, were employed. As described in the previous experimental study, the FIM samples were leached out in the water and dried. Then, the samples were cut into appropriate sizes and their acoustic absorption coefficients from 100 to 1600 Hz were measured. In the

impedance tube, the perforated surface was facing the source of the generated acoustic wave.

The measured acoustic absorption coefficients are exhibited in Figure 5.8. The coefficients were fairly low although the samples were leached and were perforated to accomplish a porous structure to a certain degree. When the injection flow rate was reduced from 100 to 20 cm³/s, the acoustic absorption behavior enhanced in some degree by accomplishing the maximum absorption coefficient over a broader range of frequency. The slower injection flow rate promoted a more cell growth dominant foaming mechanism, which led to more cell coalescence. A higher degree of cell coalescence helped to obtain a more porous structure, and a higher porosity in the acoustic samples provided positive impacts on the acoustic absorption behaviors as discussed in the literature review [36, 145, 169]. On the other hand, there was no considerable variation in terms of acoustic absorption performance witnessed when the shot size was changed from 80 vol% to 60 vol%. Finally, the actual absorption behaviors were improved dramatically when one surface of each sample was perforated. The increase was especially significant at the frequency range of 1400 Hz or higher. This enhanced performance was mainly due to the increase in the porosity of the surface that the generated acoustic normal wave first encountered.

Based on the experimental results, both the slower injection flow rate and perforation of one surface were able to contribute positively to the final acoustic absorption behaviors by increasing the structural porosity values. However, the degree of improvement was significantly greater when the perforation technique was implemented, especially at a frequency higher than 1400 Hz. Therefore, it was noticed that the surface

condition was more critical than the structural morphology when determining acoustic absorption coefficients at a lower frequency range.

5.2.2 Implementation of Mold Opening Technology

In order to effectively utilize the air-gap type of structure, the mold opening technology with conventional FIM was implemented to manufacture the desired foam structure. In this study, two processing variables, i.e., the degree of mold opening and the injection flow rate, were changed to differentiate the sample characteristics such as cellular morphology, the thickness of the air gap and the overall thickness of the foam structure. Furthermore, the open-cell content of the TPU foam structure was increased by introducing the additional melt extrusion process prior to the FIM process.

For this experimental study, a 50-ton Arburg All-rounder 270C was utilized as an injection molding machine whereas MuCell[®] was implemented as the PBA injection system. In terms of the base polymer material, Pellethane[®] 2355-75A from Lubrizol Advanced Materials Inc. was utilized. As a PBA, N₂ from Linde Canada Ltd. was employed. The original cavity shown in Figure 4.4 was used to manufacture the foam samples.

After the foam samples were manufactured, the acoustic absorption coefficients and transmission loss values were measured over the frequency range from 100 to 6300 Hz. In addition, the cellular morphologies of the foamed samples were analyzed using SEM.

5.2.2.1 Effect of Degree of Mold Opening

In this experimental study, the effect of the degree of mold opening on the cellular

morphology and on the acoustic absorption behavior was investigated. The fixed processing conditions are exhibited in Table 5.1. The injection flow rates of 20 cm³/s for the first 50 vol% of shot size and 50 cm³/s for the other half were employed. The full shot of the polymer/gas matrix was injected into the cavity first and then, the cavity pressure became very high. After the completion of the injection, there was a 6-second delay before opening up the mold to decrease the cavity pressure rapidly, which triggered foaming. This degree of mold opening was maintained for the rest of the cooling time, which was 60 seconds. The degree of mold opening was varied from 0, 4.5, and 6.0 mm.

As exhibited in Figure 5.9, the foamed samples with 0-mm and 4.5-mm mold openings did not achieve a significant amount of acoustic absorption coefficient within the frequency of 100 Hz to 1600 Hz. When the mold opening was increased to 6.0 mm, on the other hand, the maximum acoustic absorption coefficient was dramatically increased to 0.6 because this mold-opening setting was able to create the adequate thickness of an air-gap within the foam samples. According to Figure 5.10, the foam sample with a 6.0-mm mold opening obtained this air-gap throughout the structure because the growth of the nucleated cells was not able to compensate for the expansion by the mold opening. On the other hand, the foam samples with the 0-mm mold opening did not have any air-gaps within the structure because there was no room for possible expansion. This setting was identical to high pressure FIM; so the only available volume expansion was from the shrinkage of TPU during the cooling stage. In the case of the 4.5-mm mold opening, the nucleated cells were not able to fully compensate for the expansion and as a result, approximately a 2.2 mm hollow core (i.e., air-gap) was obtained. For the 6.0-mm mold opening samples, hollow cores of nearly 2.9 mm were

achieved within the samples. Consequently, it was advantageous to have an air-gap within the structure for the enhancement of acoustic absorption functionalities. This increase of acoustic absorption coefficient may also be due to the increase of overall sample thickness [36, 145].

In order to evaluate the acoustic insulation property, transmission losses were measured over the same range of frequency; the results are shown in Figure 5.11. Although the 6.0-mm mold-opening sample exhibited superior acoustic absorption behaviors than the samples with other sized mold-openings, it did not perform very well in terms of acoustic insulation. Meanwhile, the sample with the 4.5-mm mold opening accomplished the highest transmission loss values. Over the measured frequency range, the 4.5-mm mold opening sample achieved nearly 40 to 50% greater transmission loss values than that of 6.0-mm mold-opening sample. The 4.5-mm mold-opening sample accomplished 25 dB of the maximum transmission loss at 1400 Hz. In general, when the elastic modulus of the overall structure decreases, the acoustic transmission loss values deteriorate [173]. Although the overall structure became more flexible due to the existence of a hollow core (i.e., air-gap) within the structure when 4.5-mm mold opening was applied, the transmission loss behavior was still improved. Therefore, the increase of overall sample thickness did not contribute positively in terms of acoustic insulation performance.

5.2.2.2 Effect of Injection Flow Rate

In an effort to investigate the effect of the injection flow rate, the previously set injection flow rates were reduced to half, which were 10 cm³/s for the first 50 vol% of injected material and 25 cm³/s for the rest, whereas the degree of mold opening was

maintained at 6.0 mm.

Figure 5.12 displays the acoustic absorption behaviors of two different injection flow rate settings. Although the injection flow rates were reduced to half, the acoustic absorption behaviors did not vary significantly since the identical maximum absorption coefficients were achieved. The only change was a shift of the maximum acoustic absorption peak to a lower frequency. According to Figure 5.13, 2.9 and 3.1 mm of the hollow core thicknesses were from slow and fast injection flow rates, respectively. When the injection flow rate setting was decreased, the cells were significantly larger and the cell density was considerably lower in the foamed layer because cell growth became the predominant foaming mechanism. However, this morphological variation did not lead to any dramatic changes in acoustic absorption behavior in the lower frequency range although it shifted the maximum absorption peak to lower frequency. With respect to the acoustic insulation performance, the foam samples with two injection flow rate settings achieved the identical insulation behaviors despite the aforementioned morphological variations. Therefore, it was observed that the material thickness was more influential than the cellular morphology for both acoustic absorption and insulation, especially at the lower frequency range.

In order to further investigate the effects of this morphological difference, the acoustic properties at a higher frequency range were measured and analyzed. As displayed in Figure 5.15, the foamed sample with higher cell density and smaller cells was able to achieve a considerably higher acoustic absorption coefficient than the one with a lower cell density and larger cells. On the other hand, regarding the acoustic insulation behavior, the slower injection flow rate setting improved the transmission loss

over a higher frequency range because the elastic modulus of the overall structure was increased by having a lower cell density and larger cell sizes. Therefore, having smaller cells with a higher cell density definitely enhanced the acoustic absorption coefficient at a higher frequency range when the identical degree of mold opening was applied. In the past literature, smaller cells were proven to provide higher absorption coefficients at a lower frequency. The results of this study also verified that smaller cells and higher cell density were able to provide a higher acoustic absorption coefficient at a higher frequency range.

5.2.3 Utilization of Gas-Assisted Foam Injection Molding

Technology

The implementation of GAFIM technology provided the foam structure, described in Figure 4.29 and Figure 4.36; the GAFIM foam structure consisted of a solid skin layer, foam layers, and a hollow core when the gas penetration was effective. In terms of the acoustic absorption behavior, it was expected that the GAFIM could achieve higher acoustic absorption coefficients than the regular FIM samples because the GAFIM foam structure had advantageous morphological characteristics: a high cell density, small cell sizes, and a hollow core. They were verified to increase the absorption coefficients in the previous section and in other literatures. Since the solid skin layer is fixed on the foamed layer and both are backed by air cavity, furthermore, the solid skin layer is expected to serve as an impermeable film, which promotes two acoustic absorption mechanisms, the inertial effect and the piston effect. The piston effect, especially, stimulates the whole material in compression and promotes viscoelastic losses [189]. The higher degree of viscoelastic loss will improve the acoustic absorption behavior in the lower frequency

range.

The acoustic absorption coefficients were measured over a frequency range between 100 to 1600 Hz as displayed in Figure 5.17. The GAFIM sample was able to achieve the maximum absorption coefficient of 0.74, whereas the FIM sample accomplished less than 0.53. As a result, the implementation of GAFIM achieved a higher acoustic absorption coefficient than the conventional FIM sample with a 6.0-mm mold opening. Furthermore, this maximum acoustic absorption coefficient of the GAFIM sample was 28% higher than the maximum acoustic absorption coefficient of the 22-mm thickness PU foam sample. As described above, the viscoelastic loss, due to the piston effect, provided higher acoustic absorption coefficients in the low frequency range. Therefore, it was verified that GAFIM could enhance the acoustic absorption behavior without the employment of a mold opening technique.

In terms of the acoustic insulation behaviors, the GAFIM sample was able to achieve noticeably higher transmission loss values than the regular FIM sample. Initially, the GAFIM technology was expected to decrease insulation behavior because the existence of a hollow core would decrease the overall elastic modulus [173]. When the cellular morphology was carefully analyzed, however, it was observed that having appropriate cell morphology and a hollow core structure could improve the acoustic transmission loss as the previous case. The 4.5-mm mold opening TPU foam sample achieved considerably higher transmission loss than the TPU foam without any mold opening. As a result, the approximate maximum transmission loss of 20.81 dB was accomplished in the case of GAFIM; whereas the regular FIM sample obtained only about 14.4 dB according to Figure 5.18. This maximum transmission loss value from the

GAFIM was almost equivalent to the one achieved with the regular FIM with a 4.5-mm mold opening. Consequently, the GAFIM technology was able to improve the acoustic insulation behavior as well when compared to the regular FIM.

As described in the previous chapter, the cellular morphologies of the GAFIM samples varied significantly when the gas injection pressure was reduced from 13.79 to 6.89 MPa. The cells became larger and the cell density values decreased as the gas injection pressure decreased. The maximum acoustic absorption coefficient decreased from 0.74 to 0.50 because of these changes in the cellular morphology, as exhibited in Figure 5.19. In contrast, the transmission loss values increased by approximately 2 dB in terms of the acoustic insulation as the gas injection pressure decreased by 6.89 MPa. When the larger cells were obtained from the lower gas injection pressure, the transmission loss values at lower frequency increased as the previous mold opening experimental results. Consequently, the overall acoustic absorption behaviors deteriorated once the gas injection pressure decreased from 13.79 to 6.89 MPa whereas the acoustic insulation behavior was improved by the gas injection pressure decrease

5.3 Relationships between Cellular Morphologies and Acoustic Properties

In this thesis study, various types of foam structures were produced by different manufacturing technologies such as regular FIM, regular FIM with mold opening technique, and GAFIM. The acoustic characteristics, acoustic absorption coefficient and transmission loss, of these various foam structures were evaluated in this chapter. In order to optimize the acoustic performance of these foam samples, an extensive

investigation into the relationships between their cellular morphologies and their acoustic performances was required.

In the case of regular the FIM samples with the breathing mold technique, smaller cell sizes and higher cell density values were obtained by the faster injection flow rate. These morphological characteristics were preferred for obtaining higher acoustic absorption coefficients at high frequencies since the maximum absorption of the faster injection flow rate was about 0.2 higher than that of the lower injection flow rate according to Figure 5.15. On the other hand, this type of the cellular morphology was able to result in higher acoustic absorption coefficients at the lower frequency range in the case of the GAFIM samples. Another critical morphological requirement was a hollow core or an air-gap within the foam structures. For other materials and applications, it is well-known that an air-gap can enhance the acoustic absorption coefficients to some degree [169, 172, 190]. In addition, having the solid skin layer, foam layer, and a hollow cavity in the order promoted the viscoelastic loss to result in higher acoustic absorption coefficients in the lower frequency range. Consequently, a hollow core, smaller cells, and higher cell density values were preferred for improving the acoustic absorption behavior.

Regarding the acoustic insulation properties of the regular FIM with mold opening samples, having larger cells and lower cell density helped to achieve somewhat higher transmission loss values when the measured frequency range was higher than 1000 Hz. On the other hand, an increase in overall sample thickness did not improve the transmission loss values for these regular FIM samples with the mold opening.

The GAFIM samples were able to achieve higher transmission loss values than

the regular FIM samples without the mold opening over the measured frequency because having an air-gap and large-celled foamed layers also helped to increase the transmission loss values as they did for the mold opening samples. When the gas injection pressure reduced from 13.79 to 6.89 MPa, the foam structure with larger cells and lower cell density was able to enhance the transmission loss values as it did for the mold opening case. Therefore, having a foam structure with larger cells and lower cell density was advantageous to achieve higher transmission loss values when a hollow core was existed at the core of structure.

5.4 Summary

Since the proposed GAFIM technology was developed to produce a unique foam structure that can serve acoustic functions, acoustic properties such as acoustic absorption and transmission loss were studied in this chapter. In order to increase the acoustic behaviors, the traditional perforation technique was employed and its effect on the acoustic absorption coefficients of TPO injection foam molded samples was evaluated. When the perforated samples were located in front of the porous PU foam or regular foam molded samples, a significant increase in absorption coefficient was witnessed. The acoustic absorption coefficients increased dramatically at frequencies higher than 1400 Hz when only one surface was perforated using the heated perforation roller. The breathing mold or mold opening technique was adopted, and the foam structures with hollow cores were obtained when the degree of mold opening was relatively large. The varied cellular morphologies, resulting from the injection flow rate changes, led to a considerable difference in acoustic absorption coefficient at a higher frequency range. Having a foam layer with higher cell density and smaller cell sizes was more

advantageous for accomplishing higher absorption coefficients at a higher frequency. There was an optimum degree of mold opening for acoustic transmission loss because of the combined effect of the elastic modulus and air-gap thickness. As the degree of mold opening increased, the elastic modulus of the overall structure decreased, whereas the thickness of the air-gap increased. Therefore, it was important to find a balance to compensate for the effect of the elastic modulus reduction with the increase in air-gap. The slower injection flow rate was able to provide a higher acoustic transmission loss because of a thicker solid skin layer, which contributed to the modulus increase. The GAFIM samples were able to outperform the conventional FIM samples in terms of both acoustic absorption coefficients and transmission loss values. The GAFIM samples were more effective at lower frequencies by more than a 50% increase in the maximum absorption coefficient. In addition, the GAFIM samples achieved nearly 27% higher maximum absorption coefficient than that of 22-mm thick PU foam. The better absorption performance at a lower frequency range was due to the existence of the air-gap and the finer cell morphology of the foam structure. The higher degree of viscoelastic loss by the piston effect also contributed to enhance the acoustic absorption behavior over the lower frequency range. This trend was consistent in different GAFIM samples by reducing the gas injection pressure, so the maximum acoustic coefficient changed from 0.74 to 0.50. The foam samples from GAFIM were also able to provide about a 6.4 dB higher transmission loss consistently over the entire frequency range than the regular FIM sample without the mold opening. This improvement in insulation behavior was due to three morphological characteristics: thicker solid skin layers, an appropriate degree of foaming, presence of a hollow core (i.e., air-gap) at the center of structure. Furthermore,

having larger cells with lower cell density helped to increase the transmission loss values when those three morphological characteristics were satisfied.

Table 5.1 Fixed processing conditions for the mold-opening experimental study

Processing Conditions	Values
Melt Temperature [°C]	200
Mold Temperature [°C]	30
PBA Content [wt%]	0.5
Shot Size [vol%]	100

Table 5.2 Processing conditions of FIM process for the perforation study

Processing Conditions	Values
Melt Temperature [°C]	210
Mold Temperature [°C]	30
Shot Size [vol%]	70
Injection Flow Rate [cm ³ /s]	100

Table 5.3 Variable processing parameters for the perforation roller study

Exp. No.	Injection Flow Rate [cm³/s]	Shot size [vol%]
1	100	80
2	20	80
3	100	60

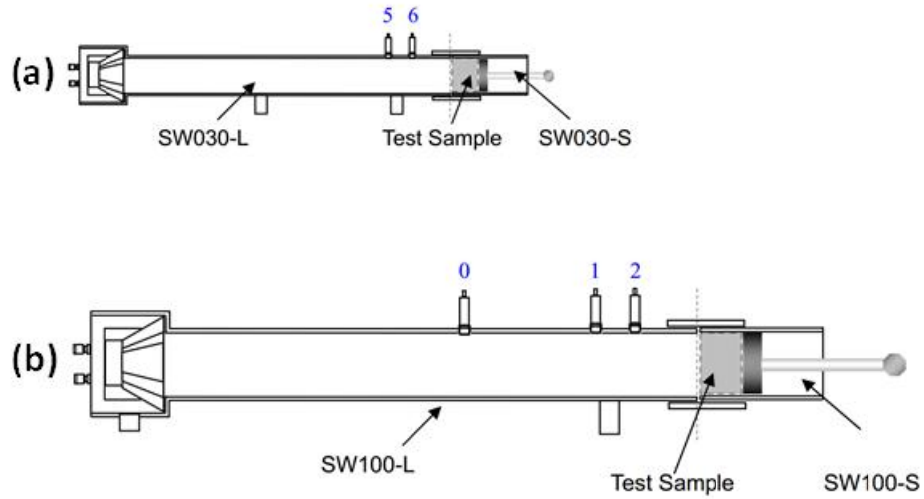


Figure 5.1 Impedance tube testing setups for acoustic absorption of (a) high frequency range with 30 mm diameter tube and (b) low frequency range with 100 mm diameter tube

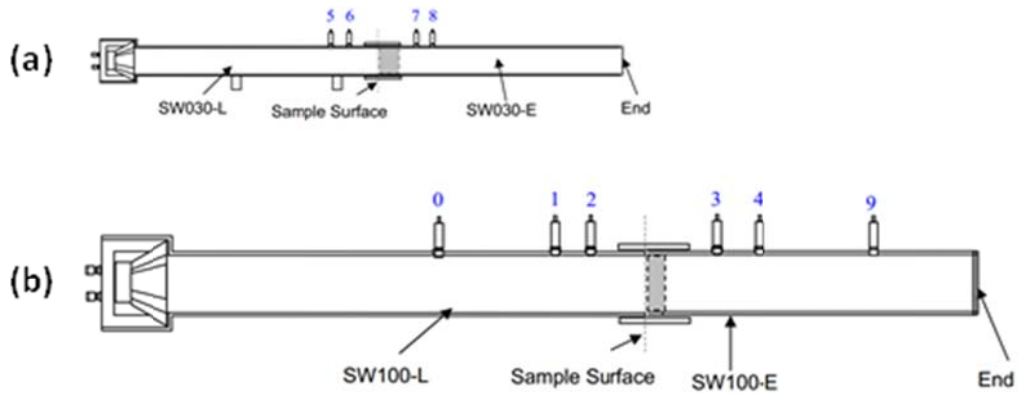


Figure 5.2 Impedance tube testing set-ups for acoustic transmission loss of (a) 30 mm diameter tube and (b) 100 mm diameter tube

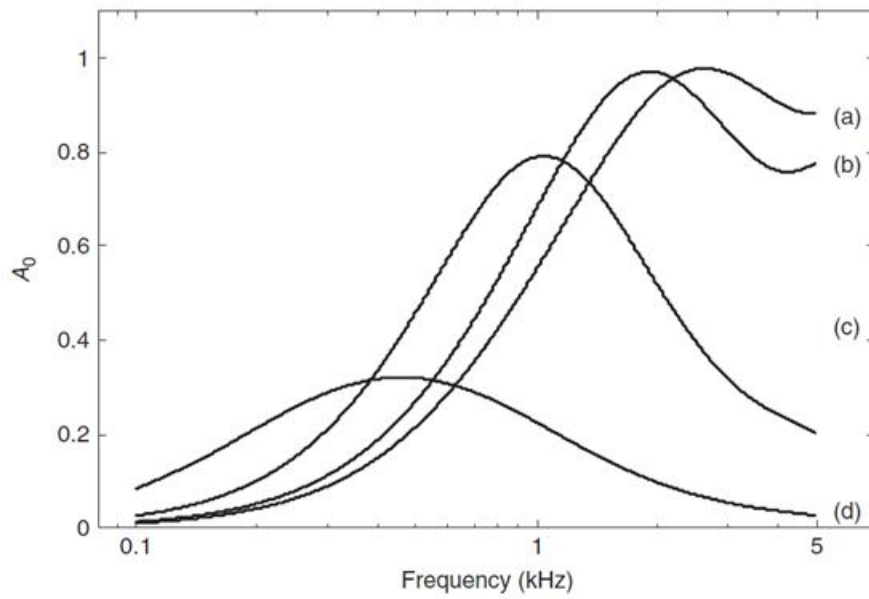


Figure 5.3 Acoustic absorption coefficients with different open area ratios of rigid cover plate (a) 0.4, (b) 0.1, (c) 0.025, and (d) 0.005

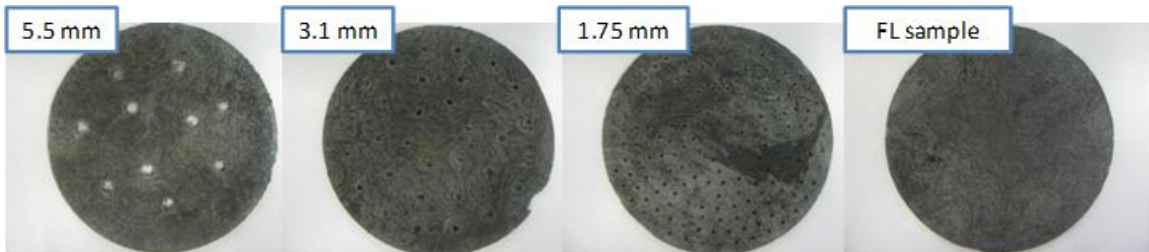


Figure 5.4 Manually perforated samples with different hole sizes

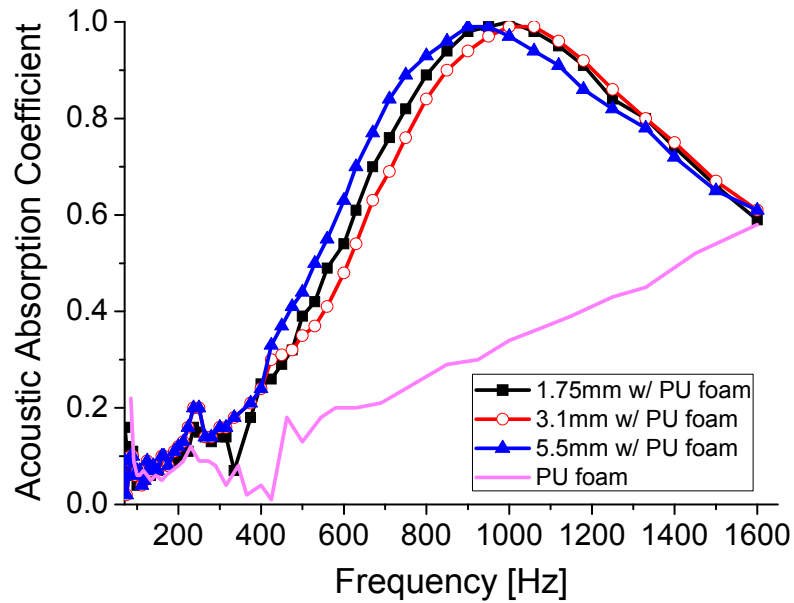


Figure 5.5 Acoustic absorption coefficients of polyurethane foam with the manually perforated samples

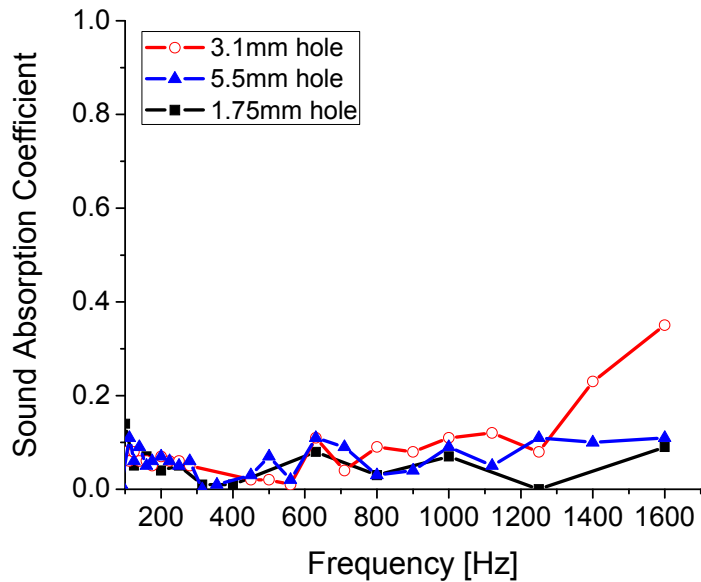


Figure 5.6 Acoustic absorption behaviors of perforated samples

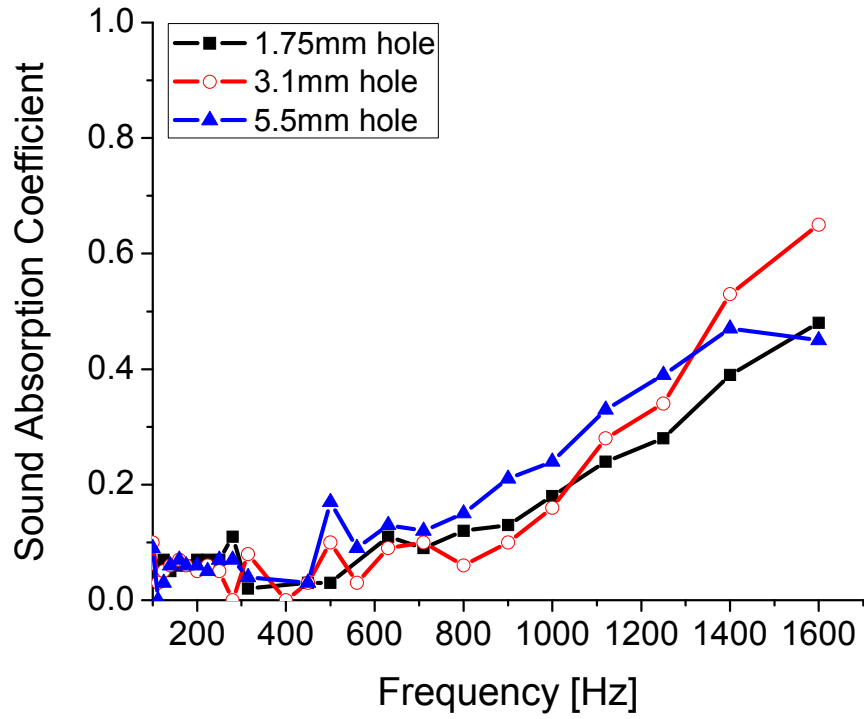
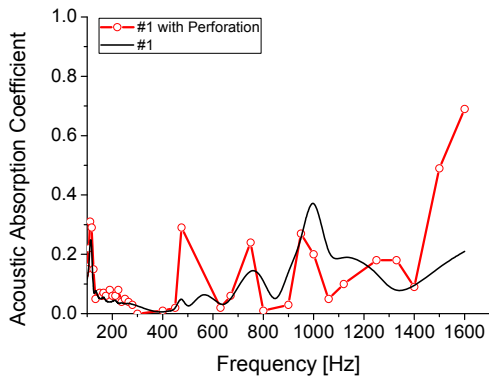
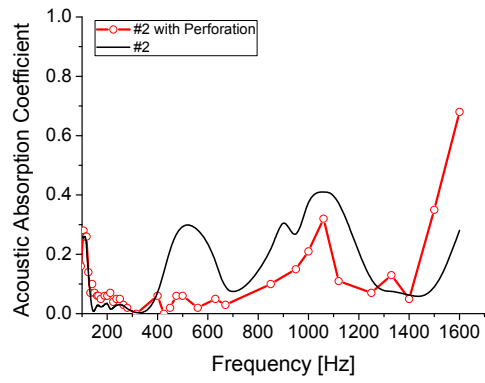


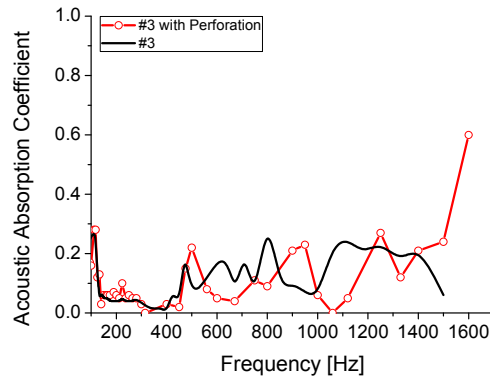
Figure 5.7 Acoustic absorption coefficients of perforated samples followed by regular foamed samples



(a)



(b)



(c)

Figure 5.8 Effects of perforation on the acoustic absorption coefficients for (a) Exp. 1, (b) Exp. 2, and (c) Exp. 3

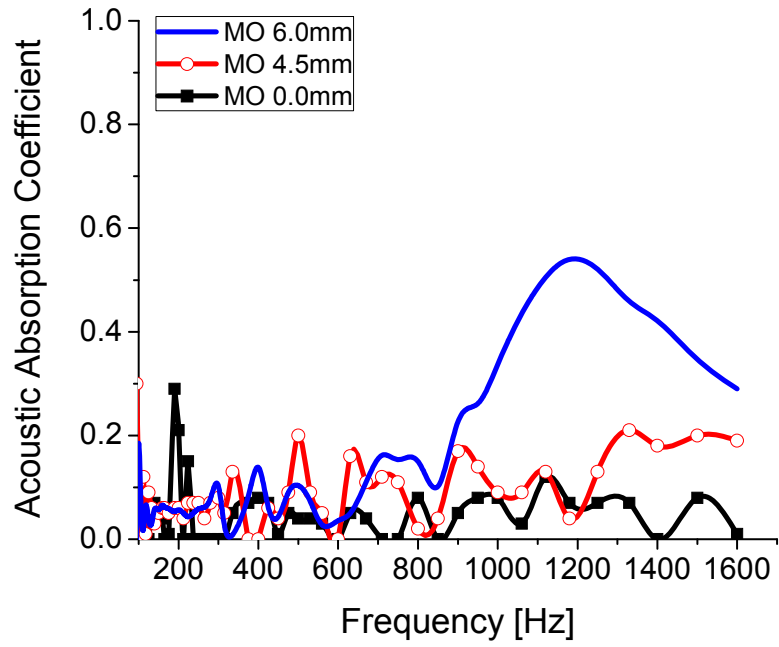


Figure 5.9 Acoustic absorption coefficients of mold opening samples

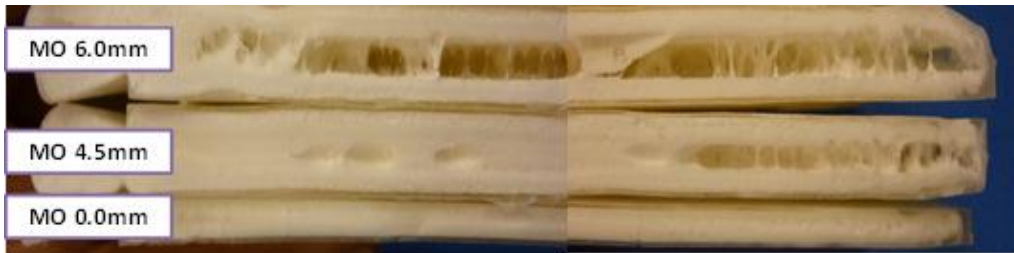


Figure 5.10 Foam samples with various degrees of mold opening

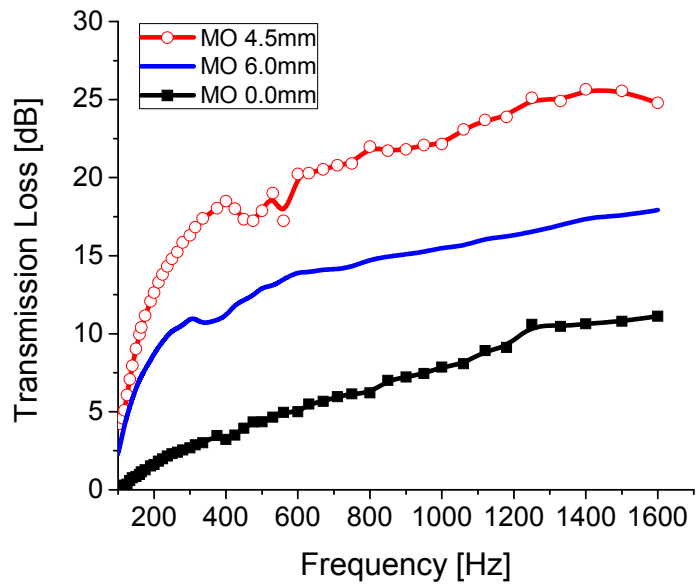


Figure 5.11 Transmission losses of different mold opening samples

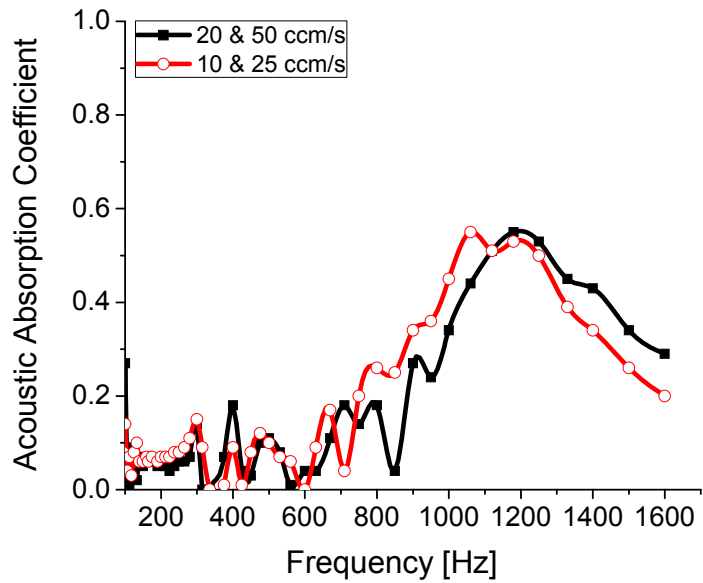
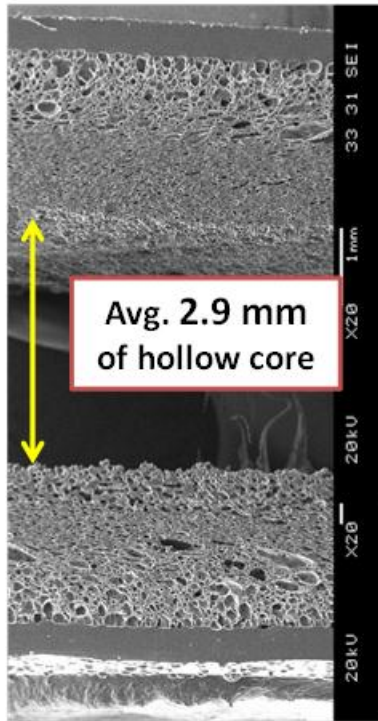


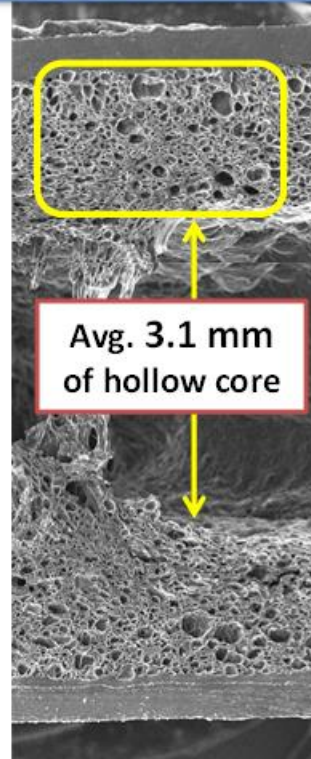
Figure 5.12 Acoustic absorption behaviors of two different injection flow rate settings

20 And 50 cm³/s IFR



(a)

10 And 25 cm³/s IFR



(b)

Figure 5.13 Cellular morphologies of (a) high injection flow rate samples and (b) low injection flow rate samples

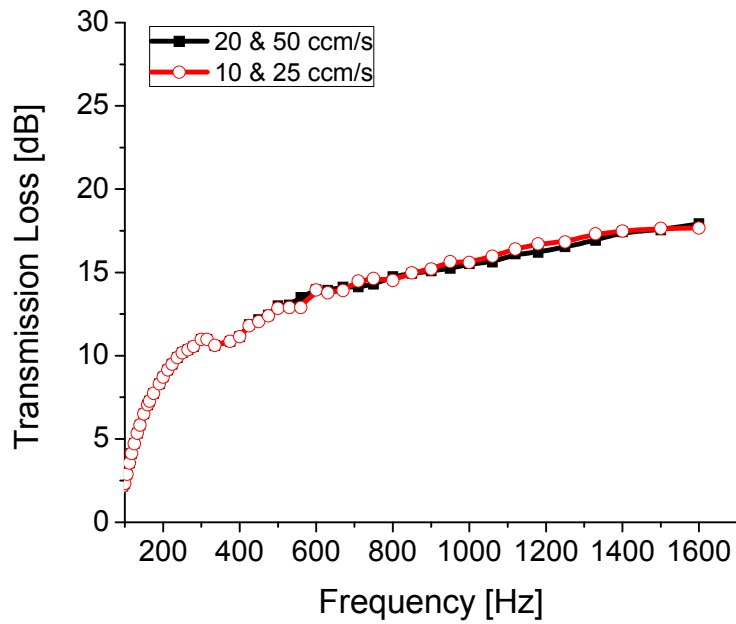


Figure 5.14 Transmission loss values for two different injection flow rate settings

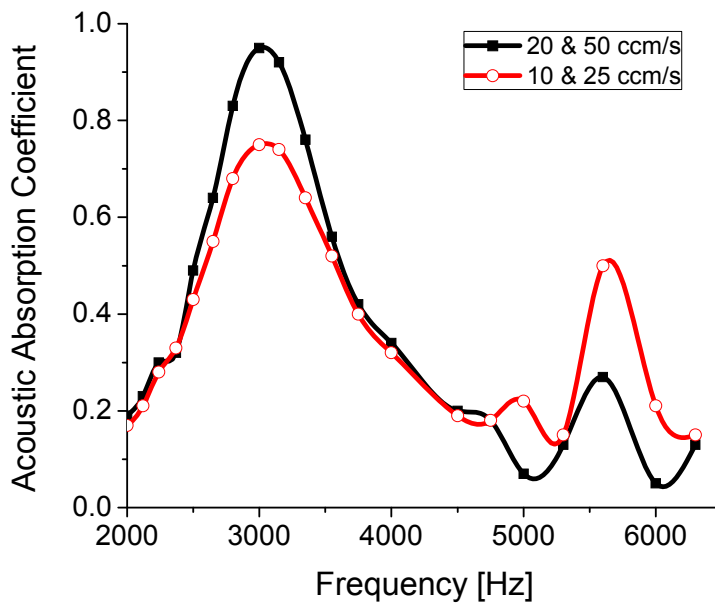


Figure 5.15 Acoustic absorption coefficients of two injection flow rate settings at higher frequency range

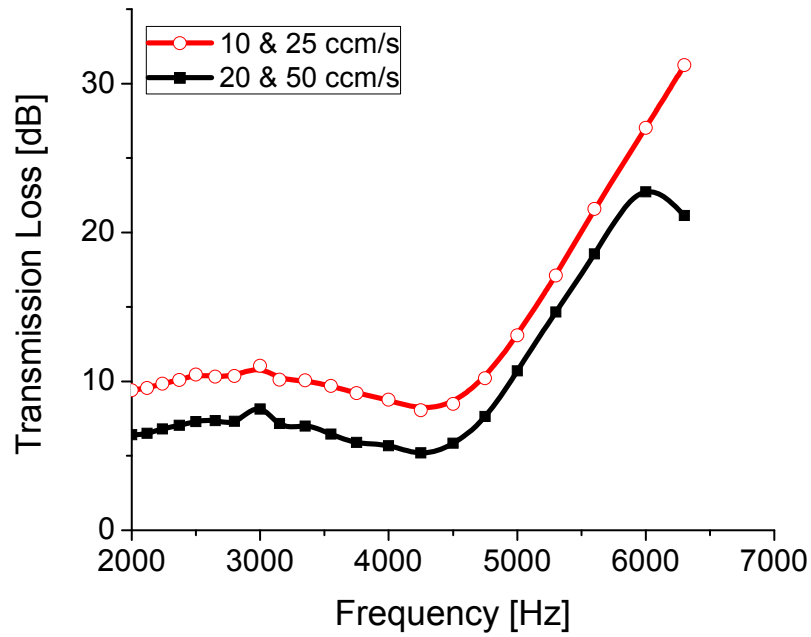


Figure 5.16 Acoustic insulation behaviors of two injection flow rate settings

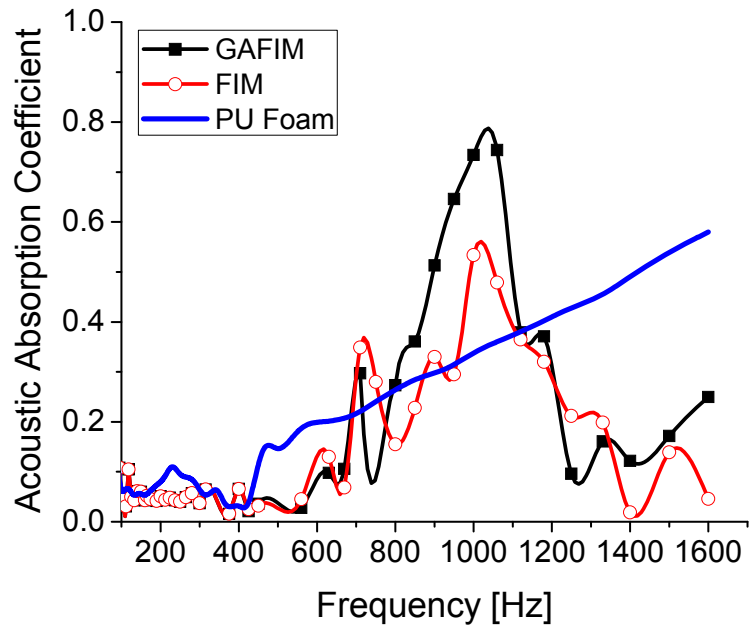


Figure 5.17 Acoustic absorption coefficients of FIM and GAFIM samples

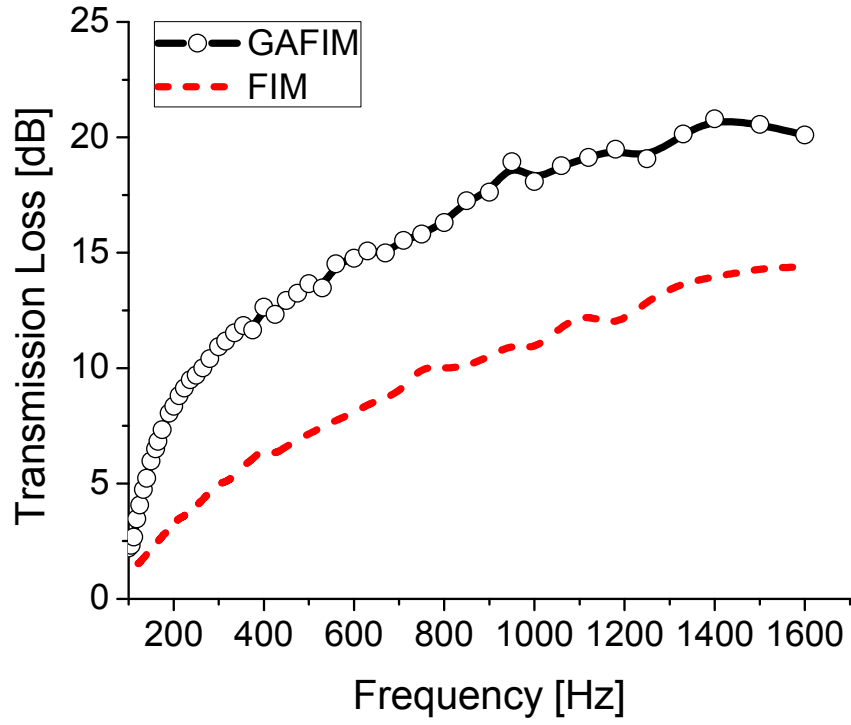


Figure 5.18 Transmission loss behaviors of FIM and GAFIM samples

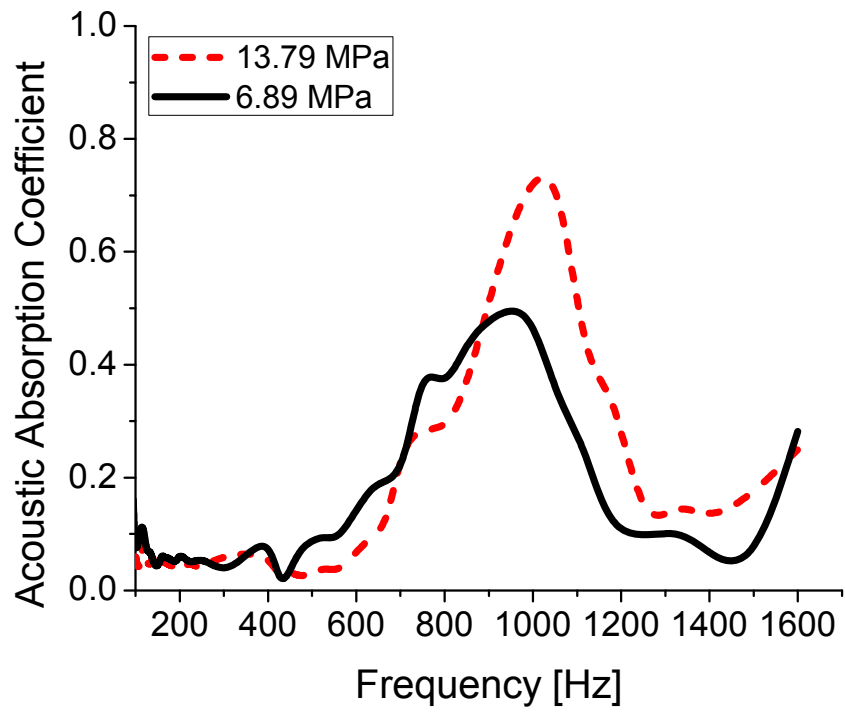


Figure 5.19 Acoustic absorption coefficients of GAFIM samples with two gas injection pressures, 13.79 and 6.89 MPa

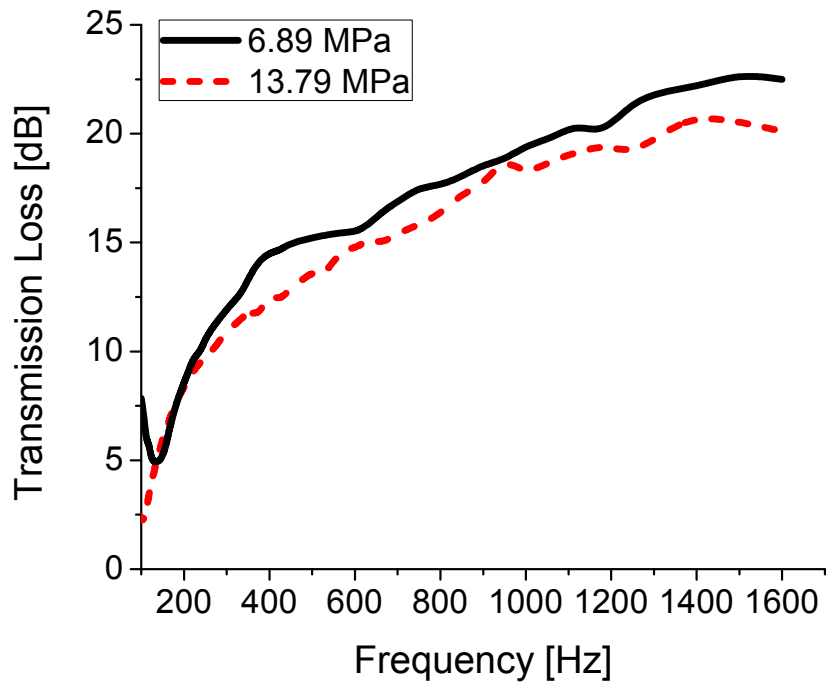


Figure 5.20 Transmission loss values of GAFIM samples with two different gas injection pressures, 13.79 and 6.89 MPa

Chapter 6 Conclusions and Recommendations for Future Research

6.1 Summary of Major Contributions

In this thesis, innovative gas-assisted foam injection molding technology has been developed to produce a unique thermoplastic foam structure that can provide effective acoustic absorption and insulation, as well as to the inherited limitation of conventional foam injection molding process. Despite the advantages of foam injection molding technology, it is very challenging to obtain a uniform cellular morphology because the filling and the foaming phases are coupled. Hence, the cells are nucleated at different locations and timings, and this nucleation characteristic varies the cell growth behaviors. Finally, the accumulated effects of these foaming behaviors result in cell growth dominant foaming and non-uniform foam structures. On the other hand, the developed gas-assisted foam injection molding technology was able to completely decouple the filling and the foaming phases and to produce a very uniform foam structure.

The technology first completed the filling and eliminated prematurely nucleated bubbles by applying high pressure with N₂ gas. Then, the primary cell nucleation was occurred via the rapid depressurization afterwards. This foaming mechanism provides very uniform on-set nucleation timings throughout the foam sample, unlike the conventional FIM samples. Furthermore, the additional extensional and shear energies from high pressure N₂ gas penetration were able to promote more cell nucleation, which

led to a higher cell density and smaller cell sizes. Last, the extensional strains and shear stresses aligned the polymer molecular chains to form the higher number of crystallites, which were effectively utilized as heterogeneous nucleation sites. The implementation of GAFIM technology provided a couple of advantages on the cell growth behaviors, which were minimizing the excessive cell growth by increasing the melt strength and eliminating the bubble travel during the growth stage. The combined effects of the advantages resulted in the very uniform morphology regardless of the flow length in the cavity.

In terms of acoustic properties, this thesis study investigated the acoustic behaviors of various foam structures, which were produced by different supplemental techniques, such as perforation and mold opening. The acoustic absorption and insulation properties of the gas-assisted injection foam molded samples were measured and evaluated. As a result, the newly developed foam structure was able to achieve higher absorption coefficients than the samples with mold opening and the conventional polyurethane acoustic foam in the lower frequency range. Furthermore, it was able to achieve nearly 25 dB of transmission loss at the lower frequency range, which was 10 dB greater than that of the regular injection foam molded sample.

The major contributions of this thesis study are summarized as follows:

- Decoupling of the filling and foaming phases led to a highly uniform foam structure.

In the case of conventional foam injection molding, bubbles are nucleated as the polymer/gas matrix travel through either the nozzle or the gate. As more polymer/gas

matrix gets injected to fill the cavity, the already nucleated cells travel further and grow. Therefore, the cell growth duration and travel distance of the nucleated cells vary depending on the timing of the injection and cell nucleation as well as the relative location of nucleation. Moreover, the injected polymer/gas matrix experiences a smaller pressure drop and pressure drop rate as the degree of filling increases. The inconsistent pressure profile during the filling and the foaming stages, therefore, often leads to a non-uniform foam structure. The GAFIM technology overcame the aforementioned issue by the complete decoupling of the filling and the foaming phases. First, the polymer/gas matrix was injected and the bubbles were nucleated during the injection phase, as part of the regular foam injection molding process. Once the injection was finished, however, the polymer/gas matrix in the cavity was highly pressurized by N₂ gas injection, and this highly pressurized circumstance forced the prematurely nucleated cells to collapse. The cavity pressure was then released to initiate foaming uniformly throughout the structure. Therefore, the proposed technology was able to provide a uniform pressure profile and eliminate the variations in nucleation timing and locations so that a highly uniform foam structure was achieved.

- Additional extensional strains and shear stresses resulted in a higher cell density and smaller cell sizes.

As the injected N₂ gas penetrated in the polymer/gas matrix, it provided additional extensional strains and shear stresses directly to the polymer/gas matrix. They provided two advantages. First, they reduced the critical radius and increased the bubble nucleation rate so that the overall foaming behavior became more cell nucleation dominant. Second, they helped the polymer molecular chains to orient and form micron-sized crystallites,

which were effectively utilized as preferred nucleation sites for heterogeneous nucleation. Among these positive effects that were provided by GAFIM technology, the crystalline induced foaming was the predominant cell nucleation mechanism that determined the final foam structure. Based on the experimental results, the implementation of GAFIM technology provided nearly 100 times higher cell density than the conventional FIM technology.

- The degree of foaming and timing of nucleation were independently and easily controlled.

In the developed technology, the cavity was pressurized first and then the pressure was suddenly released to initiate foaming. Therefore, this pressure, before its release, determined the final cellular morphology because it dictated the formation of micron-sized crystallites or degree of crystallinity. Therefore, the gas injection pressure controlled the degree of foaming. According to the experimental result, the cell density became lower as the gas injection pressure was decreased because the lower gas injection pressure provided less number of micron-sized crystallites and lower melt strength. The timing of cell nucleation could easily be controlled by timing the pressure release. Consequently, the proposed technology provided more direct and independent control on the complicated foaming mechanism.

- An acoustically functioning thermoplastic foam structure with a relatively small thickness was obtained.

The developed technology was able to manufacture a foam structure, which consisted of a solid skin layer, a foam layer, and a hollow core (i.e., air-gap). Although

the conventional mold-opening technique could provide a similar type of multi-layer structure, the foam structure from the gas-assisted foam injection molding technology outperformed the mold-opening sample in terms of acoustic properties. As a result, the acoustic absorption improved by approximately 50%, and nearly 25 dB of acoustic insulation was obtained with the smaller overall sample thickness. In terms of the acoustic absorption coefficient at the lower frequency range, the developed foam sample accomplished a 27% higher absorption coefficient than the existing 22-mm-thick polyurethane acoustic foam.

- The relationships between cellular morphological characteristics and acoustic properties were elucidated.

According to the literature review and the actual experimental studies, the relationships between the cellular morphology and the acoustic behaviors were investigated. The foam samples from both the mold-opening and the developed technology commonly had a solid skin layer, a foam layer, and a hollow core. With respect to acoustic absorption, smaller cells and a higher cell density were preferred in general. The presence of an air-gap or hollow core was proven to be necessary for enhanced acoustic absorption performances. On the other hand, when the acoustic insulation was evaluated, larger cells and a lower cell density were considerably effective at the higher frequency range. In the case of the GAFIM samples, furthermore, these characteristics also provided higher acoustic transmission values at lower frequencies.

6.2 Recommendations for Future Research

The following recommendations can be made for the direction of future research

on the developed technology:

1. In this study, TPU was mainly used as a base polymer. Different thermoplastic materials will vary the degree of impact of critical processing parameters. In addition, improvement in acoustic properties will be varied. Therefore, additional studies with different thermoplastic materials will verify the fundamental foaming mechanisms of the developed technology and its effectiveness on acoustic property enhancement.
2. In this study, it was impossible to visualize cell nucleation and growth in the cavity *in situ*. Since the developed technology presents a new foaming mechanism than the existing FIM technology, it will be very interesting to verify this newly claimed foaming mechanism using a visualization cavity and high speed camera in order to observe the cell collapsing and verify the decoupling mechanism.
3. This thesis study investigated the effect of the gas injection pressure on the cellular properties as an effort to elucidate the foaming mechanism of the proposed technology. Since other processing parameters, such as sprue-break release time and gas injection duration, are expected to control the timing of cell nucleation by affecting the crystallization kinetics, their effects on the foaming behaviors can be studied as an effort to optimize the technology.

4. Since this thesis study focused on the acoustic properties of foam structure created from innovative gas-assisted foam injection molding technology, it will be very meaningful to investigate its effects on other product functions such as thermal insulation.

References

- [1] D. Klempner and V. Sendjarevic, *Polymeric Foams and Foam Technology*, 2nd ed. Cincinnati: HANSER, 2004.
- [2] D. I. Collias, D. G. Baird, and R. J. M. Borggreve, "Impact toughening of polycarbonate by microcellular foaming," *Polymer*, vol. 35, pp. 3978-3983, 1994.
- [3] D. I. Collias and D. G. Baird, "Impact behavior of microcellular foams of polystyrene and styrene-acrylonitrile copolymer, and single-edge-notched tensile toughness of microcellular foams of polystyrene, styrene-acrylonitrile copolymer, and polycarbonate," *Polymer Engineering and Science*, vol. 35, pp. 1178-1183, 1995.
- [4] K. A. Seeler and V. Kumar, "Tension-tension fatigue of microcellular polycarbonate: initial results," *Journal of Reinforced Plastics and Composites*, vol. 12, pp. 359-376, 1993.
- [5] L. M. Matuana, C. B. Park, and J. J. Balatinez, "Structures and mechanical properties of microcellular foamed polyvinyl chloride," *Cellular Polymers*, vol. 17, pp. 1-16, 1998.
- [6] Q. Guo, J. Wang, and C. B. Park, "Visualization of PP foaming with nitrogen," 2006, pp. 2736-2740.
- [7] Q. Guo, J. Wang, C. B. Park, and M. Ohshima, "A microcellular foaming simulation system with a high pressure-drop rate," *Industrial and Engineering Chemistry Research*, vol. 45, pp. 6153-6161, 2006.
- [8] S. N. Leung and C. B. Park, "Effects of gas content and pressure drop rate on foaming," 2006, pp. 2775-2779.
- [9] S. N. Leung, C. B. Park, and H. Li, "Numerical simulation of polymeric foaming processes using modified nucleation theory," *Plastics, Rubber and Composites*, vol. 35, pp. 93-100, 2006.
- [10] S. N. Leung, C. B. Park, and A. Wong, "Effects of surface geometry of nucleating agents on heterogeneous nucleation," 2007, pp. 2987-2991.
- [11] S. N. Leung, A. Wong, and C. B. Park, "Pressure drop threshold for nucleation of PS/CO₂ foaming," 2007, pp. 3006-3010.
- [12] S. N. Leung, A. Wong, C. B. Park, and Q. Guo, "Strategies to estimate the pressure drop threshold of nucleation for polystyrene foam with carbon dioxide," *Industrial and Engineering Chemistry Research*, vol. 48, pp. 1921-1927, 2009.
- [13] S. N. Leung, A. Wong, C. B. Park, and J. H. Zong, "Ideal surface geometries of nucleating agents to enhance cell nucleation in polymeric foaming processes," *Journal of Applied Polymer Science*, vol. 108, pp. 3997-4003, 2008.
- [14] A. Wong, R. K. M. Chu, S. N. Leung, C. B. Park, and J. H. Zong, "A batch foaming visualization system with extensional stress-inducing ability," *Chemical Engineering Science*, vol. 66, pp. 55-63, 2011.
- [15] A. Wong, S. N. Leung, G. Y. G. Li, and C. B. Park, "Role of processing temperature in polystyrene and polycarbonate foaming with carbon dioxide," *Industrial and Engineering Chemistry Research*, vol. 46, pp. 7107-7116, 2007.
- [16] M. R. Barzegari, M. Nofar, and C. B. Park, "Double melting endotherms of

- polyethylene terephthalate (PET) for expanded bead foams," 2011.
- [17] M. Berghmans and K. C. Bleijenberg, "Foaming polystyrene beads: New perspectives on a maturing technology," 2006, pp. 20-24.
- [18] I. Y. Gnip, V. Kersulis, S. Vejelis, and S. Vaitkus, "Water absorption of expanded polystyrene boards," *Polymer Testing*, vol. 25, pp. 635-641, 2006.
- [19] Y. Guo, N. Hossieny, R. K. M. Chu, C. B. Park, and N. Zhou, "Critical processing parameters for foamed bead manufacturing in a lab-scale autoclave system," *Chemical Engineering Journal*, vol. 214, pp. 180-188, 2013.
- [20] Y. Guo, N. Hossieny, C. B. Park, and N. Q. Zhou, "Bead foaming in the autoclave-based EPP process," 2011, pp. 2615-2619.
- [21] M. Nofar, Y. Guo, and C. B. Park, "Simulation of epp bead manufacturing in batch foaming process through high pressure differential scanning calorimeter (HPDSC)," 2011, pp. 2773-2778.
- [22] K. Parker, J. P. Garancher, S. Shah, and A. Fernyhough, "Expanded polylactic acid - An eco-friendly alternative to polystyrene foam," *Journal of Cellular Plastics*, vol. 47, pp. 233-243, 2011.
- [23] M. Saberian-Broudjenni, G. Wild, and J. C. Charpentier, "FOAMING EFFECTS IN GAS-LIQUID FLUIDIZATION," 1985.
- [24] I. Sen, E. Dadush, and D. Penumadu, "Microwave-assisted foaming of expandable polystyrene beads," *Journal of Cellular Plastics*, vol. 47, pp. 65-79, 2011.
- [25] J. Shen, X. Cao, and L. James Lee, "Synthesis and foaming of water expandable polystyrene-clay nanocomposites," *Polymer*, vol. 47, pp. 6303-6310, 2006.
- [26] L. Tang, W. Zhai, and W. Zheng, "Autoclave preparation of expanded polypropylene/poly(lactic acid) blend bead foams with a batch foaming process," *Journal of Cellular Plastics*, vol. 47, pp. 429-446, 2011.
- [27] C. J. Waechter, "Processing foamed styrene for thermoformed packages," *Plast Des Process*, vol. 10, pp. 9-11, 1970.
- [28] H. Wang, S. L. Zhang, M. Nofar, R. Barzegari, C. B. Park, and Z. H. Jiang, "Development of bead foaming technology for high performance peek I. Thermal analysis," 2012, pp. 2355-2359.
- [29] J. Yang, S. K. Yeh, Z. Guo, Z. Cai, L. J. Lee, N. R. Chiou, and T. Daniel, "Synthesis and foaming of water expandable polystyrene-activated carbon composites," 2008, pp. 1013-1018.
- [30] S. K. Yeh, J. Yang, N. R. Chiou, T. Daniel, and L. J. Lee, "Introducing water as a coblowing agent in the carbon dioxide extrusion foaming process for polystyrene thermal insulation foams," *Polymer Engineering and Science*, vol. 50, pp. 1577-1584, 2010.
- [31] J. D. McRae, H. E. Naguib, and N. Atalla, "Mechanical and acoustic performance of compression-molded open-cell polypropylene foams," *Journal of Applied Polymer Science*, vol. 116, pp. 1106-1115, 2010.
- [32] Y. Zhang, M. Kontopoulou, M. Ansari, S. Hatzikiriakos, and C. B. Park, "Effect of molecular structure and rheology on the compression foam molding of ethylene- α -olefin copolymers," *Polymer Engineering and Science*, vol. 51, pp. 1145-1154, 2011.
- [33] R. Pop-Iliev, K. H. Lee, Y. C. Chew, and C. B. Park, "Processing fine-celled

- recyclable CBA-based polyolefin foams in compression foam molding," 2007, pp. 1172-1176.
- [34] B. Xiang, R. Guan, Q. Fang, Z. Xiao, and Y. Jiang, "Preparation and characterization of microcellular thin polycarbonate sheets," *Journal of Applied Polymer Science*, vol. 99, pp. 1760-1766, 2006.
- [35] E. Archer, E. Harkin-Jones, M. P. Kearns, and A. M. Fatnes, "The rotational molding characteristics of metallocene polyethylene skin/foam structures," *Journal of Cellular Plastics*, vol. 43, pp. 491-504, 2007.
- [36] R. K. M. Chu, H. E. Naguib, and N. Atalla, "Synthesis and characterization of open-cell foams for sound absorption with rotational molding method," *Polymer Engineering and Science*, vol. 49, pp. 1744-1754, 2009.
- [37] D. D'Agostino, E. Takács, and J. Vlachopoulos, "Foaming with polymer microspheres in rotational molding: The effect of coupling agent," *Journal of Cellular Plastics*, vol. 40, pp. 61-75, 2004.
- [38] M. Emami, E. Takacs, and J. Vlachopoulos, "Rotational foam molding of metallocene catalyzed polyethylene: CBA screening and process characteristics," *Journal of Cellular Plastics*, vol. 46, pp. 333-351, 2010.
- [39] A. Marcilla, J. C. García-Quesada, R. Ruiz-Femenia, and M. I. Beltrán, "Crosslinking of rotational molding foams of polyethylene," *Polymer Engineering and Science*, vol. 47, pp. 1804-1812, 2007.
- [40] R. Pop-Iliev, K. H. Lee, and C. B. Park, "Manufacture of integral skin PP foam composites in rotational molding," *Journal of Cellular Plastics*, vol. 42, pp. 139-152, 2006.
- [41] R. Pop-Iliev, F. Liu, G. Liu, and C. B. Park, "Rotational Foam Molding of Polypropylene with Control of Melt Strength," *Advances in Polymer Technology*, vol. 22, pp. 280-296, 2003.
- [42] R. Pop-Iliev and C. B. Park, "Processing of polypropylene foams in melt compounding based rotational foam molding," *Journal of Reinforced Plastics and Composites*, vol. 21, pp. 1079-1100, 2002.
- [43] R. Pop-Iliev and C. B. Park, "Melt compounding based rotational foam molding technology for manufacture of polypropylene foams," *Journal of Reinforced Plastics and Composites*, vol. 21, pp. 101-120, 2002.
- [44] R. Pop-Iliev and C. B. Park, "Single-step rotational foam molding of skin-surrounded polyethylene foams," *Journal of Cellular Plastics*, vol. 39, pp. 49-58, 2003.
- [45] R. Pop-Iliev, G. M. Rizvi, and C. B. Park, "The Importance of Timely Polymer Sintering While Processing Polypropylene Foams in Rotational Molding," *Polymer Engineering and Science*, vol. 43, pp. 40-54, 2003.
- [46] R. Pop-Iliev, D. Xu, and C. B. Park, "Manufacturability of fine-celled cellular structures in rotational foam molding," *Journal of Cellular Plastics*, vol. 40, pp. 13-25, 2004.
- [47] D. F. Baldwin, C. B. Park, and N. P. Suh, "Microcellular sheet extrusion system process design models for shaping and cell growth control," *Polymer Engineering and Science*, vol. 38, pp. 674-688, 1998.
- [48] M. Lee, C. B. Park, and C. Tzoganakis, "Measurements and modeling of PS/supercritical CO₂ solution viscosities," *Polymer Engineering and Science*, vol.

- 39, pp. 99-109, 1999.
- [49] P. C. Lee, W. Kaewmesri, J. Wang, C. B. Park, J. Pumchusak, R. Folland, and A. Praller, "Effect of die geometry on foaming behaviors of high-melt-strength polypropylene with CO₂," *Journal of Applied Polymer Science*, vol. 109, pp. 3122-3132, 2008.
- [50] Y. H. Lee, M. Sain, T. Kuboki, and C. B. Park, "Extrusion foaming of nano-clay-filled wood fiber composites for automotive applications," *SAE International Journal of Materials and Manufacturing*, vol. 1, pp. 641-647, 2009.
- [51] H. E. Naguib, C. B. Park, U. Panzer, and N. Reichelt, "Strategies for achieving ultra low-density polypropylene foams," *Polymer Engineering and Science*, vol. 42, pp. 1481-1492, 2002.
- [52] H. E. Naguib, C. B. Park, and N. Reichelt, "Fundamental foaming mechanisms governing the volume expansion of extruded polypropylene foams," *Journal of Applied Polymer Science*, vol. 91, pp. 2661-2668, 2004.
- [53] C. B. Park, P. C. Lee, J. Wang, and V. Padareva, "Strategies for achieving microcellular LDPE foams in extrusion," *Cellular Polymers*, vol. 25, pp. 1-18, 2006.
- [54] C. B. Park, Y. Liu, and H. E. Naguib, "Challenge to forty-fold expansion of biodegradable polyester foams using carbon dioxide as a blowing agent," *Cellular Polymers*, vol. 18, pp. 367-384, 1999.
- [55] C. B. Park and N. P. Suh, "Filamentary extrusion of microcellular polymers using a rapid decompressive element," *Polymer Engineering and Science*, vol. 36, pp. 34-48, 1996.
- [56] S. Pilla, S. G. Kim, G. K. Auer, S. Gong, and C. B. Park, "Microcellular extrusion foaming of poly(lactide)/poly(butylene adipate-co-terephthalate) blends," *Materials Science and Engineering C*, vol. 30, pp. 255-262, 2010.
- [57] A. H. Behraves and M. Rajabpour, "Experimental study on filling stage of microcellular injection molding process," *Cellular Polymers*, vol. 25, pp. 85-97, 2006.
- [58] A. K. Bledzki and O. Faruk, "Microcellular wood fibre reinforced polypropylene composites in an injection moulding process," *Cellular Polymers*, vol. 21, pp. 417-429, 2002.
- [59] A. K. Bledzki and O. Faruk, "Microcellular wood fiber reinforced PP composites: Cell morphology, surface roughness, impact, and odor properties," *Journal of Cellular Plastics*, vol. 41, pp. 539-550, 2005.
- [60] A. K. Bledzki and O. Faruk, "Effects of the chemical foaming agents, injection parameters, and melt-flow index on the microstructure and mechanical properties of microcellular injection-molded wood-fiber/polypropylene composites," *Journal of Applied Polymer Science*, vol. 97, pp. 1090-1096, 2005.
- [61] A. K. Bledzki and O. Faruk, "Influence of different endothermic foaming agents on microcellular injection moulded wood fibre reinforced PP composites," *Cellular Polymers*, vol. 25, pp. 143-158, 2006.
- [62] A. K. Bledzki and O. Faruk, "Microcellular injection molded wood fiber-PP composites: Part I - Effect of chemical foaming agent content on cell morphology and physico-mechanical properties," *Journal of Cellular Plastics*, vol. 42, pp. 63-76, 2006.

- [63] A. K. Bledzki and O. Faruk, "Microcellular injection molded wood fiber-PP composites: Part II - Effect of wood fiber length and content on cell morphology and physico-mechanical properties," *Journal of Cellular Plastics*, vol. 42, pp. 77-88, 2006.
- [64] A. K. Bledzki, H. Kirschling, M. Rohleder, and A. Chate, "Correlation between injection moulding processing parameters and mechanical properties of microcellular polycarbonate," *Journal of Cellular Plastics*, vol. 48, pp. 301-340, 2012.
- [65] A. K. Bledzki, M. Rohleder, H. Kirschling, and A. Chate, "Microcellular polycarbonate with improved notched impact strength produced by injection moulding with physical blowing agent," *Cellular Polymers*, vol. 27, pp. 327-345, 2008.
- [66] A. K. Bledzki, M. Rohleder, H. Kirschling, and A. Chate, "Correlation between morphology and notched impact strength of microcellular foamed polycarbonate," *Journal of Cellular Plastics*, vol. 46, pp. 415-440, 2010.
- [67] S. W. Cha and J. D. Yoon, "The relationship of mold temperatures and swirl marks on the surface of microcellular plastics," *Polymer - Plastics Technology and Engineering*, vol. 44, pp. 795-803, 2005.
- [68] V. Goodship, R. L. Stewart, R. Hansell, E. O. Ogur, and G. F. Smith, "Microcellular Foaming with Supercritical CO₂ in Injection Moulding," *Cellular Polymers*, vol. 23, pp. 25-37, 2004.
- [69] G. H. Hu, C. D. Jiang, and Z. S. Cui, "Relationship between microcellular foaming injection molding process parameters and cell size," *Journal of Donghua University (English Edition)*, vol. 25, pp. 308-313, 2008.
- [70] L. Kishbaugh, "Five cases where microcellular foaming paid off," *Plastics Technology*, vol. 57, pp. 54-56, 2012.
- [71] J. Lee, L. S. Turng, E. Dougherty, and P. Gorton, "A novel method for improving the surface quality of microcellular injection molded parts," *Polymer*, vol. 52, pp. 1436-1446, 2011.
- [72] J. Lee, L. S. Turng, and A. Kramschuster, "The microcellular injection molding of low-density polyethylene (LDPE) composites," *Polymer - Plastics Technology and Engineering*, vol. 49, pp. 1339-1346, 2010.
- [73] Y. Moon, S. W. Cha, and J. H. Seo, "Bubble nucleation and growth in microcellular injection molding processes," *Polymer - Plastics Technology and Engineering*, vol. 47, pp. 420-426, 2008.
- [74] J. D. Yoon, S. K. Hong, J. H. Kim, and S. W. Cha, "A Mold Surface Treatment for Improving Surface Finish of Injection Molded Microcellular Parts," *Cellular Polymers*, vol. 23, pp. 39-47, 2004.
- [75] J. W. S. Lee, "Investigation of Foaming Behaviors in Injection Molding Using Mold Pressure Profile," Ph.D., Mechanical and Engineering Department, University of Toronto, Toronto, 2009.
- [76] T. A. Osswald, L. S. Turng, and P. J. Gramann, *Injection Molding Handbook*, 2nd ed. Cincinnati: Hanser, 2008.
- [77] R. M. German, "Scientific status of metal powder injection molding," *International Journal of Powder Metallurgy (Princeton, New Jersey)*, vol. 36, pp. 31-36, 2000.

- [78] S. Walter, D. Suttor, T. Erny, B. Hahn, and P. Greil, "Injection moulding of polysiloxane/filler mixtures for oxycarbide ceramic composites," *Journal of the European Ceramic Society*, vol. 16, pp. 387-393, 1996.
- [79] A. Bose and T. S. Wei, "Near net shapes by ceramic injection molding," 2002, pp. 35-42.
- [80] P. A. Toensmeier, "Advances in magnesium molding bode well for processors seeking diversity and business," *Plastics Engineering*, vol. 62, pp. 10-12, 2006.
- [81] V. Goodship and K. Kirwan, "Interfacial instabilities in multimaterial co-injection mouldings: Part 1 - Background and initial experiments," *Plastics, Rubber and Composites Processing and Applications*, vol. 30, pp. 11-15, 2001.
- [82] V. Goodship, K. Kirwan, T. C. Goodhead, and G. F. Smith, "Interfacial instabilities in multimaterial co-injection mouldings Part 2 - Interfacial mixing in transparent mouldings," *Plastics, Rubber and Composites*, vol. 32, pp. 98-103, 2003.
- [83] G. Akay, "CO-INJECTION MOLDING OF REINFORCED POLYMERS," *Polymer Composites*, vol. 4, pp. 256-264, 1983.
- [84] Dier Paul and G. Richard, *Gas Assist Injection Molding*, 1st ed. Norfolk: Bauer Compressors Inc, 2000.
- [85] T. Katoh, R. Tokuno, Y. Zhang, M. Abe, K. Akita, and M. Akamatsu, "Micro injection molding for mass production using LIGA mold inserts," *Microsystem Technologies*, vol. 14, pp. 1507-1514, 2008.
- [86] J. Xu, *Microcellular Injection Molding*: John Wiley and Sons, Inc., 2010.
- [87] R. Gendron, *Thermoplastic Foam Processing, Principles and Development*: CRC Press, 2005.
- [88] S. T. Lee and D. Scholz, *Polymeric Foams, Technology and Developments in Regulation, Process, and Products*: CRC Press, 2008.
- [89] J. P. Beaumont, *Runner and Gating Design Handbook*. Cincinnati: Hanser, 2004.
- [90] L. S. Turng, *C-Mold Design Guide - A Resource for Plastics Engineers*, 3rd Edition ed. New York: Ithaca, 1998.
- [91] S. Subramonian, L. Remy, and D. Schroer, "Acoustics and Forming of Novel Polyolefin Blend Foams," *Cellular Polymers*, vol. 23, pp. 349-367, 2004.
- [92] A. V. Nawaby and E. Zhang, *Thermoplastic Foam Processing: Principles and Development*. Boca Raton, FL: CRC Press, 2004.
- [93] G. Woods, *The ICI Polyurethane Book*. New York: ICI Polyurethanes and Wiley, 1987.
- [94] K. C. Frisch and J. H. Saunders, *Plastics Foams*. New York: Marcel Dekker Inc, 1973.
- [95] UNEP-Ozone-Secretariat, *Handbook for the Montreal Protocol on Substances that Deplete the Ozone Layer*. Kenya: UNEP, 2006.
- [96] S. N. Leung, "Mechanisms of Cell Nucleation, Growth, and Coarsening in Plastic Foaming, Theory, Simulation, and Experiment," Ph.D. , Mechanical and Industrial Engineering, University of Toronto, Toronto, 2009.
- [97] L. A. Utracki and R. Simha, "Free Volume and Viscosity of Polymer-Compressed Gas Mixtures during Extrusion Foaming," *Journal of Polymer Science, Part B: Polymer Physics*, vol. 39, pp. 342-362, 2001.
- [98] R. Gendron, C. Vachon, M. F. Champagne, and Y. Delaviz, "Foam Extrusion of

- PS Blown with a Mixture of HFC-134a and Isopropanol," *Cellular Polymers*, vol. 23, pp. 1-23, 2004.
- [99] C. B. Park, A. H. Behraves, and R. D. Venter, "Low density microcellular foam processing in extrusion using CO₂," *Polymer Engineering and Science*, vol. 38, pp. 1812-1823, 1998.
- [100] J. W. S. Lee, K. Wang, and C. B. Park, "Challenge to extrusion of low-density microcellular polycarbonate foams using supercritical carbon dioxide," *Industrial and Engineering Chemistry Research*, vol. 44, pp. 92-99, 2005.
- [101] C. Jacob and S. K. Dey, "Inert Gases as Alternative Blowing Agents for Extruded Low-Density Polystyrene Foam " *Journal of Cellular Plastics*, vol. 31, pp. 38-47, 1995.
- [102] A. H. Behraves, C. B. Park, and R. D. Venter, "Challenge to the Production of Low-Density, Fine-Cell HDPE Foams Using CO₂," *Cellular Polymers*, vol. 17, pp. 309-326, 1998.
- [103] X. Xu, C. B. Park, D. Xu, and R. Pop-Iliev, "Effects of Die Geometry on Cell Nucleation of PS Foams Blown With CO₂," *Polymer Engineering and Science*, vol. 43, pp. 1378-1390, 2003.
- [104] A. Wong, S. N. Leung, M. M. Hasan, and C. B. Park, "The foamability of polypropylene copolymer blown with argon, nitrogen and helium," in *Society of Plastics Engineers Annual Technical Conference*, Milwaukee, WI, 2008, pp. 2534-2538.
- [105] J. W. S. Lee and C. B. Park, "Use of nitrogen as a blowing agent for the production of fine-celled high-density polyethylene foams," *Macromolecular Materials and Engineering*, vol. 291, pp. 1233-1244, 2006.
- [106] S. G. Kim, C. B. Park, B. S. Kang, and M. Sain, "Foamability of thermoplastic vulcanizates (TPVs) with carbon dioxide and nitrogen," *Cellular Polymers*, vol. 25, pp. 19-33, 2006.
- [107] S. K. Dey, C. Jacob, and M. Xanthos, "Inert-gas extrusion of rigid PVC foam," in *Society of Plastics Engineers Annual Technical Conference*, Boston, MA, USA, 1995, pp. 4138-4143.
- [108] R. Gendron, C. Vachon, M. F. Champagne, and Y. Delaviz, "Foam Extrusion of PS Blown with a Mixture of HFC-134a and Isopropanol," *Cellular Polymers*, vol. 23, pp. 1-23, 2004.
- [109] Y. Sato, T. Takikawa, A. Sorakubo, S. Takishima, H. Masuoka, and M. Imaizumi, "Solubility and diffusion coefficient of carbon dioxide in biodegradable polymers," *Industrial and Engineering Chemistry Research*, vol. 39, pp. 4813-4819, 2000.
- [110] Y. Sato, T. Iketani, S. Takishima, and H. Masuoka, "Solubility of hydrofluorocarbon (HFC-134a, HFC-152a) and hydrochlorofluorocarbon (HCFC-142b) blowing agents in polystyrene," *Polymer Engineering and Science*, vol. 40, pp. 1369-1375, 2000.
- [111] R. Gendron, M. F. Champagne, Y. Delaviz, and M. E. Polasky, "Foaming polystyrene with a mixture of CO₂ and ethanol," *Journal of Cellular Plastics*, vol. 42, pp. 127-138, 2006.
- [112] Y. Sato, K. Fujiwara, T. Takikawa, Sumarno, S. Takishima, and H. Masuoka, "Solubilities and diffusion coefficients of carbon dioxide and nitrogen in

- polypropylene, high-density polyethylene, and polystyrene under high pressures and temperatures," *Fluid Phase Equilibria*, vol. 162, pp. 261-276, 1999.
- [113] P. L. Durrill and R. G. Griskey, "Diffusion and Solution Thermally Softened or Molten Polymers: Part I. Development of Technique and Determination of Data," *American Institute of Chemical Engineers Journal*, vol. 12, pp. 1147-1151, Nov. 1966 1966.
- [114] Y. Kamiya, K. Mizoguchi, Y. Naito, and T. Hirose, "GAS SORPTION IN POLY(VINYL BENZOATE)," *Journal of Polymer Science, Part B: Polymer Physics*, vol. 24, pp. 535-547, 1986.
- [115] B. Wong, Z. Zhang, and Y. P. Handa, "High-precision gravimetric technique for determining the solubility and diffusivity of gases in polymers," *Journal of Polymer Science, Part B: Polymer Physics*, vol. 36, pp. 2025-2032, 1998.
- [116] Y. Kamiya, K. Mizoguchi, K. Terada, Y. Fujiwara, and J. S. Wang, "CO₂ sorption and dilation of poly(methyl methacrylate)," *Macromolecules*, vol. 31, pp. 472-478, 1998.
- [117] J. G. Lee and R. W. Flumerfelt, "Nitrogen solubilities in low-density polyethylene at high temperatures and high pressures," *Journal of Applied Polymer Science*, vol. 58, pp. 2213-2219, 1995.
- [118] R. Kleinrahm and W. Wagner, "Measurement and correlation of the equilibrium liquid and vapour densities and the vapour pressure along the coexistence curve of methane," *The Journal of Chemical Thermodynamics*, vol. 18, pp. 739-760, 1986.
- [119] Y. Sato, M. Wang, S. Takishima, H. Masuoka, T. Watanabe, and Y. Fukasawa, "Solubility of butane and isobutane in molten polypropylene and polystyrene," *Polymer Engineering and Science*, vol. 44, pp. 2083-2089, 2004.
- [120] Y. Sato, T. Takikawa, S. Takishima, and H. Masuoka, "Solubilities and diffusion coefficients of carbon dioxide in poly(vinyl acetate) and polystyrene," *Journal of Supercritical Fluids*, vol. 19, pp. 187-198, 2001.
- [121] G. Li, H. Li, J. Wang, and C. B. Park, "Investigating the solubility of CO₂ in polypropylene using various EOS models," *Cellular Polymers*, vol. 25, pp. 237-248, 2006.
- [122] G. Li, F. Gunkel, J. Wang, C. B. Park, and V. Altstädt, "Solubility measurements of N₂ and CO₂ in polypropylene and ethene/octene copolymer," *Journal of Applied Polymer Science*, vol. 103, pp. 2945-2953, 2007.
- [123] H. Xie and R. Simha, "Theory of solubility of gases in polymers," *Polymer International*, vol. 44, pp. 348-355, 1997.
- [124] I. C. Sanchez and R. H. Lacombe, "Statistical thermodynamics of polymer solutions," *Macromolecules*, vol. 11, pp. 1145-1156, 1978.
- [125] R. Simha and T. Somcynsky, "On the statistical thermodynamics of spherical and chain molecule fluids," *Macromolecules*, vol. 2, pp. 342-350, 1969.
- [126] Y. G. Li, C. B. Park, H. B. Li, and J. Wang, "Measurement of the PVT property of PP/CO₂ solution," *Fluid Phase Equilibria*, vol. 270, pp. 15-22, 2008.
- [127] J. W. S. Lee, "Investigation of Foaming Behaviors In Injection Molding Using Mold Pressure Profile," Ph.D., Mechanical and Industrial Engineering, University of Toronto, Toronto, 2009.
- [128] J. S. Colton and N. P. Suh, "Nucleation of Microcellular Thermoplastic Foam with Additives: Part I: Theoretical Considerations," *Polymer Engineering and*

- Science*, vol. 27, pp. 485-492, 1987.
- [129] J. S. Colton and N. P. Suh, "Nucleation of Microcellular Thermoplastic Foam With Additives: Part II: Experimental Results and Discussion," *Polymer Engineering and Science*, vol. 27, pp. 493-499, 1987.
- [130] C. B. Park, D. F. Baldwin, and N. P. Suh, "Effect of the pressure drop rate on cell nucleation in continuous processing of microcellular polymers," *Polymer Engineering and Science*, vol. 35, pp. 432-440, 1995.
- [131] M. S. Ahmed, Y. H. Lee, C. B. Park, and N. Atalla, "Effect of nanoclay on the microcellular structure and morphology of high internal phase emulsion (HIPE) foams," *Asia-Pacific Journal of Chemical Engineering*, vol. 4, pp. 120-124, 2009.
- [132] C. B. Park, L. K. Cheung, and S. W. Song, "The Effect of Talc on Cell Nucleation in Extrusion Foam Processing of Polypropylene with CO₂ and Isopentane," *Cellular Polymers*, vol. 17, pp. 221-251, 1998.
- [133] H. E. Naguib, C. B. Park, P. C. Lee, and D. Xu, "A study on the foaming behaviors of PP resins with talc as nucleating agent," *Journal of Polymer Engineering*, vol. 26, pp. 565-587, 2006.
- [134] W. G. Zheng, Y. H. Lee, and C. B. Park, "Use of nanoparticles for improving the foaming behaviors of linear PP," *Journal of Applied Polymer Science*, vol. 117, pp. 2972-2979, 2010.
- [135] A. Wong, "In Situ Observation of Plastic Foaming under Static Condition, Extensional Flow and Shear Flow," Ph.D., Mechanical and Industrial Engineering, University of Toronto, Toronto, 2012.
- [136] P. C. Lee, W. Kaewmesri, J. Wang, C. B. Park, J. Pumchusak, R. Follond, and A. Praller, "Effect of die geometry on foaming behaviors of high melt strength polypropylene with CO₂," 2007, pp. 2103-2107.
- [137] P. C. Lee, H. E. Naguib, C. B. Park, and J. Wang, "Increase of open-cell content by plasticizing the soft regions with a secondary blowing agent," 2004, pp. 2626-2630.
- [138] P. C. Lee, H. E. Naguib, C. B. Park, and J. Wang, "Increase of open-cell content by plasticizing soft regions with secondary blowing agent," *Polymer Engineering and Science*, vol. 45, pp. 1445-1451, 2005.
- [139] P. C. Lee, J. Wang, and C. B. Park, "Extruded open-cell foams using two semicrystalline polymers with different crystallization temperatures," 2005, pp. 177-181.
- [140] P. C. Lee, J. Wang, and C. B. Park, "Extrusion of microcellular open-cell LDPE-based sheet foams," *Journal of Applied Polymer Science*, vol. 102, pp. 3376-3384, 2006.
- [141] P. C. Lee, J. Wang, and C. B. Park, "Extruded open-cell foams using two semicrystalline polymers with different crystallization temperatures," *Industrial and Engineering Chemistry Research*, vol. 45, pp. 175-181, 2006.
- [142] C. B. Park, V. Padareva, P. C. Lee, and H. E. Naguib, "Extruded open-celled LDPE-based foams using non-homogeneous melt structure," *Journal of Polymer Engineering*, vol. 25, pp. 239-260, 2005.
- [143] P. C. Lee, G. Li, J. W. S. Lee, and C. B. Park, "Improvement of cell opening by maintaining a high temperature difference in the surface and core of a foam extrudate," *Journal of Cellular Plastics*, vol. 43, pp. 431-444, 2007.

- [144] A. Kramschuster and L. S. Turng, "An injection molding process for manufacturing highly porous and interconnected biodegradable polymer matrices for use as tissue engineering scaffolds," *Journal of Biomedical Materials Research - Part B Applied Biomaterials*, vol. 92, pp. 366-376, 2010.
- [145] R. K. M. Chu, H. E. Naguib, and N. Atalla, "Synthesis and characterization of open-cell foams for sound absorption with rotational molding method," 2008, pp. 1029-1033.
- [146] S. G. Mosanenzadeh, W. Lee, H. E. Naguib, C. B. Park, and N. Atalla, "Effect of water soluble polymer on acoustic performance of environmentally friendly acoustic foams," 2011.
- [147] K. T. Okamoto, *Microcellular Processing*. Cincinnati: Hanser Gardner Publications Inc., 2003.
- [148] J. W. S. Lee, J. Wang, J. D. Yoon, and C. B. Park, "Strategies to achieve a uniform cell structure with a high void fraction in advanced structural foam molding," *Industrial and Engineering Chemistry Research*, vol. 47, pp. 9457-9464, 2008.
- [149] J.-S. Wu and M.-J. Lee, "Studies on gas counter pressure and low pressure structural foam molding, part I: process design and effect of processing conditions on surface quality of molded parts," *Plastics, Rubber and Composites Processing and Applications*, vol. 21, pp. 163-171, 1994.
- [150] J.-S. Wu and M.-J. Lee, "Studies on gas counter pressure and low pressure structural foam molding, part II: effect of processing conditions on structure of molded parts," *Plastics, Rubber and Composites Processing and Applications*, vol. 21, pp. 173-182, 1994.
- [151] L. S. Turng, "Special and emerging injection molding processes," *Journal of Injection Molding Technology*, vol. 5, pp. 160-179, 2001.
- [152] B. Dong, Q. Li, C. Liu, and C. Shen, "Optimizing sink marks of ABS part with ribs by gas assisted injection," *Huagong Xuebao/Journal of Chemical Industry and Engineering (China)*, vol. 58, pp. 255-259, 2007.
- [153] T. Geng, Y. Zhang, and Q. Ren, "Effect of different section shape of gas channel on the Gas-Assisted Injection Molding," vol. 58-60, ed, 2011, pp. 2225-2230.
- [154] R. D. Chien, S. C. Chen, M. C. Lin, P. H. Lee, and C. S. Chen, "Effect of gas channel design on the molding window of gas-assisted-injection-molded polystyrene parts," *Journal of Applied Polymer Science*, vol. 90, pp. 2979-2986, 2003.
- [155] Y. S. Soh and C. H. Chung, "Flow directions in the gas assisted injection molding technology," *Journal of Reinforced Plastics and Composites*, vol. 17, pp. 935-944, 1998.
- [156] X. Lu, H. H. Chiang, L. Fong, J. Zhao, and S. C. S. Chen, "Study of "gas fingering" behavior in gas-assisted injection molding," *Polymer Engineering and Science*, vol. 39, pp. 62-77, 1999.
- [157] D. P. Dempsey, B. Beaudoin, S. H. Yoon, J. S. Lee, S. P. Johnston, J. L. Mead, and C. M. F. Barry, "Gas channel design for gas assisted micro injection molding," 2010, pp. 1727-1732.
- [158] H. Zhou and D. Li, "Computer simulation of the filling process in gas-assisted injection molding based on gas-penetration modeling," *Journal of Applied*

- Polymer Science*, vol. 90, pp. 2377-2384, 2003.
- [159] C. S. Chen, W. S. Cheng, T. S. Wang, and R. D. Chien, "Optimum design of gas-assisted injection molding," *Journal of Reinforced Plastics and Composites*, vol. 24, pp. 1577-1586, 2005.
- [160] J. Li, L. Chen, H. Zhou, and D. Li, "Surface model based modeling and simulation of filling process in gas-assisted injection molding," *Journal of Manufacturing Science and Engineering, Transactions of the ASME*, vol. 131, pp. 0110081-0110088, 2009.
- [161] D. M. Gao, "Three dimensional filling analysis of gas-assisted injection molding," *Journal of Reinforced Plastics and Composites*, vol. 20, pp. 1090-1099, 2001.
- [162] K. M. Zi and L. H. Chen, "Application of Moldflow in Gas-assisted Injection Molding," *Advanced Materials and Research*, vol. 328-330, pp. 1202-1205, 2011.
- [163] M. A. Parvez, N. S. Ong, Y. C. Lam, and S. B. Tor, "Gas-assisted injection molding: The effects of process variables and gas channel geometry," *Journal of Materials Processing Technology*, vol. 121, pp. 27-35, 2002.
- [164] G. Q. Zheng, W. Yang, M. B. Yang, J. B. Chen, Q. Li, and C. Y. Shen, "Gas-assisted injection molded polypropylene: The skin-core structure," *Polymer Engineering and Science*, vol. 48, pp. 976-986, 2008.
- [165] G. Q. Zheng, Q. Li, J. B. Chen, C. Y. Shen, W. Yang, and M. B. Yang, "Gas-assisted injection molded polypropylene/glass fiber composite: Foaming structure and tensile strength," *Polymer - Plastics Technology and Engineering*, vol. 48, pp. 170-176, 2009.
- [166] L. Wang, B. Yang, W. Yang, N. Sun, B. Yin, J. M. Feng, and M. B. Yang, "Morphology and mechanical property of high-density polyethylene parts prepared by gas-assisted injection molding," *Colloid and Polymer Science*, vol. 289, pp. 1661-1671, 2011.
- [167] R. K. M. Chu, "Synthesis and Characterization of Rotational Molded Polymeric Foams for Optimal Acoustic Absorption," M.A.Sc, Mechanical and Industrial Engineering, University of Toronto, Toronto, 2007.
- [168] C. Zwicker and C. W. Kosten, *Sound Absorbing Materials*: Elsevier Pub. Co., 1949.
- [169] J. F. Allard and N. Atalla, *Propagation of Sound in Porous Media - Modelling Sound Absorbing Materials*, Second ed.: Wiley, 2009.
- [170] J. Moir, "SOUND ABSORBENTS AS NOISE REDUCERS," *Noise Control Vib Reduct*, vol. 5, pp. 307-310, 1974.
- [171] C. C. o. O. H. a. Safety. (2012). *A Comparison of Sound Pressure and Sound Pressure Level*. Available: http://www.ccohs.ca/oshanswers/phys_agents/noise_basic.html
- [172] H. J. Kang, J. G. Ih, J. S. Kim, and H. S. Kim, "Prediction of sound transmission loss through multilayered panels by using Gaussian distribution of directional incident energy," *Journal of the Acoustical Society of America*, vol. 107, pp. 1413-1420, 2000.
- [173] J. W. Lee, J. C. Lee, J. Pandey, S. H. Ahn, and Y. J. Kang, "Mechanical Properties and Sound Insulation Effect of ABS/Carbon-black Composites," *Journal of Composite Materials*, vol. 44, pp. 1701-1706, 2010.
- [174] Q. Q. Ni, E. Lu, N. Kurahashi, K. Kurashiki, and T. Kimura, "Development of

- insulation sheet materials and their sound characterization," *Advanced Composite Materials*, vol. 17, pp. 25-40, 2008.
- [175] P. F. Soto, M. Herráez, A. González, and J. A. de Saja, "Acoustic impedance and absorption coefficient measurements of porous materials used in the automotive industry," *Polymer Testing*, vol. 13, pp. 77-88, 1994.
- [176] D. Chen, J. Li, and J. Ren, "Study on sound absorption property of ramie fiber reinforced poly(l-lactic acid) composites: Morphology and properties," *Composites Part A: Applied Science and Manufacturing*, vol. 41, pp. 1012-1018, 2010.
- [177] K. W. Suh, C. P. Park, M. J. Maurer, M. H. Tusim, R. De Genova, R. Broos, and D. P. Sophiea, "Lightweight cellular plastics," *Advanced Materials*, vol. 12, pp. 1779-1789, 2000.
- [178] A. Wong and C. B. Park, "A visualization system for observing plastic foaming processes under shear stress," *Polymer Testing*, vol. 31, pp. 417-424, 2012.
- [179] A. Wong and C. B. Park, "The effects of extensional stresses on the foamability of polystyrene-talc composites blown with carbon dioxide," *Chemical Engineering Science*, vol. 75, pp. 49-62, 2012.
- [180] C. B. Park and X. Xu, "Apparatus and Method for Advanced Structural Foam Molding," U.S.A Patent, 2005.
- [181] C. B. Park and X. Xu, "Apparatus and Method for Advanced Structural Foam Molding," Canada Patent, 2005.
- [182] C. B. Park and X. Xu, "Apparatus and Method for Advanced Structural Foam Molding," 2006.
- [183] C. B. Park, J. W. S. Lee, and J. Wang. (2008) Advanced Structural Foam Molding Using Supercritical Fluid (SCF). *Plastics Age*.
- [184] K. Blizard, K. T. Okamoto, and J. R. Anderson, "Microcellular articles and methods of their production," USA Patent 6169122, 2001.
- [185] J. Xu, "Methods of manufacturing foam material including systems with pressure restriction element," USA Patent 6322347, 2001.
- [186] (Feb.14). *MuCell Injection Molding - The Process*. Available: http://www.trexel.com/injection-molding-solutions/the_process.php
- [187] Rapidwerks, "Rapidwerks-Precision Injection Molding Services," ed.
- [188] BSWA-TECH, "User's Manual - Impedance Tube Test System," ed: BSWA Tech, 2010.
- [189] *Materials and Acoustics Handbook*: Wiley.
- [190] J. Yao, L. Ma, W. Lua, L. Jiang, and Y. Li, "Acoustic absorption performance research of coir density board," vol. 549, ed, 2012, pp. 589-592.